A Density-Functional Theory Including Dispersion Interactions

by
Erin R. Johnson

A thesis submitted to the Department of Chemistry
in conformity with the requirements for
the degree of Doctorate of Philosophy

Queen's University
Kingston, Ontario
November, 2007

Abstract

The London dispersion interaction is responsible for attraction between non-polar molecules and is of great importance in describing structure and reactivity in many areas of chemistry. Dispersion is difficult to model accurately. Density Functional Theory (DFT) methods, widely used in computational chemistry today, do not include the necessary physics. This often leads to qualitatively incorrect predictions when DFT is applied to dispersion-bound systems. A novel DFT method has been developed which is capable of accurately modeling dispersion. Dispersion attraction between molecules arises when an instantaneous dipole moment in one molecule induces a dipole moment in a second molecule. Our approach proposes that the source of these instantaneous dipole moments is the position-dependent dipole moment of the exchange hole. The model is no more computationally expensive than existing DFTs and gives remarkably accurate dispersion coefficients, intermolecular separations, intermolecular binding energies, and intramolecular conformational energies. Our dispersion theory is also combined with previous post-exact-exchange models of dynamical and nondynamical correlation, yielding a unified exact-exchange-based energy functional called DF07. DF07 overcomes many of the outstanding problems in DFT arising from local exchange approximations. The DF07 model is shown to provide highly accurate results for thermochemistry, kinetics, and van der Waals interactions.

Acknowledgments

I wish to express my gratitude to Dr. Axel Becke for his guidance and supervision over the past three years. Working with Axel has provided an unparalleled learning experience and has helped me to become a better scientist.

In the course of any research project there are points where difficulties arise. I would like to acknowledge Drs. Daniel Matusek, William Meath, and Jane Murray for discussions that provided valuable insight towards the solutions of these problems. I would also like to thank my longtime friend and collaborator Dr. Gino DiLabio, who is largely responsible for my ongoing career in science.

I am very fortunate to have the continuing love and support of my parents, Ray and Jane Johnson. Thanks also to my friends Owen Clarkin, Amanda Kenney, Lindsay Patrick, Chris Rowley, Manuel Smeu, and Richard Verver. In particular, a special thank you to Brad Lutwick for one of the longest two-hour drives in history.

Finally, the financial support of the Natural Sciences and Engineering Research Council of Canada (NSERC) is gratefully acknowledged.

Statement of Originality

The work contained in this thesis is the result of original research. Three years ago my supervisor proposed the idea of a relationship between the dispersion interaction and the exchange-hole dipole moment. During the course of my graduate studies I developed and tested this idea. I also surveyed the literature, assembled benchmark and calibration data, performed reference calculations, and wrote code for parameter optimizations. The results contained in this thesis have all been published in, or submitted to, peer-reviewed journals. No part of this thesis has been counted towards another degree at Queen's University or any other institution.

Contents

List of Tables

List of Figures

List of Acronyms

BDE Bond dissociation enthalpy

BE Binding energy

CP Counterpoise correction

DC Dynamical correlation

DFT Density functional theory

DNA Deoxyribonucleic acid

GGA Generalized gradient approximation

HAT Hydrogen atom transfer

LDA Local density approximation

LSDA Local spin-density approximation

MAE Mean absolute error

MAPE Mean absolute percent error

MaxAE Maximum absolute error

MaxAPE Maximum absolute percent error

MaxE Maximum error

MaxPE Maximum percent error

MBPT Many-body perturbation theory

ME Mean error

MM Molecular mechanics

MPE Mean percent error

NDC Nondynamical correlation

PES Potential energy surface

RC Repulsion correction

RMSE Root-mean-square error

RMSPE Root-mean-square percent error

vdW van der Waals

XC Exchange-correlation

XDM Exchange-hole dipole moment

XNDC Exchange plus nondynamical correlation

XX Exact exchange

Chapter 1

Introduction

The London dispersion interaction [1] is the weakest of the van der Waals interactions, arising when an instantaneous dipole in the charge distribution of one atom or molecule induces an instantaneous dipole in a nearby atom or molecule. This interaction is responsible for condensation of non-polar species, such as noble gases, homonuclear diatomics, and hydrocarbons. It is also important in physisorption of molecules on surfaces, in protein folding, and ligand-receptor binding. Thus, dispersion interactions play a major role in determining the chemistry of a wide range of systems and a physically correct description of dispersion is clearly a key requirement for any general purpose electronic structure method.

Since dispersion energies are much smaller in magnitude than electronic energies, dispersion is naturally modeled in the framework of perturbation theory, as summarized by Dalgarno and Davison [2]. The angle averaged dispersion energy between two atoms or molecules at large interatomic (or intermolecular) separation, R, takes the general form of a series expansion:

$$E_{disp} = -\frac{C_6}{R^6} - \frac{C_8}{R^8} - \frac{C_{10}}{R^{10}} - \ldots , \tag{1.1}$$

where the C_i's are system-dependent dispersion coefficients. The C_6 coefficients can be determined experimentally from dipole oscillator strengths [3].

The dispersion coefficients between monomers A and B can also be determined theoretically from frequency dependent polarizabilities, $\alpha(i\omega)$, [4] although this is very computationally intensive. For example, C_6 can be accurately computed by the Casimir-Polder formula [5, 6]:

$$C_6 = \frac{3}{\pi}\int_0^\infty \alpha_A(i\omega)\alpha_B(i\omega)d\omega. \tag{1.2}$$

There are also a number of simple theoretical approximations to the dispersion coefficients, including the London [1], Slater-Kirkwood [7], Salem [8] (or generalized Unsöld [9]), and Kirkwood-Müller [10, 11] models. These models are all obtained from second-order perturbation theory with the closure approximation [12]. The London model gives the dispersion coefficient in terms of the polarizability, α, and mean excitation energy (taken to be the ionization potential, I) of the monomers:

$$C_6 = \frac{3}{2}\alpha_A\alpha_B\frac{I_A I_B}{I_A + I_B}. \tag{1.3}$$

The Slater-Kirkwood model approximates the dispersion coefficient in terms of the polarizability and the number, N, of electrons in the outer subshell of the monomers:

$$C_6 = \frac{3}{2}\frac{\alpha_A\alpha_B}{(\alpha_A/N_A)^{1/2} + (\alpha_B/N_B)^{1/2}}. \tag{1.4}$$

The Salem (or generalized Unsöld) model gives the dispersion coefficient in terms of the polarizability and the quantum mechanical expectation value of the squared

dipole moment operator, $< \mu^2 >$:

$$C_6 = \frac{\alpha_A \alpha_B}{\alpha_A / < \mu^2 >_A + \alpha_B / < \mu^2 >_B}. \tag{1.5}$$

Finally, the Kirkwood-Müller model can be viewed as a further approximation to the Salem model for atomic dispersion coefficients, assuming independent or uncorrelated electron motion. This allows $< \mu^2 >$ to be replaced by $< r^2 >$ for an electron at distance r from the atomic nucleus:

$$C_6 = \frac{\alpha_A \alpha_B}{\alpha_A / < r^2 >_A + \alpha_B / < r^2 >_B}. \tag{1.6}$$

However, if one is interested in dispersion binding energies rather than dispersion coefficients, these simple models which are valid only at large intermonomer separations must be abandoned in favour of more sophisticated electronic structure theories.

Accurate modeling of dispersion interactions is a notoriously difficult problem in computational chemistry. In the wavefunction picture, dispersion arises from electron correlation and accurate modeling requires inclusion of a large manifold of excited-state configurations. Thus, the uncorrelated Hartree-Fock method does not capture any of the dispersion interaction and predicts completely repulsive potential energy curves for dispersion-bound complexes. Correlated wavefunction methods such as configuration interaction or coupled-cluster theory give an accurate treatment of dispersion. Due to the weakness of this interaction (interaction energies of 0.01-5 kcal/mol), very large basis sets must be used to isolate the binding energies from the basis set superposition error [13]. The dual requirements of highly correlated methods and large basis sets mean that dispersion can only be practically modeled with *ab initio* methods for very small systems.

Density-functional theory (DFT) has achieved widespread popularity as an alter-

native to correlated wavefunction methods thanks to its balance between computational cost and accuracy. DFTs have evolved to the point where they are capable of providing thermochemistry predictions approaching the accuracy of correlated wavefunction methods in some applications [14]. However, contemporary functionals have several shortcomings, leading to qualitatively incorrect predictions for certain classes of systems. These failures include over-stabilization of delocalized odd-electron systems [15], underestimation of the band gap [16], and a total neglect of dispersion physics [17, 18].

Contemporary DFTs are based on *local* models of the exchange-correlation energy in molecular systems and the long-range electron correlation that gives rise to dispersion is neglected. Depending on the exchange models inherent in the functionals, DFTs give widely varying results for dispersion-bound complexes, ranging from completely repulsive curves to drastic overbinding [18]. Repulsion versus overbinding is related to the long-range behaviour of the exchange functional [19].

Attempts to incorporate dispersion into DFT have taken one of two general routes. The first is computationally expensive approaches such as symmetry-adapted perturbation theory [20] or "*ab initio* DFT" [21] that make use of virtual orbitals as in correlated wavefunction theory. The second is the incorporation of empirical correction terms with parameterized atom-dependent dispersion coefficients reminiscent of molecular mechanics force fields [22, 23]. Another empirical approach employs parameterized effective core potentials with attractive terms at long-range to mimic dispersion physics [24]. None of these alternatives is particularly desirable for general use. It would be ideal to have a physically motivated framework for inexpensive calculation of the dispersion energy based only on occupied orbitals and without resorting to atom-dependent empirical parameters.

The object of this thesis is to develop a unified density-functional model capable of providing accurate prediction of thermochemistry, kinetics (i.e. reaction barrier

heights), and all classes of van der Waals interactions, including dispersion, to within "chemical accuracy". We begin by developing a parameter-free model for calculation of the C_6 dispersion coefficients in Chapter 3. We then decompose these coefficients into atomic components which are used to compute potential-energy surfaces for a test set of van der Waals complexes in Chapters 4 and 5. The model is subsequently extended to higher-order C_8 and C_{10} dispersion coefficients, and applied to both intermolecular and intramolecular van der Waals interactions in Chapters 6-8 and 10. The dispersion theory is added to Becke's 2005 exact-exchange-based correlation functional [25] in Chapter 9 to give the desired unified DFT, which is called DF07. Finally, DF07 is extensively tested on a series of thermochemical and kinetic benchmark sets in Chapter 11.

This thesis consists of a sequence of papers, published or to be published, detailing the evolution of our dispersion model and development of our unified DFT. First, in Chapter 2, we provide a brief review of DFT, with a focus on the particular functionals used in this work.

Chapter 2

An Overview of Density Functionals

Density-functional theory is an appealing alternative to correlated wavefunction methods in computational chemistry. While correlated wavefunction methods can generate extremely accurate wavefunctions and energies, their poor computational scaling renders them intractable for large systems [26, 27, 28].

In wavefunction theory, all properties, including the energy, are uniquely determined by the wavefunction, Ψ. In a landmark paper, Hohenberg and Kohn [29] showed that all properties are uniquely determined by the electron density, ρ, as well. The total electronic energy can be expressed as a functional of the density as follows:

$$E(\rho) = T(\rho) + V_{ee}(\rho) + \int v\rho, \tag{2.1}$$

where the total kinetic energy (T) and the total electron-electron repulsion energy (V_{ee}) are functionals of the density in principle, but whose explicit functional dependence is not exactly known. The third term in Eq. (2.1) is the interaction between the electrons and the nuclei, arising from the nuclear potential v. Hohenberg and Kohn

proved that there exists a variational principle in which the ground-state density is the density that minimizes the energy in Eq. (2.1) [29].

The Hohenberg-Kohn variational theorem had the potential to revolutionize electronic structure theory, since the density is a 3-dimensional function that is much easier to work with than the 3N-dimensional wavefunction of an N-electron system. Unfortunately, direct application of this variational principle is of little practical utility. All trial densities in the Hohenberg-Kohn proof must be "v-representable", meaning that each must correspond to the density generated by *some* external potential v, not necessarily the potential of the system in question [30]. There are no known simple constraints on ρ that guarantee v-representability. This difficulty was resolved a year later with the introduction of Kohn-Sham theory [31].

2.1 Kohn-Sham Theory

All contemporary implementations of DFT use the Kohn-Sham formalism [31]. In Kohn-Sham theory, the density is v-representable by construction. This is achieved by introducing a single Slater-determinant reference wavefunction, composed of "Kohn-Sham" orbitals, ψ_i, that generates the electron density. Assuming a closed-shell system, the density is

$$\rho = 2\sum_i \psi_i^2. \tag{2.2}$$

In Kohn-Sham theory, the total electronic energy of the system is partitioned as follows [30, 31, 32]:

$$E(\rho) = T_0(\rho) + J(\rho) + \int v\rho + E_{\mathrm{XC}}(\rho). \tag{2.3}$$

Here $T_0(\rho)$ and $J(\rho)$ have explicit and simple orbital-dependent or density-dependent

forms and are good first approximations to the functionals $T(\rho)$ and $V_{ee}(\rho)$ of Eq. (2.1). $T_0(\rho)$ is the kinetic energy of the reference Slater determinant,

$$T_0(\rho) = -\sum_i \int \psi_i \nabla^2 \psi_i d\mathbf{r}_i, \tag{2.4}$$

and the second term, $J(\rho)$, is the classical electron-electron repulsion energy,

$$J(\rho) = \frac{1}{2} \int \int \frac{\rho(\mathbf{r}_1)\rho(\mathbf{r}_2)}{r_{12}} d\mathbf{r}_1 d\mathbf{r}_2. \tag{2.5}$$

The last term in Eq. (2.3), $E_{\mathrm{XC}}(\rho)$, is called the *exchange-correlation* energy. This term contains the differences, in both kinetic and potential energy, between $T_0 + J$ and $T + V_{ee}$ due to the effects of exchange and correlation:

$$E_{\mathrm{XC}}(\rho) = T(\rho) - T_0(\rho) + V_{ee}(\rho) - J(\rho). \tag{2.6}$$

Since $T_0(\rho)$ and $J(\rho)$ are good approximations to $T(\rho)$ and $V_{ee}(\rho)$, $E_{\mathrm{XC}}(\rho)$ is a relatively small part of the total energy.

To obtain an equation for the Kohn-Sham orbitals, we apply the variational theorem to Eq. (2.3). Minimizing the energy with respect to orbital variations and imposing orthonormalization conditions gives the following orbital equation [30, 31, 32]:

$$-\frac{1}{2}\nabla^2 \psi_i + \left(v + v_{el} + v_{\mathrm{XC}}\right) \psi_i = \epsilon_i \psi_i. \tag{2.7}$$

Here v_{el} is the Coulomb potential of the electron density,

$$v_{el}(\mathbf{r}_1) = \int \frac{\rho(\mathbf{r}_2)}{r_{12}} d\mathbf{r}_2, \tag{2.8}$$

and $v_{\rm XC}$ is the functional derivative of the exchange-correlation energy,

$$v_{\rm XC} = \frac{\delta E_{\rm XC}}{\delta \rho}. \tag{2.9}$$

The functional derivative is related to the first-order change in $E_{\rm XC}$ due to a small variation in the density, $\delta\rho$. See Appendix A of Ref. [30] for a thorough discussion of functional derivatives.

Kohn-Sham theory reduces the electronic structure problem to finding good approximations for the exchange-correlation energy. Let us analyze the *potential-energy* component of the exchange-correlation energy. Consider the interelectronic Coulomb repulsion operator, G, in atomic units:

$$G = \sum_{i>j} \frac{1}{r_{ij}}, \tag{2.10}$$

where r_{ij} is the separation between the electron coordinates $\mathbf{r}_i$ and $\mathbf{r}_j$. The Coulomb repulsion energy is given by [32],

$$V_{ee}(\rho) = \frac{1}{2} \int \int \frac{\Pi(\mathbf{r}_1, \mathbf{r}_2)}{r_{12}} d\mathbf{r}_1 d\mathbf{r}_2, \tag{2.11}$$

where $\Pi(\mathbf{r}_1, \mathbf{r}_2)$ is the pair density. The pair density is the probability of simultaneously finding an electron in the volume element $d\mathbf{r}_1$ and an electron in $d\mathbf{r}_2$. The exchange-correlation potential energy is thus

$$\begin{aligned} V_{ee}(\rho) - J(\rho) &= \frac{1}{2} \int \int \frac{\Pi(\mathbf{r}_1, \mathbf{r}_2)}{r_{12}} d\mathbf{r}_1 d\mathbf{r}_2 - \frac{1}{2} \int \int \frac{\rho(\mathbf{r}_1)\rho(\mathbf{r}_2)}{r_{12}} d\mathbf{r}_1 d\mathbf{r}_2 \\ &= \frac{1}{2} \int \int \frac{1}{r_{12}} \left[\Pi(\mathbf{r}_1, \mathbf{r}_2) - \rho(\mathbf{r}_1)\rho(\mathbf{r}_2) \right] d\mathbf{r}_1 d\mathbf{r}_2, \end{aligned} \tag{2.12}$$

from Eqs. (2.5) and (2.11). Multiplying and dividing by $\rho(\mathbf{r}_1)$ in the integrand gives:

$$V_{ee}(\rho) - J(\rho) = \frac{1}{2} \int \int \frac{\rho(\mathbf{r}_1)}{r_{12}} \left[\frac{\Pi(\mathbf{r}_1, \mathbf{r}_2)}{\rho(\mathbf{r}_1)} - \rho(\mathbf{r}_2) \right] d\mathbf{r}_1 d\mathbf{r}_2. \tag{2.13}$$

The expression in square brackets, $\frac{\Pi(\mathbf{r}_1,\mathbf{r}_2)}{\rho(\mathbf{r}_1)} - \rho(\mathbf{r}_2)$, has a nice physical interpretation. The first term is the *conditional* probability of finding an electron at position $\mathbf{r}_2$, provided that an electron is located at $\mathbf{r}_1$. The second term is the probability of finding an electron at $\mathbf{r}_2$ in the uncorrelated system. Thus, this expression represents the *change* in conditional probability (a "hole") due to the effects of electron exchange and correlation.

While the potential energy contribution to the exchange-correlation energy is easy to represent in terms of this hole, the kinetic energy contribution is not. However, the kinetic energy contribution can be included through the so-called "adiabatic connection" or "coupling strength integration" formalism of Refs. [30, 31, 32, 33, 34, 35, 36]. We introduce a coupling strength parameter, λ, in the Hamiltonian that turns on the Coulomb repulsion between electrons,

$$\mathbf{H}_\lambda = \sum_i \left(-\frac{1}{2} \nabla_i^2 + v_{\lambda,i} \right) + \lambda \sum_{i>j} \frac{1}{r_{ij}}, \tag{2.14}$$

while, at the same time, the external potential v_λ holds the density distribution ρ fixed. $\lambda = 1$ corresponds to the "real" system. $\lambda = 0$ corresponds to a system of noninteracting electrons whose wavefunction is the Kohn-Sham reference Slater determinant. Eq. (2.14) literally "connects" the real system with the Kohn-Sham reference determinant through λ:

$$E_{\lambda=1} = E_{\lambda=0} + \int_0^1 dE_\lambda. \tag{2.15}$$

It can be shown that the total energy of the real system is given by

$$E(\rho) = T_0(\rho) + \int v\rho + \frac{1}{2}\int\int \frac{\Pi_{avg}(\mathbf{r}_1, \mathbf{r}_2)}{r_{12}} d\mathbf{r}_1 d\mathbf{r}_2, \tag{2.16}$$

where $\Pi_{avg}(\mathbf{r}_1, \mathbf{r}_2)$ is the pair density *averaged over the coupling strength parameter*:

$$\Pi_{avg} = \int_0^1 \Pi_\lambda d\lambda. \tag{2.17}$$

Adding and subtracting the classical Coulomb repulsion energy J in Eq. (2.16) gives

$$E(\rho) = T_0(\rho) + J(\rho) + \int v\rho + \frac{1}{2}\int\int \frac{\rho(\mathbf{r}_1)}{r_{12}} \left[\frac{\Pi_{avg}(\mathbf{r}_1, \mathbf{r}_2)}{\rho(\mathbf{r}_1)} - \rho(\mathbf{r}_2)\right] d\mathbf{r}_1 d\mathbf{r}_2. \tag{2.18}$$

Comparing with Eq. (2.3), the exchange-correlation energy is therefore

$$E_{\mathrm{XC}}(\rho) = \frac{1}{2}\int\int \frac{\rho(\mathbf{r}_1)}{r_{12}} \left[\frac{\Pi_{avg}(\mathbf{r}_1, \mathbf{r}_2)}{\rho(\mathbf{r}_1)} - \rho(\mathbf{r}_2)\right] d\mathbf{r}_1 d\mathbf{r}_2. \tag{2.19}$$

This has the same form as the exchange-correlation *potential* energy of Eq. (2.13), but also includes *kinetic* energy effects at the expense of introducing the coupling strength integration. We call the bracketed expression the *exchange-correlation hole*, h_{XC}:

$$E_{\mathrm{XC}} = \frac{1}{2}\int\int \frac{\rho(\mathbf{r}_1)}{r_{12}} h_{\mathrm{XC}}(\mathbf{r}_1, \mathbf{r}_2) d\mathbf{r}_1 d\mathbf{r}_2, \tag{2.20}$$

with

$$h_{\mathrm{XC}}(\mathbf{r}_1, \mathbf{r}_2) = \frac{\Pi_{avg}(\mathbf{r}_1, \mathbf{r}_2)}{\rho(\mathbf{r}_1)} - \rho(\mathbf{r}_2). \tag{2.21}$$

The exchange-correlation (XC) hole is a central quantity in DFT. It measures

the depletion in density (relative to the classical or non-interacting density) around a reference electron located at $\mathbf{r}_1$ due to the effects of exchange and correlation. In real space, picture an electron traveling in the classical potential of the nuclei and the remaining electrons, accompanied by its XC hole. If the reference electron is at position $\mathbf{r}_1$ (called the "reference point"), its hole is given by a distribution in space over coordinate $\mathbf{r}_2$.

The exchange-correlation energy is linked to the XC hole by Eq. (2.20). Development of new XC functionals can therefore be motivated by development of better descriptions of the XC hole. The hole is a convenient quantity to model since it has a nice physical interpretation and can be visualized in real space. The hole also obeys several well-known constraints, which will be discussed in the following section.

2.2 Properties of the Exchange-Correlation Hole

In this section several useful properties of the exchange-correlation hole [32, 39] will be reviewed.

First, the XC hole is normalized to -1 electron at any reference point $\mathbf{r}_1$:

$$\int h_{\mathrm{XC}}(\mathbf{r}_1, \mathbf{r}_2) d\mathbf{r}_2 = -1. \tag{2.22}$$

This follows from Eq. (2.21) and the interpretation of its first term $\Pi_{avg}(\mathbf{r}_1, \mathbf{r}_2)/\rho(\mathbf{r}_1)$ as the *conditional* probability of finding an electron at $\mathbf{r}_2$ *if an electron is at* $\mathbf{r}_1$. Therefore it must integrate, over $\mathbf{r}_2$, to $N-1$. The normalization constraint is very powerful and will be used many times in later chapters.

Further insights may be obtained by defining four spin-dependent holes as follows:

$$h_{\mathrm{XC}}^{\sigma\sigma'}(\mathbf{r}_1, \mathbf{r}_2) = \frac{\Pi_{avg}^{\sigma\sigma'}(\mathbf{r}_1, \mathbf{r}_2)}{\rho_\sigma(\mathbf{r}_1)} - \rho_{\sigma'}(\mathbf{r}_2), \tag{2.23}$$

where ρ_σ is the σ-spin density (either α-spin or β-spin). The XC energy is given in terms of the spin-dependent holes by the following generalization of Eq. (2.20):

$$E_{\rm XC} = \frac{1}{2}\sum_{\sigma\sigma'}\int\int \frac{\rho_\sigma(\mathbf{r}_1)}{r_{12}} h_{\rm XC}^{\sigma\sigma'}(\mathbf{r}_1,\mathbf{r}_2)d\mathbf{r}_1 d\mathbf{r}_2. \tag{2.24}$$

The physical interpretation of each spin-dependent hole is similar to before. $h_{\rm XC}^{\sigma\sigma'}(\mathbf{r}_1,\mathbf{r}_2)$ is the change in conditional probability of finding a σ'-spin electron at $\mathbf{r}_2$ if a σ-spin electron is located at $\mathbf{r}_1$. $h_{\rm XC}^{\sigma\sigma'}(\mathbf{r}_1,\mathbf{r}_2)$ has *parallel*-spin components, $\sigma = \sigma'$, and *opposite*-spin components, $\sigma \neq \sigma'$.

Since electrons are Fermions, there is zero probability of finding two electrons of the same spin at the same point. Thus the parallel-spin pair densities $\Pi_{avg}^{\sigma\sigma}(\mathbf{r}_1,\mathbf{r}_2)$ must vanish when $\mathbf{r}_1 = \mathbf{r}_2$ and the parallel σ-spin hole totally depletes the σ-spin density at the reference point [see Eq. (2.23)]:

$$h_{\rm XC}^{\sigma\sigma}(\mathbf{r}_1,\mathbf{r}_1) = -\rho_\sigma(\mathbf{r}_1). \tag{2.25}$$

Also, if a σ-spin electron is at $\mathbf{r}_1$, the probability of finding another σ-spin electron elsewhere (over all $\mathbf{r}_2$) is $N_\sigma - 1$, and the probability of finding an electron of σ'-spin elsewhere is $N_{\sigma'}$. Therefore, the parallel-spin holes must be normalized to -1 electron while the opposite-spin holes are normalized to zero:

$$\int h_{\rm XC}^{\sigma\sigma}(\mathbf{r}_1,\mathbf{r}_2)d\mathbf{r}_2 = -1, \tag{2.26}$$

$$\int h_{\rm XC}^{\alpha\beta}(\mathbf{r}_1,\mathbf{r}_2)d\mathbf{r}_2 = \int h_{\rm XC}^{\beta\alpha}(\mathbf{r}_1,\mathbf{r}_2)d\mathbf{r}_2 = 0. \tag{2.27}$$

The opposite-spin holes are purely "correlation" holes, but the parallel-spin holes

can be further subdivided into "exchange" and "correlation" components:

$$h_{\mathrm{XC}}^{\sigma\sigma}(\mathbf{r}_1, \mathbf{r}_2) = h_X^{\sigma\sigma}(\mathbf{r}_1, \mathbf{r}_2) + h_C^{\sigma\sigma}(\mathbf{r}_1, \mathbf{r}_2). \tag{2.28}$$

The exchange hole is the hole that delivers, through Eq. (2.24), the Hartree-Fock exchange energy using the Kohn-Sham orbitals instead. It is given by [32]

$$h_X^{\sigma\sigma}(\mathbf{r}_1, \mathbf{r}_2) = -\frac{1}{\rho_\sigma(\mathbf{r}_1)} \left[\sum_i \psi_{i\sigma}(\mathbf{r}_1)\psi_{i\sigma}(\mathbf{r}_2) \right]^2. \tag{2.29}$$

The exchange hole is always negative, completely depletes the σ-spin density at the reference point,

$$h_X^{\sigma\sigma}(\mathbf{r}_1, \mathbf{r}_1) = -\rho_\sigma(\mathbf{r}_1), \tag{2.30}$$

and is normalized to -1 electron,

$$\int h_X^{\sigma\sigma}(\mathbf{r}_1, \mathbf{r}_2) d\mathbf{r}_2 = -1. \tag{2.31}$$

Since the opposite-spin holes are purely correlation holes, we replace the subscript XC with C:

$$\int h_C^{\alpha\beta}(\mathbf{r}_1, \mathbf{r}_2) d\mathbf{r}_2 = \int h_C^{\beta\alpha}(\mathbf{r}_1, \mathbf{r}_2) d\mathbf{r}_2 = 0. \tag{2.32}$$

The XC hole is generally not spherically symmetric, except in the uniform electron gas or at reference points at the center of systems with spherically symmetric densities. However, from Eq. (2.17) or Eq. (2.24) it can be seen that the exchange-correlation energy is dependent only on the *spherical average* of the XC hole around each $\mathbf{r}_1$. Therefore, only the spherically-averaged hole needs to be modeled in order to obtain

$E_{\rm XC}$ approximations.

These properties of the spin-dependent components of the exchange, correlation, and total exchange-correlation holes are very useful and will reappear throughout this thesis. Representative sketches of the parallel-spin XC hole and the opposite-spin correlation hole are shown in Fig. 2.1.

Figure 2.1: Sketch of the spherically-averaged parallel-spin XC hole and the opposite-spin correlation hole in a free atom.

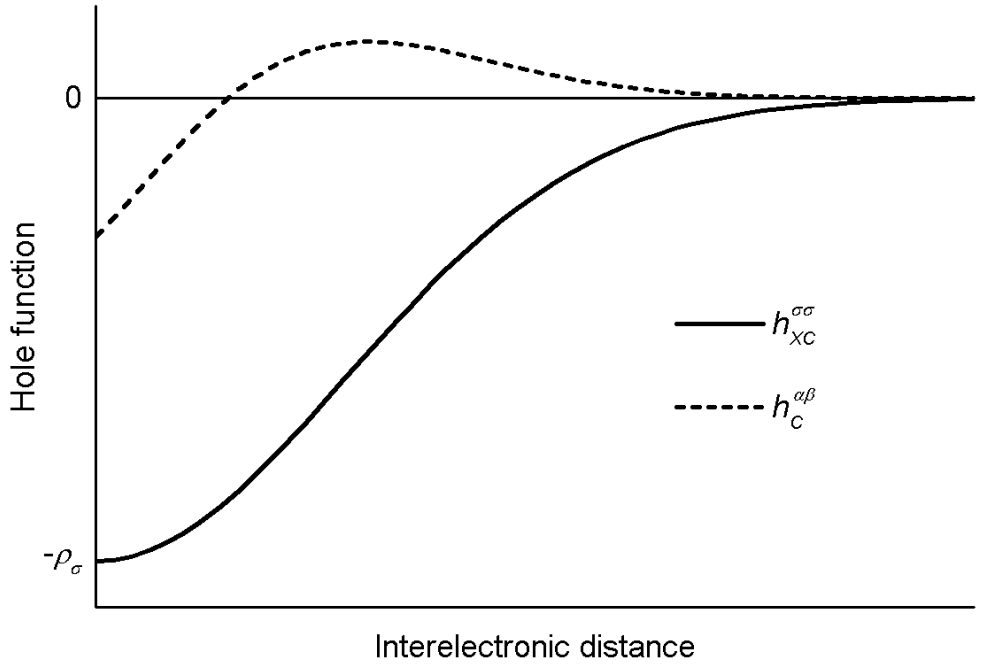

2.3 The LSDA

The simplest exchange-correlation approximation is the local spin-density approximation (LSDA), in which the XC hole is approximated by the XC hole of a spin-dependent uniform electron gas [30, 31, 32, 37, 38]. This gives an XC energy that

depends only on the spin density at each reference point,

$$E_{\mathrm{XC}}^{\mathrm{LSDA}} = \int e_{\mathrm{XC}}^{\mathrm{UEG}}[\rho_\alpha(\mathbf{r}_1), \rho_\beta(\mathbf{r}_1)] d\mathbf{r}_1, \tag{2.33}$$

where $e_{\mathrm{XC}}^{\mathrm{UEG}}(\rho_\alpha, \rho_\beta)$ is the XC energy density of the uniform electron gas with spin densities ρ_α and ρ_β. The LSDA exchange-energy part is given by the following simple expression:

$$E_X^{\mathrm{LSDA}} = -\frac{3}{2}\left(\frac{3}{4\pi}\right)^{1/3} \sum_\sigma \int \rho_\sigma^{4/3}. \tag{2.34}$$

The correlation part is most accurately obtained by fitting quantum Monte Carlo simulations, and several parameterizations are available in the literature [37, 38]. The performance of the LSDA is somewhat comparable to HF, in that it predicts reasonable molecular geometries but very poor energetics (from our own unpublished calculations, the mean absolute errors for the "G3/99" benchmark set of 222 atomization energies [40] are 225 kcal/mol with HF and 120 kcal/mol with the LSDA). However, while HF underbinds molecules the LSDA has an overbinding tendency.

2.4 GGA Exchange Functionals

The exchange energy is generally much larger in magnitude than the correlation energy [32]. We focus in this section on exchange energy. Substantial improvement over the LSDA is obtained with a class of functionals called the "generalized gradient approximation" (GGA), where the exchange energy is dependent on both the spin-density *and its gradient* at each reference point.

Two very popular GGA exchange functionals are the B86 [41] and B88 [42] functionals. They give similar results for thermochemistry, but have very different long-

range behaviour. The B86 functional is

$$E_X^{\mathrm{B86}} = E_X^{\mathrm{LSDA}} - \beta \sum_\sigma \int \rho_\sigma^{4/3} \frac{\chi_\sigma^2}{1+\gamma\chi_\sigma^2}, \tag{2.35}$$

where χ_σ is the dimensionless gradient

$$\chi_\sigma = \frac{|\nabla \rho_\sigma|}{\rho_\sigma^{4/3}} \tag{2.36}$$

and β and γ are parameters determined by least-squares fits to exact atomic exchange energies. Their values are $\beta = 0.0036$ and $\gamma = 0.004$ [41].

While the B86 form gives excellent atomic exchange energies, it has the incorrect behaviour in the limit $\chi_\sigma \to \infty$, which corresponds to reference points far from a finite system. For reference points far removed from a finite system, the exchange hole must remain localized on the system and the reference electron should experience an exchange potential of $-1/r$. Thus, the correct long-range behaviour for the integrand of the exchange energy expression (e_X) is [see Eq. (2.24)]

$$\lim_{\chi_\sigma \to \infty} e_X = -\frac{1}{2}\frac{\rho_\sigma}{r}. \tag{2.37}$$

In both the LSDA and B86, e_X has the asymptotic behaviour $\rho_\sigma^{4/3}$ and, since the spin-density decays exponentially, the exchange energy falls off too rapidly. This incorrect long-range behaviour causes B86-based functionals to predict binding in some dispersion-bound complexes [18, 19]. However, this binding does not arise for good physical reasons, as evidenced by the fact that the errors grow rapidly larger with increasing polarizability in the series of noble-gas pairs.

The B88 functional was designed to achieve the correct long-range behaviour and

has the form:

$$E_X^{\mathrm{B88}} = E_X^{\mathrm{LSDA}} - \beta \sum_\sigma \int \rho_\sigma^{4/3} \frac{\chi_\sigma^2}{1 + 6\beta\chi_\sigma \mathrm{arcsinh}\chi_\sigma}. \tag{2.38}$$

The optimum value of the parameter $\beta = 0.0042$ was determined by least-squares fitting to exact atomic exchange energies [42]. Since B88 has the correct asymptotic behaviour of e_X, like exact or Hartree-Fock exchange, it predicts completely repulsive curves for dispersion-bound complexes [17, 18].

The functionals discussed up to this point all have the uniform electron gas as their starting point. However, for chemistry applications this is not a particularly important system. The hydrogen atom may be a more relevant starting point for functional development. Unlike B86 and B88, the Becke-Roussel (BR) exchange model [43] was designed to give the exact exchange hole at any reference point in any hydrogenic atom. The BR model is a "meta-GGA" method, meaning that, in addition to including the density and its gradient, it also makes use of the kinetic-energy density, and the Laplacian of the density.

The BR functional approximates the exchange hole by an exponential function $-Ae^{-ar}$ centered at a distance b from the reference point. This gives the following analytical expression for the spherically-averaged exchange hole [43]:

$$h_{X\sigma}^{\mathrm{BR}}(\mathbf{r}, s) = -\frac{a}{16\pi bs} \left[(a|b-s|+1)\, e^{-a|b-s|} - (a|b+s|+1)\, e^{-a|b+s|} \right], \tag{2.39}$$

where the arguments $(\mathbf{r}, s)$ denote the spherical average on a shell of radius s around the reference point $\mathbf{r}$. The three parameters in the model (A, a, b) are determined by enforcing the correct hole normalization of -1 electron and constraining the model hole to give the same first two terms in the Taylor expansion about the reference point as the exact exchange hole.

The short-range behaviour of the exact exchange hole is given by the Taylor expansion [39],

$$h_{X\sigma}(\mathbf{r}, s) = -\rho_\sigma - Q_\sigma s^2 + \dots , \tag{2.40}$$

where

$$Q_\sigma = \frac{1}{6}\left(\nabla^2\rho_\sigma - 2D_\sigma\right), \tag{2.41}$$

with

$$D_\sigma = \tau_\sigma - \frac{1}{4}\frac{(\nabla\rho_\sigma)^2}{\rho_\sigma}, \tag{2.42}$$

and τ_σ is the positive-definite kinetic energy density defined in terms of the Kohn-Sham orbitals by

$$\tau_\sigma = \sum_i |\nabla\psi_{i\sigma}|^2. \tag{2.43}$$

The Taylor expansion of the BR model hole is [43]

$$h_{X\sigma}^{\mathrm{BR}}(\mathbf{r}, s) = -Ae^{-x} - \frac{Aa^2}{6}\left(1 - \frac{2}{x}\right)e^{-x}s^2 + \dots , \tag{2.44}$$

with $x = ab$ and $A = a^3/8\pi$ for normalization to unit charge. Solving the remaining two constraints leads to the following nonlinear equation for the dimensionless variable x:

$$\frac{xe^{-2x/3}}{x-2} = \frac{2}{3}\pi^{2/3}\frac{\rho_\sigma^{5/3}}{Q_\sigma}, \tag{2.45}$$

which must be solved numerically. The value of b is then given by

$$b^3 = \frac{x^3 e^{-x}}{8\pi\rho_\sigma} \tag{2.46}$$

and $a = x/b$. The final expression for the BR exchange energy is

$$E_{X\sigma}^{\mathrm{BR}} = -\frac{1}{2}\int \frac{\rho_\sigma}{b}\left(1 - e^{-x} - \frac{1}{2}xe^{-x}\right) d\mathbf{r}. \tag{2.47}$$

The BR exchange functional is appealing because it is free of empirical parameters and it reproduces both the exact exchange potential for the ground state of any hydrogenic atom and the correct $-1/r$ asymptotic limit of the exchange potential in all finite systems. The detailed shape of the exact exchange hole is also well reproduced at all reference points in non-hydrogenic atoms as seen from plots in Ref. [43].

2.5 GGA Correlation Functionals

There are several popular GGA models for correlation that can be paired with the GGA exchange models described above, including P86 [44], PW91 [45], and LYP [46]. In this work frequent use is made of the 1988 correlation model of Becke [39], which is a meta-GGA. This correlation model is based on the known constraints on the shapes of both the opposite and parallel-spin correlation holes.

Since both the opposite and parallel-spin correlation holes integrate to zero, they must change sign at some value of the interelectronic separation s, which we call the "correlation length". Since correlation decreases the probability of finding a second electron near the reference electron, the correlation hole is negative inside the correlation length and positive outside as in Fig. 2.1. In the B88 model, the correlation length is denoted as $z_{\alpha\beta}$ for opposite spins and $z_{\sigma\sigma}$ for parallel spins.

Enforcing interelectronic cusp conditions for the spherically-averaged correlation holes, and zero normalization, gives the following functionals for the correlation energy [39]:

$$E_C^{\alpha\beta+\beta\alpha} = A^{\alpha\beta} \int \rho_\alpha \rho_\beta z_{\alpha\beta}^2 \left(1 - \frac{\ln(1+z_{\alpha\beta})}{z_{\alpha\beta}}\right) d\mathbf{r}, \tag{2.48}$$

$$E_C^{\sigma\sigma} = A^{\sigma\sigma} \int \rho_\sigma D_\sigma z_{\sigma\sigma}^4 \left[1 - \frac{2}{z_{\sigma\sigma}} \ln\left(1 + \frac{z_{\sigma\sigma}}{2}\right)\right] d\mathbf{r}, \tag{2.49}$$

where $A^{\alpha\beta}$ and $A^{\sigma\sigma}$ are constants whose values are dependent on the shape of the correlation hole at large distances from the reference point. Their values are $A^{\alpha\beta} = -0.8$ and $A^{\sigma\sigma} = -0.01$ in Ref. [39] assuming exponential decay of the hole at large interelectronic separation, characteristic of Coulomb systems.

The correlation length between two electrons is assumed to be related to the distance at which their respective exchange-hole "radii" overlap. The *mean inverse* radius of the exchange hole at reference point $\mathbf{r}$ is

$$< s_\sigma^{-1} >= 4\pi \int \frac{1}{s} |h_X^{\sigma\sigma}(\mathbf{r}, s)| s^2 ds = |U_{X\sigma}|, \tag{2.50}$$

which equals the magnitude of the exchange-hole potential $U_{X\sigma}$. Thus, we define the exchange-hole radius to be $|U_{X\sigma}|^{-1}$, giving the following definition of the correlation lengths:

$$z_{\sigma\sigma'} = c_{\sigma\sigma'} \left(|U_{X\sigma}|^{-1} + |U_{X\sigma'}|^{-1}\right), \tag{2.51}$$

where $c_{\alpha\beta} = 0.63$ and $c_{\sigma\sigma} = 0.88$ are constants of proportionality for opposite and parallel-spin correlations respectively, determined from fits to exact atomic correlation energies [47]. This definition of the correlation lengths means that the B88

correlation functional can be naturally paired with any exchange functional by using the appropriate exchange potential in Eq. (2.51).

From our own (unpublished) calculations, the B86, B88, and BR exchange-correlation functionals all give similar performance for the G3/99 atomization energies [40], with mean absolute errors of 13-14 kcal/mol. While this is a vast improvement over the LSDA, these models are still far from "chemical accuracy."

2.6 Hybrid Functionals

The most popular and accurate density functionals today are so-called "hybrids", which employ a mixing of GGA exchange and exact (or Hartree-Fock) exchange as in Eq. (2.29). The introduction of hybrid DFTs was motivated by the coupling-strength average in Eq. (2.21). This can be shown more explicitly as

$$h_{\mathrm{XC}}^{\sigma\sigma'}(\mathbf{r}_1, \mathbf{r}_2) = \int_0^1 h_{\mathrm{XC}\lambda}^{\sigma\sigma'}(\mathbf{r}_1, \mathbf{r}_2) d\lambda. \tag{2.52}$$

While the XC hole tends to be *localized* in the interacting system ($\lambda > 0$), it is relatively more *delocalized* in the non-interacting ($\lambda = 0$) limit. GGA model holes are intrinsically *more localized* than exact exchange holes, especially in *multicenter* systems. Description of the XC hole in molecules can therefore be improved by combining the localized GGA hole with the exact *multi-center* exchange hole. This was done by Becke [48], who proposed hybrid exchange-correlation of the form

$$E_{\mathrm{XC}}^{hybrid} = E_{\mathrm{XC}}^{\mathrm{GGA}} + a_0(E_X^{exact} - E_X^{\mathrm{GGA}}). \tag{2.53}$$

Hybrids show substantial improvement over pure GGAs in thermochemical tests (see data below).

The popular "B3LYP", "B3PW91", and "B3P86" functionals [48, 49] have the

general form:

$$E_{\rm XC} = E_{\rm XC}^{\rm LSDA} + a_0(E_X^{exact} - E_X^{\rm LSDA}) + a_X \Delta E_X^{\rm B88} + a_C \Delta E_C, \qquad (2.54)$$

where $\Delta E_X^{\rm B88}$ is the gradient correction term of the B88 exchange functional and ΔE_C is the gradient correction term of the selected correlation functional (or in the case of LYP, which does not go to the uniform-electron-gas limit, $\Delta E_C = E_C^{\rm LYP} - E_C^{\rm LSDA}$, as implemented in the Gaussian program [50]). The three semi-empirical coefficients are determined from fits to experimental data, usually atomization energies. B3LYP gives a mean absolute error (MAE) of 4.8 kcal/mol for the 222 atomization energies of the G3/99 benchmark set [40].

Another possible form for 3-parameter fits, employing the particular functionals of interest in the present work, is

$$E_{\rm XC} = a_0 E_X^{exact} + (1 - a_0) E_X^{local} + a_C^{opp} E_C^{\alpha\beta+\beta\alpha} + a_C^{par}(E_C^{\alpha\alpha} + E_C^{\beta\beta}), \qquad (2.55)$$

where E_X^{local} is either the B86, B88, or BR exchange energy and the opposite and parallel-spin correlation energies are given by the B88 correlation functionals of Eqs. (2.48) and (2.49).

The three-parameter hybrids obtained from Eq. (2.55) are among the best DFTs we know for thermochemistry. For the G3/99 atomization-energy set they give MAEs of 2-3 kcal/mol (unpublished calculations), approaching the accuracy of correlated wavefunction methods [51].

Another popular hybrid functional examined in this work is B97 [52]. This functional was proposed by Becke in order to reach the limits of what is possible with

GGAs. The B97 exchange-correlation energy is:

$$E_{\rm XC}^{\rm B97} = c_X E_X^{exact} + E_X^{\rm B97} + E_{C\alpha\beta}^{\rm B97} + \sum_\sigma E_{C\sigma\sigma}^{\rm B97}. \tag{2.56}$$

The individual components are:

$$E_X^{\rm B97} = \sum_\sigma \int e_{X\sigma}^{\rm LSDA}(\rho_\sigma) g_{X\sigma}(\chi_\sigma^2) d\mathbf{r}, \tag{2.57a}$$

$$E_{C\alpha\beta}^{\rm B97} = \int e_{C\alpha\beta}^{\rm LSDA}(\rho_\alpha, \rho_\beta) g_{C\alpha\beta}(\chi_{avg}^2) d\mathbf{r}, \tag{2.57b}$$

$$E_{C\sigma\sigma}^{\rm B97} = \int e_{C\sigma\sigma}^{\rm LSDA}(\rho_\sigma) g_{C\sigma\sigma}(\chi_\sigma^2) d\mathbf{r}, \tag{2.57c}$$

and $\chi_{avg}^2 = \frac{1}{2}(\chi_\alpha^2 + \chi_\beta^2)$. The g's are polynomials of the following form:

$$g = \sum_{i=0}^{2} c_i u^i \tag{2.58}$$

$$u_{X\sigma} = \frac{\gamma_{X\sigma}\chi_\sigma^2}{1 + \gamma_{X\sigma}\chi_\sigma^2} \tag{2.59a}$$

$$u_{C\alpha\beta} = \frac{\gamma_{C\alpha\beta}\chi_{avg}^2}{1 + \gamma_{C\alpha\beta}\chi_{avg}^2} \tag{2.59b}$$

$$u_{C\sigma\sigma} = \frac{\gamma_{C\sigma\sigma}\chi_\sigma^2}{1 + \gamma_{C\sigma\sigma}\chi_\sigma^2} \tag{2.59c}$$

The γ's are fit to exact atomic exchange and correlation energies and the c_i's are fit

to thermochemical data, along with the fraction of exact exchange (c_X). There are several parameterizations of this functional in the literature [52, 53, 54]. The original B97 parameterization gives a MAE of 1.8 kcal/mol for the "G2" atomization energies (a subset of the G3/99 set) [52]. This is an improvement over the 3-parameter hybrids B3B86, B3B88, and B3BR which have MAEs of 2.1-2.4 kcal/mol. However, B97 has a total of 10 empirical fit parameters.

2.7 Comparison of Local and Exact Exchange

GGA exchange-correlation approximations (such as B86, B88, and BR) give reasonably good thermochemistry. This is improved by adding a small fraction (20-25%) of exact HF (Hartree-Fock) exchange as in the previous section. One might wonder, therefore, if using 100% HF exchange paired with one of the GGA correlation functionals would be even better. However, this fails horribly in fact, with "HF plus GGA correlation" giving large MAEs of 65-70 kcal/mol for the G3/99 atomization energies (unpublished calculations).

GGA exchange functionals such as B86, B88, and BR perform much better than exact exchange when combined with GGA correlation functionals because they give a better representation of the full exchange-correlation hole in closed-shell molecules. As illustrated in Fig. 2.2 for H_2, the *exact* exchange and correlation holes in molecules are highly delocalized, while the exchange-correlation hole is localized around the atom nearest the reference electron. The GGA exchange and correlation holes are localized by construction, thus giving the same qualitative behaviour as the full exchange-correlation hole.

If exact *exchange* is used, *nonlocal* approximations to the exact correlation hole must also be used in order to extinguish those parts of the exact exchange hole on atoms far from the reference point and localize the exchange-correlation hole onto a

Figure 2.2: Sketch of the exchange-correlation hole and its components in the H_2 molecule for a reference electron near the right nucleus. See Ref. [55] for more accurate plots of these holes.

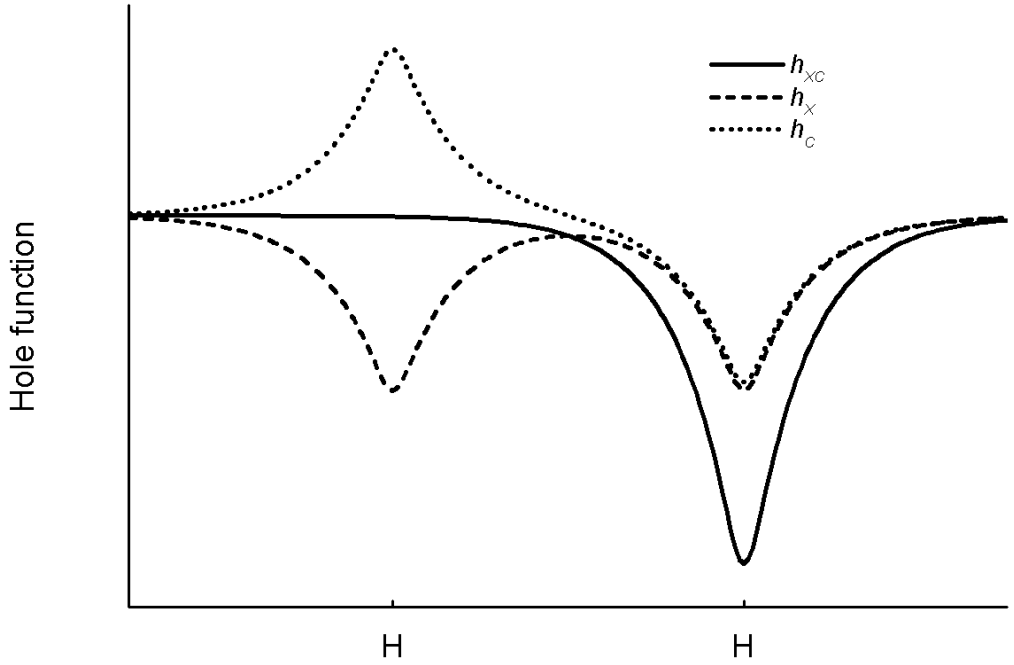

single atomic center. GGA exchange and correlation holes are completely determined by properties of the density at the reference point. Therefore a GGA correlation hole cannot localize the exact exchange hole, explaining why "HF plus GGA correlation" yields poor thermochemistry.

This can be further understood by separating electron correlation into two distinct types: dynamical and nondynamical. Dynamical correlation is *short-range* correlation between electrons within an atom in a molecule, due to mixing of high-energy excited-state configurations. Conversely, nondynamical correlation is *longer* range or *multi-centered* correlation between electrons on different atoms in a molecule. In configuration space, it arises from mixing of low-lying excited-state configurations nearly

degenerate with the ground state. In real space, it arises from Coulomb repulsions pushing electron pairs in multi-center molecular orbitals to different atomic centers. The multi-centered correlation hole of the H_2 molecule, Fig. 2.2, is representative of nondynamical correlation. GGA correlation models account for dynamical correlation, but cannot describe nondynamical correlation. Nondynamical correlation is crudely accounted for, however, by the GGA exchange models that implicitly assume a localized hole.

Though qualitatively correct in closed-shell molecules, local exchange-hole models are qualitatively incorrect in delocalized *odd*-electron molecules. The classic example is H_2^+ at the dissociation limit. Since this is a one-electron system, there is no electron correlation and the exchange-correlation hole is simply the exact exchange hole. The exact exchange hole in stretched H_2^+ is split over both centers, with *half* an electron around each center. However, local DFTs always assume a localized exchange hole with a normalization of -1 electron at each atomic center. This causes local DFTs to give an exchange energy for stretched H_2^+ that is much too large in magnitude [15]. Consequently, local DFTs give a dissociation limit for H_2^+ far below the exact limit, as shown in Fig. 2.3.

While the H_2^+ molecule may seem unimportant, this problem appears in many guises throughout chemical applications. For example, radical reactions are prevalent in chemistry and biology, and have transition states where an unpaired electron may be delocalized over several atomic centers. Local DFTs tend to over-stabilize these transition states leading to underestimation of the barrier heights. In many cases the transition state is predicted to be more stable than the separated reactants or products [56]. This radical delocalization problem has prompted the development of exact-exchange-based functionals that explicitly include both dynamical and nondynamical correlation. Two such models have recently been proposed: B05 [25, 57] and MCY [58]. Both yield accurate thermochemistry and correct the over-stabilization of radical

Figure 2.3: The H_2^+ potential energy curve.

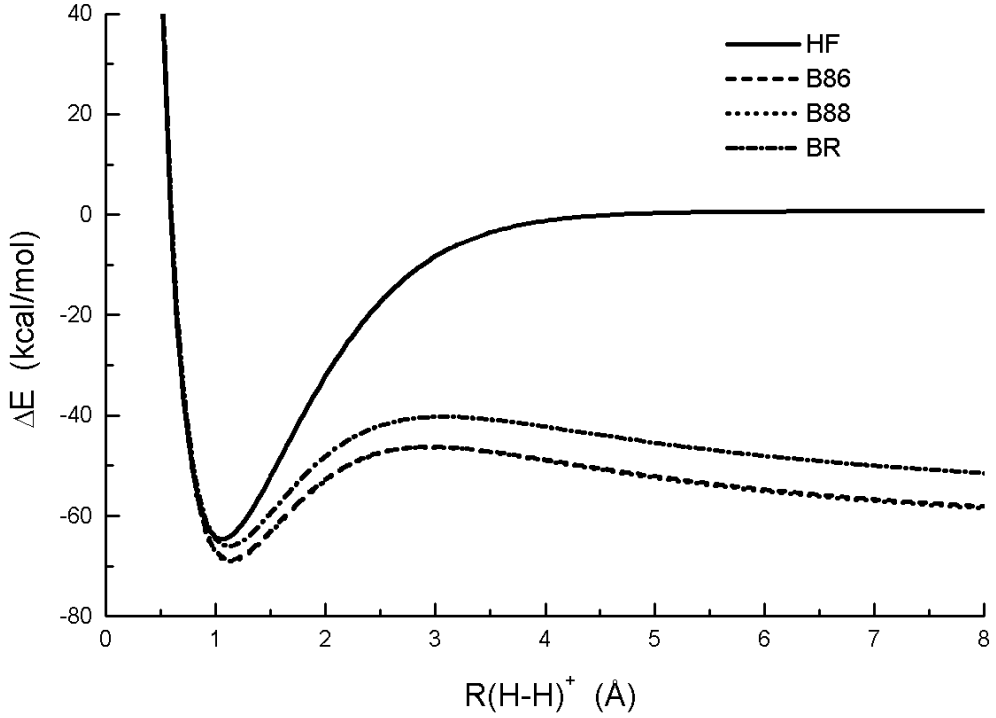

reaction transition states. These methods represent the current state of the art in density functionals. B05 and MCY are complicated functionals whose forms will not be reviewed in this introduction. B05 is discussed in Chapter 9.

2.8 Dispersion in DFT

None of the functionals considered so far incorporates dispersion physics. Thus, it should not be surprising that no conventional DFT can model dispersion-bound complexes with even qualitative accuracy [18]. This demonstrates a fundamental principle of functional development - a DFT model can only yield meaningful results if the correct physics is built into the model at the outset.

To our knowledge only two attempts have been described in the literature to develop a unified DFT model including the physics of dispersion [59, 60]. One of

these is the approach of Sato, Tsuneda, and Hirao [59], which extends the dispersion model of Andersson, Langreth, and Lundqvist (ALL) [61].

The ALL method is based on the dispersion interaction energy between two separated uniform-electron-gas-like regions. For an intermolecular complex, the total dispersion energy has the form

$$E_{disp} = -\frac{6}{(4\pi)^{3/2}} \int_{V_1} d\mathbf{r}_1 \int_{V_2} d\mathbf{r}_2 \frac{\rho^{1/2}(\mathbf{r}_1)\rho^{1/2}(\mathbf{r}_2)}{\rho^{1/2}(\mathbf{r}_1) + \rho^{1/2}(\mathbf{r}_2)} \frac{1}{r_{12}^6}. \tag{2.60}$$

V_1 and V_2 correspond to the volumes of the constituent monomers. Remarkably, while based on electron-gas physics, the ALL model gives atomic C_6's in fairly good agreement with experiment, with a mean absolute percent error (MAPE) of 15.5% for a set of 45 noble-gas and alkali-atom pairs [61].

To compute potential-energy surfaces, the dispersion energy is decomposed into a sum over atomic pair terms for atoms A and B in V_1 and V_2 [59],

$$E_{disp} = \sum_{A \in V_1} \sum_{B \in V_2} E_{AB}, \tag{2.61}$$

with

$$E_{AB} = -\frac{6}{(4\pi)^{3/2}} \int_{A} d\mathbf{r}_1 \int_{B} d\mathbf{r}_2 \frac{\rho^{1/2}(\mathbf{r}_1)\rho^{1/2}(\mathbf{r}_2)}{\rho^{1/2}(\mathbf{r}_1) + \rho^{1/2}(\mathbf{r}_2)} \frac{1}{r_{12}^6} f_{damp}(r_{12}) \tag{2.62}$$

and where the A and B integrations are performed on numerical atom-centered grids. The damping function,

$$f_{damp}(r_{12}) = \exp\left[-\left(\frac{a_{AB}}{r_{12}}\right)^6\right], \tag{2.63}$$

prevents unphysical behaviour at small r_{12}. The parameter a_{AB} is linearly related to

the sum of atomic van der Waals radii, R_m, as follows:

$$a_{AB} = c_1 R_m + c_2. \tag{2.64}$$

The constants $c_1 = 0.4290$ and $c_2 = 1.8949$ au are universal parameters fit to accurate potential-energy curves of noble-gas dimers [59].

This model has been applied to noble-gas pairs and noble-gas - diatomic complexes [59], and later to the benzene dimer [62], but has not been systematically benchmarked. More importantly, since the system must be divided into separated monomers, the ALL dispersion model is not applicable to *intramolecular* dispersion interactions.

The B97-D method of Grimme [60] is more widely applicable than the above model but is also more empirical. There is a substantial history in the literature of adding empirical dispersion corrections to existing quantum chemistry methods [22, 23, 63, 64, 65, 66, 67]. The B97-D method is similar, but stands out because it includes a reparameterization of the underlying DFT functional, in this case B97 [52], in the presence of the dispersion term.

In B97-D, the dispersion energy has the form [60]

$$E_{disp} = -s_6 \sum_{i>j} \frac{C_{6,ij}}{R_{ij}^6} f_{damp}(R_{ij}), \tag{2.65}$$

where the sum is over atom pairs, s_6 is a scale factor with value 1.25, and f_{damp} is a damping function to prevent divergence of the dispersion energy at small interatomic separations:

$$f_{damp}(R_{ij}) = \frac{1}{1 + e^{-d(R_{ij}/R_r - 1)}}. \tag{2.66}$$

R_r is a sum of atomic van der Waals radii (defined as 1.1 times the radius of the

$0.01a_0^{-3}$ electron density contour from atomic ROHF calculations) and $d = 20$ is another empirical parameter. The dispersion coefficients are obtained from a London-type approximation:

$$C_{6,i} = 0.05NI_i\alpha_i, \tag{2.67}$$

where I is the ionization potential and α is the polarizability of the free atom i as obtained from PBE calculations [68]. N has values of 2, 10, 18, 36, and 54 for the first five rows of the periodic table, and the constant 0.05 was determined from fits. The dispersion coefficients for atomic pairs are obtained from the empirical combination rule

$$C_{6,ij} = \sqrt{C_{6,i}C_{6,j}}. \tag{2.68}$$

The 9 parameters of the B97 functional excluding the exact exchange term (see Section 2.6) were refit in the presence of the dispersion term of Eq. (2.65) to give a consistent treatment of thermochemistry and dispersion with a total of 13 parameters. B97-D gives a MAE of 3.8 kcal/mol for the G2 atomization energies and a MAPE of 17.3% for the binding energies of a set of 40 van der Waals complexes [60]. Major criticisms of this model are that the dispersion coefficients are highly empirical, are fixed for all atomic environments, and do not resemble accurate values for free-atom pairs. For example, B97-D gives C_6 dispersion coefficients with a MAPE of 42.5% for the set of all pair-wise combinations of the atoms H, He, Ne, Ar, Kr, and Xe.

Clearly there is a need for a non-empirical dispersion model that has accurate long-range behaviour, can be applied both to intermolecular and intramolecular dispersion interactions, and can be combined with existing density functionals to give highly accurate thermochemistry and kinetics. The following chapters detail the development

of such a model.

The basic idea underlying our dispersion model is that we can treat the instantaneous dipoles responsible for the dispersion interaction as the position-dependent dipole of the exchange hole. An electron and its exchange hole have a non-zero dipole moment in atomic and molecular systems, except at highly symmetric reference points. The interactions between the exchange-hole dipole moments in neighboring atoms or molecules capture the long-range electron correlation responsible for dispersion. While we should properly consider the dipole moment of an electron and its full exchange-correlation hole, the exchange hole is much easier to model and we expect that correlation effects on the dipole moment of the hole will be small. This gives a conceptually simple model of dispersion correlation in terms of easily computed quantities within the DFT framework.

Chapter 3

Exchange-Hole Dipole Moment and the Dispersion Interaction

Original reference: A. D. Becke and E. R. Johnson, J. Chem. Phys. **122**, 154104 (2005).

Abstract

A simple model is presented in which the instantaneous dipole moment of the exchange hole is used to generate a dispersion interaction between non-overlapping systems. The model is easy to implement, requiring no electron correlation (in the usual sense) or time dependence, and has been tested on various atomic and molecular pairs. The resulting C_6 dispersion coefficients are remarkably accurate.

3.1 Introduction

The classical explanation of the dispersion or van der Waals interaction between chemically inert systems is familiar even to introductory chemistry students. Given two inert or widely separated systems, an *instantaneous* dipole moment on one system

induces a dipole moment on the other. The attraction between these moments results in an interaction which, in the limit of large separation R, has the behaviour

$$E_{disp} = -\frac{C_6}{R^6}, \tag{3.1}$$

where C_6 is a constant whose value depends on the systems involved. This picture begs the obvious question. How do "instantaneous" dipole moments arise in systems which may otherwise have a zero permanent dipole moment? How, for example, do instantaneous dipole moments originate in a noble gas atom?

The usual quantum mechanical approach is complicated (we recommend Ref. [12] for a nice treatment). Electron correlation invokes the mixing of *excited* states with the ground state, creating virtual or "transition" dipole moments that interact with each other. Second-order perturbation theory and additional approximations [12] give the famous London formula (in atomic units) for the dispersion energy between two systems A and B,

$$E_{disp} = -\frac{3}{2}\left(\frac{I_A I_B}{I_A + I_B}\right)\frac{\alpha_A \alpha_B}{R^6}, \tag{3.2}$$

which conveniently depends on properties, the ionization energy I and polarizability α, that are experimentally accessible. The London formula is instructive for understanding trends but is prone to large errors.

Correlated *ab initio* calculations of high quality can produce accurate dispersion energy curves [13] but are very demanding and provide little physical insight. Also, a rigorous expression for C_6 involving frequency dependent polarizability $\alpha(i\omega)$ is known [69],

$$C_6 = \frac{3}{\pi}\int_0^\infty \alpha_A(i\omega)\alpha_B(i\omega)d\omega, \tag{3.3}$$

which can be used to compute accurate C_6 values from time-dependent electronic structure calculations [70, 71]. These are also very demanding, however, and must be performed with care.

Methods able to produce C_6 coefficients of *reasonable* quality, without the demands of the highly accurate approaches, are widely useful. Here we present such a method. It is based on a novel answer to the question posed at the outset. How do "instantaneous" dipole moments arise in a quantum system? We propose that *spherical asymmetries* in the *exchange hole* are the source.

3.2 The Present Model

Consider an electron of σ spin in an atomic or molecular system. As it moves through the system it is accompanied by an *exchange* or *Fermi hole* whose shape depends on the electron's instantaneous position $\mathbf{r}_1$. The hole is given by the expression

$$h_{X\sigma}(\mathbf{r}_1, \mathbf{r}_2) = -\frac{1}{\rho_\sigma(\mathbf{r}_1)} \sum_{ij} \psi_{i\sigma}(\mathbf{r}_1)\psi_{j\sigma}(\mathbf{r}_1)\psi_{i\sigma}(\mathbf{r}_2)\psi_{j\sigma}(\mathbf{r}_2), \tag{3.4}$$

where $\mathbf{r}_2$ defines the shape of the hole and $\mathbf{r}_1$ is called the "reference" point. Summation is over all orbitals of σ spin (Hartree-Fock or Kohn-Sham, and assumed in this paper to be real) and ρ_σ is the total σ-spin electron density. The σ-spin exchange energy, $E_{X\sigma}$, is related to the exchange hole by

$$E_{X\sigma} = \frac{1}{2} \int \int \rho_\sigma(\mathbf{r}_1) \frac{h_{X\sigma}(\mathbf{r}_1, \mathbf{r}_2)}{r_{12}} d^3\mathbf{r}_2 d^3\mathbf{r}_1. \tag{3.5}$$

This simple deconstruction of the exchange energy of a Slater determinant has great conceptual power [72] which will be exploited presently.

The exchange-hole definition enables us to *visualize* the effects of self-interaction correction and exchange. When an electron is at $\mathbf{r}_1$, the hole measures the depletion

of probability (with respect to the total electron density ρ) of finding another same-spin electron at $\mathbf{r}_2$. The probability of finding another same-spin electron at $\mathbf{r}_2 = \mathbf{r}_1$ is completely extinguished,

$$h_{X\sigma}(\mathbf{r}_1, \mathbf{r}_1) = -\rho_\sigma(\mathbf{r}_1), \tag{3.6}$$

as required by the Pauli exclusion principle. The hole is always negative, as can be seen by rewriting Eq. (3.4) as

$$h_{X\sigma}(\mathbf{r}_1, \mathbf{r}_2) = -\frac{1}{\rho_\sigma(\mathbf{r}_1)} \left[\sum_i \psi_{i\sigma}(\mathbf{r}_1)\psi_{i\sigma}(\mathbf{r}_2) \right]^2 \tag{3.7}$$

and the hole always contains exactly (minus) one electron:

$$\int h_{X\sigma}(\mathbf{r}_1, \mathbf{r}_2) d^3\mathbf{r}_2 = -1. \tag{3.8}$$

This is easy to prove from Eq. (3.4) and the orthonormality of the orbitals $\psi_{i\sigma}$. Eq. (3.8) guarantees that the electron *plus its hole* always has *zero charge* overall.

The hole is not, in general, spherically symmetric around $\mathbf{r}_1$. Only in a uniform electron gas does it have spherical symmetry. Even in systems with spherically symmetric densities, the hole is aspherical unless $\mathbf{r}_1$ is at the center of the system. Thus the electron plus its Fermi hole, though of zero charge overall, generally has a *non-zero dipole moment*. Since the exchange energy, Eq. (3.5), senses only the spherical average of the hole around each $\mathbf{r}_1$, a non-zero dipole moment has no effect on the energy of the system containing the electron. Might the asphericity of the hole be the source, however, of the "instantaneous" dipole moment responsible for the dispersion interaction with *other* systems?

Consider a second system (B) at position $\mathbf{R}$ relative to the first (A) and assume that the distance R is large compared to the sizes of A and B. The instantaneous

dipole moment $\mathbf{d}_{X\sigma}(\mathbf{r}_1)$ of the exchange hole plus its electron at point $\mathbf{r}_1$ in system A generates an electric field

$$\mathbf{E} = \frac{3(\mathbf{d}_{X\sigma} \cdot \mathbf{R})\mathbf{R}}{R^5} - \frac{\mathbf{d}_{X\sigma}}{R^3} \tag{3.9}$$

at position $\mathbf{R}$. If system B has polarizability α_B, then a dipole moment of value

$$\mathbf{d}_{ind} = \alpha_B \mathbf{E} \tag{3.10}$$

is induced in B. The electrostatic interaction between these dipoles has energy

$$V_{dip-dip} = \frac{\mathbf{d}_{X\sigma} \cdot \mathbf{d}_{ind}}{R^3} - \frac{3(\mathbf{d}_{X\sigma} \cdot \mathbf{R})(\mathbf{d}_{ind} \cdot \mathbf{R})}{R^5}, \tag{3.11}$$

which, after substituting Eqs. (3.10) and (3.9), becomes

$$V_{dip-dip} = -\alpha_B \left[\frac{d_{X\sigma}^2}{R^6} + \frac{3(\mathbf{d}_{X\sigma} \cdot \mathbf{R})^2}{R^8} \right]. \tag{3.12}$$

The *orientation averaged* isotropic interaction (i.e. averaged over all orientations of $\mathbf{d}_{X\sigma}$) is obtained by integrating over angles as follows:

$$V_{dip-dip}^{avg} = -\frac{\alpha_B}{4\pi} \int_0^{2\pi} \int_0^{\pi} \left(\frac{d_{X\sigma}^2}{R^6} + \frac{3d_{X\sigma}^2}{R^6} \cos^2\theta \right) \sin\theta d\theta d\phi = -\frac{2d_{X\sigma}^2 \alpha_B}{R^6}, \tag{3.13}$$

where θ and ϕ are polar angles with respect to the direction $\mathbf{R}$. The resulting $V_{dip-dip}^{avg}$ thus depends on the magnitude squared, $d_{X\sigma}^2(\mathbf{r}_1)$, of the exchange-hole dipole moment at each *body centered* reference point $\mathbf{r}_1$ in system A.

Now integrate over $\mathbf{r}_1$ in system A and over α and β spins as well. Denoting this

integral by $< d_X^2 >$, we have

$$< d_X^2 >_A = \int \rho_\alpha(\mathbf{r}_1) d_{X\alpha}^2(\mathbf{r}_1) d^3\mathbf{r}_1 + \int \rho_\beta(\mathbf{r}_1) d_{X\beta}^2(\mathbf{r}_1) d^3\mathbf{r}_1, \tag{3.14}$$

and we obtain the following formula for the total dipole-dipole interaction energy:

$$U_{dip-dip}^{AB} = -2 < d_X^2 >_A \alpha_B / R^6. \tag{3.15}$$

The same derivation with systems A and B interchanged gives

$$U_{dip-dip}^{BA} = -2 < d_X^2 >_B \alpha_A / R^6, \tag{3.16}$$

which is not, unfortunately, the same as Eq. (3.15). For unlike systems our model lacks A-B symmetry. An appropriate averaging of Eqs. (3.15) and (3.16) will be suggested below. For like systems, however, there is no ambiguity and the dipole-dipole interaction energy is

$$U_{dip-dip} = -2 < d_X^2 > \alpha / R^6. \tag{3.17}$$

Initial tests of Eq. (3.17) on various atomic dimers (computation of $< d_X^2 >$ is described in the next section) gave interesting results. Despite the simplicity of the underlying model, Eq. (3.17) reproduces known C_6 values with remarkable accuracy if divided by a factor of four! An incorrect prefactor is not surprising. Our model takes dipole-dipole potential energy into account, but not kinetic energy [73] or charge rearrangement [74] effects. These, especially the latter, are very difficult to model. That Eq. (3.17) *does* work well with a modified prefactor is, in our opinion, fascinating.

We therefore take a heuristic approach (for now) and propose the formula

$$C_6 = \frac{1}{2} < d_X^2 > \alpha \tag{3.18}$$

for like-system interactions.

For unlike systems a suitable average of Eqs. (3.15) and (3.16) needs to be taken with, in light of the above, prefactors divided by four. Straightforward algebraic averaging is unsuccessful. Geometric averaging also fails. Recognizing that successful combination formulas in the literature (eg. London formula or Slater-Kirkwood formula [75]) feature a sum of some property of A and B in a *divisor*, we propose averaging *inverses* as follows:

$$\frac{2}{C_6} = \frac{1}{C_6^{AB}} + \frac{1}{C_6^{BA}}, \tag{3.19}$$

which, after inserting C_6 coefficients divided by four from Eqs. (3.15) and (3.16), gives

$$C_6 = \frac{< d_X^2 >_A < d_X^2 >_B \alpha_A \alpha_B}{< d_X^2 >_A \alpha_B + < d_X^2 >_B \alpha_A}. \tag{3.20}$$

If this heuristic approach is unsatisfying, Eq. (3.20) can be derived by strong theoretical arguments as well. There are connections between the formulas of this section and the second-order perturbation theory of the dispersion interaction. We draw these connections in the Appendix rather than digressing now. In the next section, Eq. (3.20) is applied without further ado to a wide variety of atomic and molecular, like and unlike, interactions.

3.3 Computations and Applications

The calculation of C_6 dispersion coefficients in the present model requires only $< d_X^2 >$ and α for individual systems. We take polarizability data from tables instead of computing α ourselves. Accurate values are readily available [76]. This leaves as our only task the computation of $< d_X^2 >$.

$< d_X^2 >$ is a sum of two terms, one for each spin, as in Eq. (3.14):

$$< d_X^2 >=< d_{X\alpha}^2 > + < d_{X\beta}^2 >, \tag{3.21}$$

where

$$< d_{X\sigma}^2 >= \int \rho_\sigma(\mathbf{r}_1) d_{X\sigma}^2(\mathbf{r}_1) d^3\mathbf{r}_1. \tag{3.22}$$

Recall that $d_{X\sigma}^2(\mathbf{r}_1)$ is the magnitude squared of the dipole moment of the electron plus its exchange hole at reference point $\mathbf{r}_1$. Given a set of occupied orbitals $\psi_{i\sigma}$, the dipole moment is easily computed by integrating over $\mathbf{r}_2$ in Eq. (3.4):

$$\mathbf{d}_{X\sigma}(\mathbf{r}_1) = \left[\frac{1}{\rho_\sigma(\mathbf{r}_1)} \sum_{ij} \mathbf{r}_{ij\sigma} \psi_{i\sigma}(\mathbf{r}_1) \psi_{j\sigma}(\mathbf{r}_1) \right] - (\mathbf{r}_1), \tag{3.23}$$

$$\mathbf{r}_{ij\sigma} = \int \mathbf{r} \psi_{i\sigma}(\mathbf{r}) \psi_{j\sigma}(\mathbf{r}) d^3\mathbf{r}. \tag{3.24}$$

Note that the dipole moment of a neutral object is origin independent and we therefore conveniently use the molecular origin in Eq. (3.23). All integrations, the moment integrations of Eq. (3.24) and the 1-integration of Eq. (3.22), are performed numerically [77]. The cost of computing $< d_X^2 >$ is negligible compared to the cost of computing the orbitals themselves.

Orbitals are obtained in this work from the grid-based NUMOL program of Becke and Dickson [78]. We use (spin unrestricted) Hartree-Fock orbitals in these first tests [79]. Hartree-Fock orbitals are preferable to, eg., LDA or GGA Kohn-Sham orbitals because the Fermi-hole dipole moment is sensitive to orbital behaviour at long range. We therefore avoid the well-known long-range deficiencies of the LDA and GGA Kohn-Sham potentials. The dependence of $< d_X^2 >$ on orbitals and electron correlation will be explored in greater detail in future work.

In Tables 3.1 and 3.2, we present C_6 dispersion coefficients obtained from Eq. (3.18) for like systems and Eq. (3.20) for unlike systems for a variety of atomic and molecular pairs. The mean absolute percent error (MAPE) of our atom-atom C_6's in Table 3.1 relative to highly accurate literature values [80] is 14.0%. The potassium atom is a significant outlier. Omitting all cases involving potassium leads to a reduced MAPE of 9.8%. Our C_6s are in slightly better agreement with literature values than the approximate density-functional method of Andersson, Langreth, and Lundqvist [61], which yields a MAPE of 15.5% for the same set of 45 noble gas an alkali atom pairs.

Isotropic C_6 coefficients for molecule-molecule pairs are reported in Table 3.2. We use B3LYP/6-31G(2df,p) [46, 48, 81] geometries obtained from the Gaussian 98 program package [49]. Our calculated values tend to be smaller than accurate literature values [22, 71], but a reasonably good MAPE of 12.5% is achieved. C_6's from Eq. (3.3) combined with time-dependent Hartree-Fock calculations of frequency dependent polarizabilities have been reported by Spackman [71] for eight of the sixteen systems in this set. His results also underestimate accurate values, and their MAPE of 12.6% is similar to the 12.5% obtained from our much simpler time-independent model.

The present method performs remarkably well given its simplicity. Neither time dependence, nor excited states, are necessary. The "instantaneous" dipole moment

of the exchange hole, and the polarizability of the partner system, is all we require.

3.4 Conclusions

This work proposes an elegant connection between exchange-hole asphericity and the dispersion interaction. If the position dependent dipole moment of the exchange hole (plus its electron) in a system A is considered to induce dipole moments in another system B, then a C_6 dispersion coefficient of very good accuracy can be obtained through Eq. (3.20). The model works for molecular as well as atomic systems.

This approach may have practical benefits in addition to its fundamental theoretical appeal. We hope to incorporate it into molecular structure and molecular mechanics codes in future work in order to efficaciously handle long range interactions.

3.5 Appendix

We refer the reader to Ref. [12] for an excellent and comprehensible account of the 2nd-order perturbation theory of the dispersion interaction. We will here adopt notation and formulas from Chapter 12 of this book.

Eq. (12.32) of Ref. [12] is obtained when all excitation energies in system A are approximated by a constant "average" value ΔE_A and similarly for system B:

$$E_{disp} = -\frac{2}{3}\left(\frac{1}{\Delta E_A + \Delta E_B}\right)\frac{<\mu_A^2><\mu_B^2>}{R^6}. \tag{3.25}$$

The quantity $<\mu^2>$ is the expectation value of the squared dipole moment operator

$$\mu^2 = \left(\sum_i q_i \mathbf{r}_i\right)^2 = \sum_k q_k^2 \mathbf{r}_k^2 + \sum_{i\neq j} q_i q_j \mathbf{r}_i \cdot \mathbf{r}_j, \tag{3.26}$$

where the sums are over all particles including nuclei. It is assumed that A and

B have zero total charge and zero permanent dipole moment. From the analogous 2nd-order perturbation theory of polarizability α, and again making an "average" excitation-energy approximation, one obtains [12]

$$\alpha = \frac{2 < \mu^2 >}{3\Delta E}. \tag{3.27}$$

This equation can be used to eliminate $< \mu^2 >$ from Eq. (3.25) thus deriving the London formula, Eq. (3.2), after further approximating ΔE by the ionization energy. Alternatively, we can eliminate ΔE from Eq. (3.25) and derive another formula,

$$E_{disp} = -\left[\frac{< \mu_A^2 >< \mu_B^2 >}{< \mu_A^2 > \alpha_B + < \mu_B^2 > \alpha_B}\right] \frac{\alpha_A \alpha_B}{R^6}, \tag{3.28}$$

the focus of which is $< \mu^2 >$. The μ^2 operator, Eq. (3.26), consists of nuclear and electron one-body operators and two-body operators arising from the cross terms. In an *atom* the nuclear parts can be ignored and $< \mu^2 >$ in the Hartree-Fock approximation is given by

$$< \mu^2 >= \int r^2 \rho(\mathbf{r}) d^3\mathbf{r} - \sum_{ij} \left(\mathbf{r}_{ij\alpha}^2 + \mathbf{r}_{ij\beta}^2\right), \tag{3.29}$$

where r is distance from the nucleus, $\rho(\mathbf{r})$ is the total electron density, and $\mathbf{r}_{ij\sigma}$ is the moment integral of Eq. (3.24).

$< \mu^2 >$ is not the same quantity as $< d_X^2 >$. For atoms containing only s electrons, however, $< \mu^2 >$ and $< d_X^2 >$ are identical and are both given by

$$< d_X^2 >=< \mu^2 >= \int r^2 \rho(\mathbf{r}) d^3\mathbf{r}. \tag{3.30}$$

The fact that $< d_X^2 >$ equals $< \mu^2 >$ in atoms such as H, He, Li, and Be suggests an obvious way to incorporate $< d_X^2 >$ into a dispersion model. Simply replace $< \mu^2 >$

everywhere in Eq. (3.28) by $< d_X^2 >$. This gives Eq. (3.20) of the text and confirms our heuristically obtained result.

How well does Eq. (3.28) itself perform? C_6 values from Eq. (3.28) are presented in Table 3.3 for the same atom-atom pairs as in Table 3.1. We see that C_6 values from Eq. (3.20) are superior to those from Eq. (3.28). The MAPE arising from Eq. (3.28) is 31.7%, more than twice the MAPE of 14.0% arising from Eq. (3.20). Our exchange-hole-based model therefore offers, in addition to conceptual beauty, a significant advance over the putative model of Eq. (3.28).

Individual values of $< d_X^2 >$, $< \mu^2 >$, and α for the atoms comprising our atomic C_6 test set are presented in Table 3.4. These may be of interest to some readers.

Table 3.1: Calculated C_6 coefficients for atomic pairs, in atomic units.

Atoms	Calculated C_6	Literature C_6^a
He-He	1.64	1.47
He-Ne	3.09	3.13
He-Ar	9.81	9.82
He-Kr	14.08	13.6
He-Xe	20.91	18.3
Ne-Ne	5.83	6.87
Ne-Ar	18.61	20.7
Ne-Kr	26.72	28.7
Ne-Xe	39.73	37.8
Ar-Ar	62.71	67.2
Ar-Kr	90.93	94.3
Ar-Xe	137.4	129
Kr-Kr	132.1	133
Kr-Xe	200.1	184
Xe-Xe	304.7	261
H-H	6.76	6.49
H-Li	71.64	66.4
H-Na	85.76	71.8
H-K	143.2	109
Li-Li	1528	1390
Li-Na	1683	1450
Li-K	2910	2320
Na-Na	1879	1510
Na-K	3230	2410
K-K	5567	3890
He-H	2.99	2.82
He-Li	24.17	22.6
He-Na	29.53	24.4
He-K	48.88	38.0
Ne-H	5.69	5.71
Ne-Li	46.51	44.0
Ne-Na	56.79	47.7
Ne-K	94.02	74.9
Ar-H	20.13	20.0
Ar-Li	185.7	175
Ar-Na	224.8	189
Ar-K	373.6	292
Atoms	Calculated C_6	Literature C_6^a

continued on next page

Kr-H	29.44	28.5
Kr-Li	278.7	259
Kr-Na	336.7	281
Kr-K	560.0	433
Xe-H	45.14	40.9
Xe-Li	446.5	404
Xe-Na	537.5	438
Xe-K	895.3	669
MAPE[b]	14.0 (9.8[c])	–

[a]Literature values from Ref. [80]. [b]Mean absolute percent error relative to the literature values. [c]Excluding atomic pairs involving potassium.

Table 3.2: Isotropic C_6 coefficients for molecular pairs, in atomic units.

Molecules	Calculated C_6	Literature C_6^a
H_2-H_2	14.01	12.11
N_2-N_2	66.62	73.39
CH_4-CH_4	115.3	129.6
CH_4-CO_2	128.7	142.6
CO_2-CO_2	143.7	158.7
methane-acetylene	147.5	162.5
acetylene-CO_2	164.7	178.2
acetylene-acetylene	188.7	204.1
acetylene-ethylene	225.3	247.7
acetylene-ethane	241.9	278.9
ethylene-ethylene	270.1	300.5
acetylene-propylene	320.2	367.6
ethane-ethane	310.6	381.8
acetylene-propane	332.8	395.6
propylene-propylene	548.6	662.8
propane-propane	589.4	768.1
MAPE[b]	12.5	–

[a]Literature values from Refs. [22] and [71]. [b]Mean absolute percent error relative to the literature values.

Table 3.3: Calculated C_6 coefficients for atomic pairs, in atomic units.

Atoms	Eq. (3.20) C_6	Eq. (3.28) C_6	Literature C_6^a
He-He	1.64	1.64	1.47
He-Ne	3.09	3.61	3.13
He-Ar	9.81	12.19	9.82
He-Kr	14.08	17.95	13.6
He-Xe	20.91	27.87	18.3
Ne-Ne	5.83	8.12	6.87
Ne-Ar	18.61	26.58	20.7
Ne-Kr	26.72	39.02	28.7
Ne-Xe	39.73	60.21	37.8
Ar-Ar	62.71	91.02	67.2
Ar-Kr	90.93	134.3	94.3
Ar-Xe	137.4	209.1	129
Kr-Kr	132.1	198.4	133
Kr-Xe	200.1	309.2	184
Xe-Xe	304.7	482.7	261
H-H	6.76	6.76	6.49
H-Li	71.64	71.64	66.4
H-Na	85.76	89.97	71.8
H-K	143.2	157.2	109
Li-Li	1528	1528	1390
Li-Na	1683	1727	1450
Li-K	2910	3062	2320
Na-Na	1879	1992	1510
Na-K	3230	3522	2410
K-K	5567	6230	3890
He-H	2.99	2.99	2.82
He-Li	24.17	24.17	22.6
He-Na	29.53	31.16	24.4
He-K	48.88	54.25	38.0
Ne-H	5.69	6.20	5.71
Ne-Li	46.51	47.38	44.0
Ne-Na	56.79	61.38	47.7
Ne-K	94.02	106.8	74.9
Ar-H	20.13	22.94	20.0
Ar-Li	185.7	191.7	175
Ar-Na	224.8	246.4	189
Atoms	Eq. (3.20) C_6	Eq. (3.28) C_6	Literature C_6^a

continued on next page

Ar-K	373.6	429.1	292
Kr-H	29.44	34.19	28.5
Kr-Li	278.7	289.1	259
Kr-Na	336.7	371.3	281
Kr-K	560.0	646.7	433
Xe-H	45.14	54.11	40.9
Xe-Li	446.5	467.5	404
Xe-Na	537.5	599.3	438
Xe-K	895.3	1044	669
MAPE[b]	14.0	31.7	–

[a]Literature values from Ref. [80]. [b]Mean absolute percent error relative to the literature values.

Table 3.4: Atomic values of $< d_X^2 >$, $< \mu^2 >$, and α, in atomic units.

Atom	$< d_X^2 >$	$< \mu^2 >$	α
He	2.37	2.37	1.38
Ne	4.36	6.08	2.67
Ar	11.31	16.42	11.09
Kr	15.74	23.64	16.78
Xe	22.30	35.34	27.32
H	3.00	3.00	4.50
Li	18.61	18.61	164
Na	23.10	24.49	163
K	37.98	42.50	293

Chapter 4

A Post-Hartree-Fock Model of Intermolecular Interactions

Original reference: E. R. Johnson and A. D. Becke, J. Chem. Phys. **123**, 024101 (2005).

Abstract

Intermolecular interactions are of great importance in chemistry but are difficult to model accurately with computational methods. In particular, Hartree-Fock and standard density functional approximations do not include the physics necessary to properly describe dispersion. These methods are sometimes corrected to account for dispersion by adding a pairwise C_6/R^6 term, with C_6 dispersion coefficients dependent on the atoms involved. We present a post-Hartree-Fock model in which C_6 coefficients are generated by the instantaneous dipole moment of the exchange hole. This model relies on occupied orbitals only, and involves only one, universal, empirical parameter to limit the dispersion energy at small interatomic separations. The model is extensively tested on isotropic C_6 coefficients of 178 intermolecular pairs. It is also applied to the calculation of the geometries and binding energies of 20 inter-

molecular complexes involving dispersion, dipole-induced dipole, dipole-dipole, and hydrogen-bonding interactions, with remarkably good results.

4.1 Introduction

The dispersion or van der Waals interaction between molecules is a weak attraction attributed to an instantaneous dipole moment in one molecule inducing a dipole moment in another molecule. The resulting dipole-induced-dipole interaction leads, in the limit of large intermolecular separation (R), to a dispersion energy (E_{disp}) of the form [12]

$$E_{disp} = -\frac{C_6}{R^6}, \tag{4.1}$$

where the dispersion coefficient C_6 is a constant depending on the molecules involved.

While dispersion interactions are very important in chemistry, efficient modeling of dispersion remains a long-standing computational problem. Correlated *ab initio* methods with large basis sets provide an accurate treatment of dispersion (eg. see Ref. [13] and references therein) but are computationally expensive, rendering these methods impractical for all but the smallest systems. There is considerable interest, therefore, in modifying the more economical Hartree-Fock (HF) or density functional theory (DFT) methods to approximately account for dispersion.

Such modifications often involve addition of a dispersion term of the following form to the HF or DFT electronic energy [22, 23, 63, 64, 65, 66]:

$$E_{disp} = -\sum_{i>j} \frac{C_{6,ij}}{R_{ij}^6}. \tag{4.2}$$

The summation is over all atom pairs and the C_6 coefficients depend on the atoms i and j. This approach is commonly used to model dispersion in molecular mechanics

(MM) methods [82], and it is natural to use a similar correction in molecular orbital methods, such as HF, which do not contain the essential physics of dispersion.

But how does one determine the values of the interatomic C_6 coefficients? Intermolecular C_6's can be obtained from experimental dipole oscillator strengths [83] and can be rigorously calculated from frequency dependent polarizabilities [69, 71] or from a recent approximate model based on the exchange-hole dipole moment [84]. However, it is unclear how intermolecular C_6's can be decomposed into interatomic components as in Eq. (4.2). The simplest conceivable assumption, that $C_{6,ij}$ is equal to its value for free atoms, fails badly. Interatomic C_6 coefficients are highly dependent on the molecular environment of the atoms involved.

Interatomic C_6's are commonly obtained from empirical fits. An example is the Slater-Kirkwood approach [64, 66] in which C_6's are obtained from atomic polarizabilities fit to molecular polarizability data [85]. The atomic polarizabilities are dependent on the molecular environment and involve explicit atom types such as sp^3, sp^2, or sp carbons, as in MM force fields. Wu and Yang [22] have suggested that interatomic C_6's be directly fit to a reference set of intermolecular C_6 data. Wu and Yang's fitted C_6's were averaged over atom types to obtain a more general parameter set and used in more extensive calculations by Grimme [23]. Interatomic C_6 values have also been obtained by fitting to intermolecular potential energy surfaces from *ab initio* calculations [86].

The empirical fitting approach has obvious limitations. Atom typing leads to difficulties in calculating potential energy surfaces in reactions where atom types may change. Also, the existing C_6 parameterizations only have C, H, N, O, and halogen atoms in their training sets. Applications involving other elements will require additional fits. Furthermore, schemes involving many-parameter fits may yield large errors for species outside the training set.

A general model for interatomic dispersion terms not involving empirical fits or

atom typing would be greatly advantageous. This paper proposes such a model and tests it on calculation of intermolecular C_6 values, binding energies, and minimum energy separations.

4.2 The Present Model

Our approach is based on a model of the dispersion interaction recently proposed by us in Ref. [84]. The model requires nothing more than time-independent occupied Hartree-Fock, or DFT, orbitals as input and the polarizabilities of the interacting systems. We use a previously unexploited property of the exchange hole, its dipole moment, to generate dispersion interactions.

Consider the exchange hole of an atom or molecule, $h_{X\sigma}(\mathbf{r}_1, \mathbf{r}_2)$. When a σ-spin electron is at position $\mathbf{r}_1$ the hole measures the depletion of probability, with respect to the total electron density, of finding another σ-spin electron at position $\mathbf{r}_2$. The electron plus its hole has zero net charge. However, the hole is generally not spherically symmetric around $\mathbf{r}_1$ [87] and the electron plus its exchange hole therefore has a non-zero dipole moment. We proposed in Ref. [84] that the exchange-hole instantaneous dipole moment is the source of dispersion interactions between nonoverlapping systems. This led to a simple but remarkably accurate formula for calculating C_6 dispersion coefficients.

For the isotropic C_6 coefficient between two systems (atoms or molecules) A and B, we obtained [84]

$$C_6 = \frac{< d_X^2 >_A < d_X^2 >_B \alpha_A \alpha_B}{< d_X^2 >_A \alpha_B + < d_X^2 >_B \alpha_A}, \tag{4.3}$$

where $< d_X^2 >$ is the expectation value of the squared exchange-hole dipole moment and α is the isotropic molecular polarizability. $< d_X^2 >$ is easily computed by numer-

ical integration, over HF or DFT orbitals, as follows:

$$< d_X^2 >=< d_{X\alpha}^2 > + < d_{X\beta}^2 >, \tag{4.4a}$$

$$< d_{X\sigma}^2 >= \int \rho_\sigma(\mathbf{r}_1) d_{X\sigma}^2(\mathbf{r}_1) d^3\mathbf{r}_1, \tag{4.4b}$$

where ρ_σ is the σ-spin density and the dipole moment of the σ-spin exchange hole at reference point $\mathbf{r}_1$ is given by

$$d_{X\sigma}(\mathbf{r}_1) = \left[\frac{1}{\rho_\sigma(\mathbf{r}_1)} \sum_{ij} \psi_{i\sigma}(\mathbf{r}_1)\psi_{j\sigma}(\mathbf{r}_1) \int \mathbf{r}\psi_{i\sigma}(\mathbf{r})\psi_{j\sigma}(\mathbf{r}) d^3\mathbf{r} \right] - \mathbf{r}_1. \tag{4.5}$$

The model was tested by calculating C_6 coefficients for 45 atomic and 16 molecular pairs and performed quite well, with mean absolute percent errors (MAPE) relative to accurate literature values of 14.0% and 12.5% respectively [84].

We introduce in the present work a very nice further feature of our model. Equation (4.3) for the C_6 of an intermolecular interaction can be algebraically decomposed into a sum of interatomic C_6's as required by Eq. (4.2). We derive this decomposition in the following paragraphs.

We begin by partitioning the molecular $< d_X^2 >$ into atomic components using the Hirshfeld scheme [88]. A promolecule density is defined by

$$\rho^{pro}(\mathbf{r}_1) = \sum_i \rho_i^{at}(\mathbf{r}_1), \tag{4.6}$$

where the functions $\rho_i^{at}(\mathbf{r}_1)$ are free spherically-averaged ground-state densities of the constituent atoms. Atomic weight functions $w_i(\mathbf{r}_1)$ are then defined by

$$w_i(\mathbf{r}_1) = \frac{\rho_i^{at}(\mathbf{r}_1)}{\rho^{pro}(\mathbf{r}_1)}, \tag{4.7a}$$

such that

$$\sum_i w_i(\mathbf{r}_1) = 1. \tag{4.7b}$$

For molecule A with atoms A_i, we thus obtain the dipole-density decomposition

$$< d_X^2 >_A = \sum_i < d_X^2 >_{A_i}, \tag{4.8}$$

where $< d_X^2 >_{A_i}$ is

$$< d_X^2 >_{A_i} = \int w_{A_i}(\mathbf{r}_1) \left[\rho_\alpha(\mathbf{r}_1) d_{X\alpha}^2(\mathbf{r}_1) + \rho_\beta(\mathbf{r}_1) d_{X\beta}^2(\mathbf{r}_1)\right] d^3\mathbf{r}_1. \tag{4.9}$$

This has the same form as Eq. (4.4) with Hirshfeld weights inserted in the integrand.

The molecular polarizability may also be partitioned into atomic terms,

$$\alpha_A = \sum_i \alpha_{A_i}, \tag{4.10}$$

though not as straightforwardly as $< d_X^2 >$. It is well known that molecular polarizabilities are not given by sums of free atomic polarizabilities. We propose that the polarizability of atom A_i be defined by

$$\alpha_{A_i} = \frac{< d_X^2 >_{A_i}}{< d_X^2 >_A} \alpha_A, \tag{4.11}$$

which is a reasonable definition (viz. the atomic polarizability is proportional to the fraction of the exchange-hole dipole moment owned by the atom).

With the above partitionings of $< d_X^2 >$ and α, an exact decomposition of our model C_6 into interatomic terms is possible. Using Eqs. (4.8) and (4.11) it is easily

shown that Eq. (4.3) decomposes to

$$C_6 = \sum_{i,j} \frac{< d_X^2 >_{A_i} < d_X^2 >_{B_j} \alpha_{A_i} \alpha_{B_j}}{< d_X^2 >_{A_i} \alpha_{B_j} + < d_X^2 >_{B_j} \alpha_{A_i}}. \tag{4.12}$$

Thus the interatomic C_6's required, eg. in Eq. (4.2), are

$$C_{6,ij} = \frac{< d_X^2 >_{A_i} < d_X^2 >_{B_j} \alpha_{A_i} \alpha_{B_j}}{< d_X^2 >_{A_i} \alpha_{B_j} + < d_X^2 >_{B_j} \alpha_{A_i}}. \tag{4.13}$$

These are determined from the occupied orbitals, without fitting or atom typing of any kind.

The dispersion correction of Eq. (4.2) diverges at small interatomic separations R_{ij} and must be modified at $R_{ij} \approx 0$. This is commonly done by multiplying each C_6/R^6 term by a suitable damping function. Many damping functions have been proposed which involve the ratio of R_{ij} to the sum of the atomic van der Waals radii, R_m, and an empirical parameter c_{damp}. Examples are the damping function of Ahlrichs *et al.* [63]

$$f_{damp}(R) = \begin{cases} \exp\left[-\left(\frac{1.28R_m}{R} - 1\right)^2\right], & \text{if } R < 1.28R_m, \\ 1, & \text{if } R \geq 1.28R_m, \end{cases} \tag{4.14}$$

the damping function of Mooij *et al.* [86]

$$f_{damp}(R) = \left[1 - \exp\left(-c_{damp}\left(\frac{R}{R_m}\right)^3\right)\right]^2. \tag{4.15}$$

and the damping function of Wu and Yang [22]

$$f_{damp}(R) = \frac{1}{1 + \exp\left[-c_{damp}\left(\frac{R}{R_m} - 1\right)\right]} \tag{4.16}$$

Wu and Yang found that the cut-off of Mooij *et al*, Eq. (4.15), performs better than others. It is perhaps noteworthy, therefore, that the damped combination $f_{damp}(R)C_6/R^6$ approaches a finite, though small, non-zero value at $R = 0$ for Eq. (4.15) but goes to zero for the others.

In this work we introduce a novel energy-based cut-off which also has the property that the dispersion energy is finite at $R_{ij} = 0$. We argue that, at small interatomic separation, dispersion energy need not necessarily vanish, but should be very small in comparison with other characteristic correlation energies of the system. We suggest that the dispersion energy of the atomic pair ij should not exceed some small fraction $(1/\kappa)$ of the sum of the correlation energies of the free atoms i and j. Thus, we propose the following modified formula for the dispersion energy:

$$E_{disp} = -\sum_{i>j} \frac{C_{6,ij}}{(\kappa C_{6,ij}/E_{C,ij}) + R_{ij}^6}. \tag{4.17}$$

This expression retains the C_6/R^6 form at large R, but at small R approaches $E_{C,ij}/\kappa$ where $E_{C,ij}$ is the sum of the absolute values of the correlation energies of the free atoms i and j. A plot of the dispersion energy for the neon dimer with both the unaltered C_6/R^6 formula and this modified formula is shown in Fig. 4.1.

The dispersion energy correction of Eq. (4.17) offers many advantages over others in the literature. It contains only one universal parameter κ (to be determined in Sections 4.3 and 4.4) with all other quantities easily computable. The coefficients $C_{6,ij}$ are computed from Eq. (4.13) using, in the present work, Hartree-Fock orbitals. The free atomic correlation energies in $E_{C,ij}$ are unique and unambiguously defined (except for the H atom, for which we take half the correlation energy of the He atom). No empirical fitting of $C_{6,ij}$ coefficients is necessary and no van der Waals atomic radii, impossible to unambiguously define in any case, are required. Eq. (4.17) omits C_8/R_{ij}^8 and C_{10}/R_{ij}^{10} terms at long range, but we make no attempt to model these here and

their omission is inconsequential.

In the following sections we expand our original tests of Eq. (4.3), or equivalently Eq. (4.12), to a much larger and diverse set of molecular pairs than in our previous work [84]. Then we apply our proposed Eq. (4.17) for the post-Hartree-Fock dispersion energy to calculation of geometries and binding energies for a test set of 20 intermolecular complexes, and we compare our results to CCSD(T) results.

4.3 Computations

4.3.1 Intermolecular C_6's

A database of accurate C_6 coefficients for 178 complexes (Table 4.1) involving 32 atoms and molecules was compiled from literature data [83]. Geometry optimizations were performed on all molecules in this set using B3LYP/6-31G(2df,p) as implemented in the Gaussian program package [49]. The $< d_X^2 >$ values of all species were obtained from fully-numerical HF single-point energy calculations, at the B3LYP optimized geometries, using the grid-based NUMOL program of Becke and Dickson [78, 79]. C_6's for the set of 178 complexes were computed using these $< d_X^2 >$ values, according to Eq. (4.3), with atomic and molecular polarizabilities taken from Ref. [76].

4.3.2 CCSD(T) binding energies

Highly accurate binding energies (BEs) are available in the literature for noble gas pairs [13], triplet H_2 [89], He-N_2 [90], and He-FCl [91]. For the other complexes in our binding energy test set (Table 4.2), reference BEs were calculated with the Gaussian program using the same method as in Ref. [92]. Geometry optimizations on the monomers were performed with CCSD/aug-cc-pvtz [93]. Potential energy surfaces (PES's) for the complexes were generated by keeping the monomers frozen at the

CCSD/aug-cc-pvtz optimized geometries and varying a single coordinate corresponding to the intermonomer separation in 0.1 Å increments. Single-point energy calculations were performed at each point on the PES using counterpoise (CP) corrected [94] CCSD(T)/aug-cc-pvdz and CCSD(T)/aug-cc-pvtz. The CP corrected energies were extrapolated to the basis-set limit using the extrapolation scheme of Martin [95].

For each complex, the minimum energy point on the basis-set extrapolated PES was deemed the optimized intermolecular separation. Each BE is the energy difference between the optimized complex and the separated monomers. The BEs do not include zero-point correction and are tabulated as positive quantities.

4.3.3 Post-HF binding energies

The BEs of the 20 test complexes in Table 4.2 were then calculated using the dispersion model of Section 4.2. The geometries of all monomers were fixed at the CCSD geometries described above. N_2 and FCl bond lengths were constrained to 1.098 Å(N_2) and 1.63 Å(FCl) as in Refs. [90] and [91]. As with the CCSD(T) calculations, PES's were generated by varying one coordinate corresponding to the intermonomer separation in 0.1 Å increments. Fully numerical HF calculations [78, 79] were performed at each point followed by evaluation of a dynamical correlation energy approximation [47], denoted BR (Becke-Roussel) in this work, using the Hartree-Fock orbitals. Dynamical correlation has a significant effect on intermolecular PES's. We choose the BR approximation because it well represents the local physics of dynamical correlation through its use of the local density, gradient and Laplacian of the density, and the local kinetic energy density. The sum of the Hartree-Fock energy and the post-HF Becke-Roussel dynamical correlation energy will be denoted HF+BR.

As in the work of Johnson *et al.* [18] it was found that calculated potential energy curves showed oscillations unless rather large grids were employed. NUMOL radial grids of 80, 120, and 160 points were used for first, second, and third row elements

respectively. For the complexes involving noble gas atoms, and triplet H_2, angular grids of 194 points were used. Angular grids of 302 points were used for all other calculations.

The dispersion energy E_{disp} of Eq. (4.17) was added to the HF+BR energy at each point on the PES. Free atomic correlation energies were obtained from Ref. [96] except for hydrogen, for which we assume an atomic "correlation energy" of 0.021 hartree (half of the helium value). Molecular polarizabilities were taken from Ref. [76] except for FCl for which no data was available. The polarizability of FCl was calculated using HF/aug-cc-pvtz [49].

The lowest-energy point on the HF+BR+E_{disp} PES was deemed the optimized intermolecular separation. BEs were computed as the energy difference between the optimized complex and the separated monomers and for several trial values of the cut-off parameter κ from 400-800, in increments of 100.

4.4 Results and Discussion

The calculated C_6 values of Eq. (4.3) for 178 atomic and molecular pairs are listed in Table 4.1 and are compared to accurate literature values. The mean absolute percent error (MAPE), mean (signed) percent error (MPE), and maximum percent error (MaxPE) relative to the accurate literature values are also shown.

In our previous work, we calculated isotropic C_6's for a test set of only 16 molecular pairs and obtained a MAPE of 12.5% [84]. For this much more extensive set of 178 complexes, our method continues to perform well and yields a slightly better MAPE of 11.1%. As indicated by the MPE of -6.3%, our computed C_6 values are generally too low, particularly for large hydrocarbons and systems involving Cl. Similar underestimation of C_6's was seen in our previous work [84] as well as in the time-dependent HF calculations of molecular C_6's of Spackman [71].

Equation (4.3) has a maximum error of 60.2% for the SiF_4-Li complex and a second large error of 45.5% for SF_6-Li. Overestimation of C_6's involving alkali atoms was also observed in Ref. [84] for potassium. However, other cases involving Li in Table 4.1 are well treated due to error cancellation. Excepting the two large errors for complexes involving Li, the largest error is -25.7% for the pentane dimer.

The HF+BR+E_{disp} binding energies of our 20 test complexes are presented in Table 4.2 for the cut-off parameter value $\kappa = 500$. The model BEs are compared to reference data consisting of our CCSD(T) calculations and literature data as described in Section 4.3.2. The conformers of the complexes and their CCSD(T) optimized geometries are shown in Fig. 4.2. CCSD(T) and HF+BR+E_{disp} PES's for the methane dimer are plotted in Fig. 4.3.

The HF+BR+E_{disp} model shows excellent agreement with CCSD(T) over the entire range of the methane dimer PES in Fig. 4.3. HF+BR without the dispersion term is essentially repulsive, showing only slight binding at large intermolecular separations.

The MAPE, MPE, and MaxPE of our model BEs, relative to the reference data, are shown in Table 4.3 as a function of the cut-off parameter κ. The MAPE is minimized at a value of ca. 500, but is reassuringly insensitive to the value of this parameter. The MPE and MaxPE show the expected trends. BEs are underestimated when a larger cut-off is used and overestimated when a smaller cut-off is used.

The model performs remarkably well for these test BEs, with a MAPE of 12.8% at $\kappa = 500$. Our errors are lower than those attained with standard DFT methods. Standard DFTs reproduce BEs of hydrogen-bonded systems to within ca. 20% [97] but poorly treat dispersion-bound systems [18, 97], failing to yield even qualitative agreement with high-level theory in some cases. Also, our HF+BR+E_{disp} model gives very good geometries, with intermonomer separations agreeing to within 0.1 Å with the results of the reference calculations.

Our results also compare favourably to the results of Grimme [23], who added an empirical dispersion correction to several standard density functionals. Grimme calculated BEs for a diverse set of 28 intermolecular complexes spanning a large range of BEs (0.08-28.8 kcal/mol). The best performance relative to correlated *ab initio* data was obtained by adding a dispersion term to the BLYP functional [42, 46], yielding a MAPE of 20.4% and a MaxPE of 52.0%. While Grimme's study involved a different test set of molecules, the superior performance of the present model is promising and we will apply it to larger aromatic complexes (as in Grimme's test set) in future work.

4.5 Conclusions

The present work extends our previous work [84] on a new Hartree-Fock-based model for calculating intermolecular C_6 dispersion coefficients. The method has been tested on a much more extensive and diverse set of complexes than in Ref. [84] and shows slightly smaller errors. A MAPE of 11.1% relative to accurate literature values was obtained for 178 isotropic C_6's.

A decomposition of our model C_6 into interatomic pair terms has been derived using Hirshfeld partitioning of the dipole moment density. Unlike other models in the literature, our decomposition does not require empirical fits or atom typing. A novel energy-based cut-off of each interatomic dispersion term at small values of the interatomic separation, involving a single universal parameter κ, has been introduced and applied to the calculation of binding energies of 20 intermolecular complexes. Our calculated binding energies have a MAPE of 12.8% relative to CCSD(T) values. These results are remarkably accurate for such a simple model.

In future work, the model will be applied to larger complexes and will be extended in order to handle intramolecular dispersion energies as well.

Table 4.1: Isotropic C_6 coefficients for intermolecular complexes, in atomic units.

System	Calc[a]	Lit[b]	System	Calc[a]	Lit[b]	System	Calc[a]	Lit[b]
H_2-H_2	14.01	12.11	SiH_4-N	91.30	89.76	CCl_4-CH_4	438.9	512.2
CH_4-CH_4	115.3	129.6	SiH_4-N_2	147.3	154.6	CCl_4-C_2H_2	561.7	642.4
CH_4-C_2H_2	147.5	162.5	SiH_4-CO_2	222.9	227.6	CCl_4-C_2H_4	675.6	779.7
CH_4-C_6H_6	383.5	472.1	SiH_4-O	71.08	68.37	CCl_4-C_2H_6	723.7	879.0
C_2H_2-C_2H_2	188.7	204.1	SiH_4-O_2	131.3	140.2	CCl_4-C_3H_6	964	1157
C_2H_2-C_3H_6	320.2	367.6	SiH_4-Ne	39.15	41.77	CCl_4-C_3H_8	998	1247
C_2H_2-C_3H_8	332.8	395.6	SiH_4-SiH_4	356.1	343.9	CCl_4-C_4H_8	1269	1512
C_2H_2-C_4H_8	420.1	480.2	SiH_4-CS_2	576.2	546.5	CCl_4-C_4H_{10}	1278	1602
C_2H_2-C_4H_{10}	425.2	508.3	SiH_4-SF_6	459.3	420.3	CCl_4-C_5H_{12}	1548	1963
C_2H_2-C_5H_{12}	514.6	622.9	SiH_4-Cl_2	349.2	363.6	CCl_4-C_6H_6	1489	1866
C_2H_2-C_6H_6	491	593	SiH_4-Ar	141.7	145.3	CCl_4-C_6H_{14}	1827	2316
C_2H_2-C_6H_{14}	606.8	734.7	SiH_4-Kr	208.2	208.4	CCl_4-C_7H_{16}	2097	2671
C_2H_4-C_2H_2	225.3	247.7	SiH_4-Xe	321.7	312.3	CCl_4-C_8H_{18}	2398	3024
C_2H_4-C_2H_4	270.1	300.5	SiF_4-H	51.92	43.28	CCl_4-N	201.9	220.5
C_2H_4-C_6H_6	592.2	719.5	SiF_4-H_2	72.85	61.19	CCl_4-N_2	326.2	382.7
C_2H_6-C_2H_2	241.9	278.9	SiF_4-He	22.38	21.90	CCl_4-CO_2	490.3	563.1
C_2H_6-C_2H_6	310.6	381.8	SiF_4-Li	574.9	358.9	CCl_4-O	158.0	170.6
C_2H_6-C_6H_6	633.8	810.1	SiF_4-CH_4	213.3	202.3	CCl_4-O_2	290.4	348.6
C_3H_6-C_3H_6	548.6	662.8	SiF_4-C_2H_2	273.0	251.9	CCl_4-Ne	87.8	106.3
C_3H_8-C_3H_8	589.4	768.1	SiF_4-C_2H_4	328.4	306.2	CCl_4-SiH_4	775.4	828.6
C_4H_8-C_4H_8	951	1130	SiF_4-C_2H_6	351.7	347.4	CCl_4-CS_2	1254	1312
C_4H_{10}-C_4H_{10}	965	1268	SiF_4-C_3H_6	468.5	455.1	CCl_4-SF_6	1004	1053
C_5H_{12}-C_5H_{12}	1415	1905	SiF_4-C_3H_8	485.2	492.7	CCl_4-CCl_4	1694	2024
C_6H_6-C_3H_6	846	1068	SiF_4-C_4H_8	617.0	595.5	CCl_4-Cl_2	767.4	887.5
C_6H_6-C_3H_8	875	1149	SiF_4-C_4H_{10}	621.3	633.3	CCl_4-Ar	314.2	359.1
C_6H_6-C_4H_8	1116	1395	SiF_4-C_5H_{12}	752.4	776.8	CCl_4-Kr	460.8	511.6
C_6H_6-C_4H_{10}	1121	1476	SiF_4-C_6H_6	723.6	732.2	CCl_4-Xe	709.2	760.0
C_6H_6-C_5H_{12}	1358	1809	SiF_4-C_6H_{14}	888.1	916.1	Cl_2-H	48.67	49.76
C_6H_6-C_6H_6	1311	1723	SiF_4-C_7H_{16}	1019	1057	Cl_2-H_2	69.52	68.58
C_6H_6-C_6H_{14}	1604	2134	SiF_4-C_8H_{18}	1166	1197	Cl_2-He	21.94	22.93
C_6H_{14}-C_6H_{14}	1971	2650	SiF_4-N_2	158.5	154.8	Cl_2-Li	501.2	465.7
N_2-N_2	66.62	73.39	SiF_4-CO_2	238.3	227.7	Cl_2-CH_4	201.2	224.6
CO_2-CH_4	128.7	142.6	SiF_4-O_2	141.1	142.3	Cl_2-C_2H_2	257.4	281.7
CO_2-C_2H_2	164.7	178.2	SiF_4-Ne	42.68	45.40	Cl_2-C_2H_4	307.6	341.9
CO_2-C_6H_6	428.5	517.8	SiF_4-SiH_4	377.0	318.7	Cl_2-C_2H_6	330.1	385.4
CO_2-CO_2	143.7	158.7	SiF_4-SiF_4	400.3	330.2	Cl_2-C_3H_6	437.4	507.5
System	Calc[a]	Lit[b]	System	Calc[a]	Lit[b]	System	Calc[a]	Lit[b]

continued on next page

O_2-H_2	27.04	26.76	SiF_4-CS_2	609.8	502.5	Cl_2-C_3H_8	454.4	546.6
O_2-He	8.82	9.41	SiF_4-SF_6	488.3	436.9	Cl_2-C_4H_8	574.1	663.2
O_2-N_2	58.94	67.16	SiF_4-CCl_4	823.5	798.2	Cl_2-C_4H_{10}	580.8	702.4
O_2-O_2	52.18	61.57	SiF_4-Cl_2	373.0	349.5	Cl_2-C_5H_{12}	702.9	860.8
O_2-Ne	16.73	19.41	SiF_4-Ar	152.7	144.6	Cl_2-C_6H_6	671.2	818.3
O_2-Ar	57.12	62.76	SiF_4-Kr	223.9	203.7	Cl_2-C_6H_{14}	829	1015
O_2-Kr	83.01	88.71	SiF_4-Xe	344.7	298.4	Cl_2-C_7H_{16}	951	1171
O_2-Xe	125.9	130.5	SF_6-H	63.39	57.05	Cl_2-C_8H_{18}	1086	1326
SiH_4-H	48.72	47.25	SF_6-H_2	89.19	80.69	Cl_2-N	93.48	96.67
SiH_4-H_2	67.70	64.24	SF_6-He	27.52	28.99	Cl_2-N_2	151.4	167.7
SiH_4-He	20.51	20.78	SF_6-Li	693.5	476.7	Cl_2-CO_2	224.6	246.7
SiH_4-Li	562.9	474.9	SF_6-N	120.1	116.3	Cl_2-O	73.82	74.72
SiH_4-CH_4	199.5	209.4	SF_6-N_2	194.1	204.5	Cl_2-O_2	134.5	152.7
SiH_4-C_2H_2	255.4	264.0	SF_6-CO_2	291.2	300.9	Cl_2-Ne	41.75	46.50
SiH_4-C_2H_4	308.3	320.0	SF_6-O	94.12	92.68	Cl_2-CS_2	564.6	575.7
SiH_4-C_2H_6	329.9	359.3	SF_6-O_2	172.8	188.2	Cl_2-SF_6	455.7	461.2
SiH_4-C_3H_6	440.7	474.7	SF_6-Ne	52.46	60.21	Cl_2-Cl_2	351.2	389.2
SiH_4-C_3H_8	455.6	509.7	SF_6-SF_6	595.7	578.2	Cl_2-Ar	146.3	157.4
SiH_4-C_4H_8	581.4	619.8	SF_6-Ar	187.1	190.9	Cl_2-Kr	213.6	224.3
SiH_4-C_4H_{10}	584.0	654.8	SF_6-Kr	274.2	268.9	Cl_2-Xe	326.5	333.3
SiH_4-C_5H_{12}	707.5	802.1	SF_6-Xe	421.5	393.8			
SiH_4-C_6H_6	683.1	766.5	CCl_4-H	106.8	113.4	MAPE[c]	11.1	
SiH_4-C_6H_{14}	835.5	946.2	CCl_4-H_2	149.9	156.4	MPE[d]	-6.3	
SiH_4-C_7H_{16}	959	1091	CCl_4-He	46.07	52.39	MaxPE[e]	60.2	
SiH_4-C_8H_{18}	1098	1236	CCl_4-Li	1182	1058			

[a]Calculated C_6's from Eq. (4.3). [b]Literature values from Ref. [83]. [c]Mean absolute percent error relative to the literature values. [d]Mean (signed) percent error. [e]Maximum percent error.

Table 4.2: Intermonomer separations (R in Å) and binding energies (BE in kcal/mol) of intermolecular complexes.

Complex	Post-HF[a]		Reference[b]	
	R	BE	R	BE
H-H	4.1	0.012	4.2[c]	0.013[c]
He-He	2.9	0.023	3.0[d]	0.022[d]
He-Ne	2.9	0.050	3.0[d]	0.041[d]
He-Ar	3.4	0.060	3.5[d]	0.057[d]
Ne-Ne	3.0	0.079	3.1[d]	0.084[d]
Ne-Ar	3.5	0.107	3.5[d]	0.134[d]
Ar-Ar	3.8	0.211	3.8[d]	0.285[d]
He-N_2 linear	3.9	0.039	3.9[e]	0.053[e]
He-N_2 T-shape	3.3	0.057	3.4[e]	0.066[e]
He-FCl linear	3.9	0.081	3.9[f]	0.097[f]
FCl-He linear	3.4	0.204	3.5[f]	0.182[f]
Methane-Ethylene[h]	4.3	0.44	4.2	0.50
Methane-Methane[h]	3.6	0.49	3.6	0.53
Ammonia-Methane[h]	3.9	0.75	3.9	0.73
Silane-Methane[h]	3.7	0.85	3.8[g]	0.81[g]
Ethylene-ethylene[h]	3.7	1.52	3.7	1.47
Methane-HF[h]	2.3	1.74	2.3	1.65
Formaldehyde dimer[h]	3.6	4.61	3.7	3.37
Water-Ammonia[h]	2.9	6.82	3.0	6.09
HCN-HF linear	1.8	8.14	1.9	7.30

[a]Calculated with the HF+BR+E_{disp} model as described in the text, using $\kappa = 500$. [b]Reference data obtained from basis-set extrapolated, counterpoise corrected CCSD(T) calculations as described in the text, unless otherwise specified. [c]Ref. [89]. [d]Ref. [13]. [e]Ref. [90]. [f]Ref. [91]. [g]Ref. [92]. [h]Intermonomer coordinates are shown in Fig. 4.2.

Table 4.3: Percent errors in HF+BR+E_{disp} binding energies as a function of the cut-off parameter κ.

κ^a	MAPE^b	MPE^c	MaxPE^d
800	15.2	-9.1	-32.4
700	14.0	-6.7	32.8
600	12.9	-4.0	34.7
500	12.8	-0.9	36.8
400	13.3	2.6	39.3

[a]Value of the cut-off parameter κ in Eq. (4.17). [b]Mean absolute percent error in the 20 HF+BR+E_{disp} binding energies, relative to the reference data in Table 4.2. [c]Mean (signed) percent error. [d] Maximum percent error.

Figure 4.1: Dispersion energy of the neon dimer with and without the cut-off of Eq. (4.17), with $\kappa = 500$. The dispersion energy with the cut-offs of Ahlrichs *et al.* [63] given by Eq. (4.14) and Mooij *et al.* [86] given by Eq. (4.15), $R_m = 3.08$Å[98], are also shown for comparison.

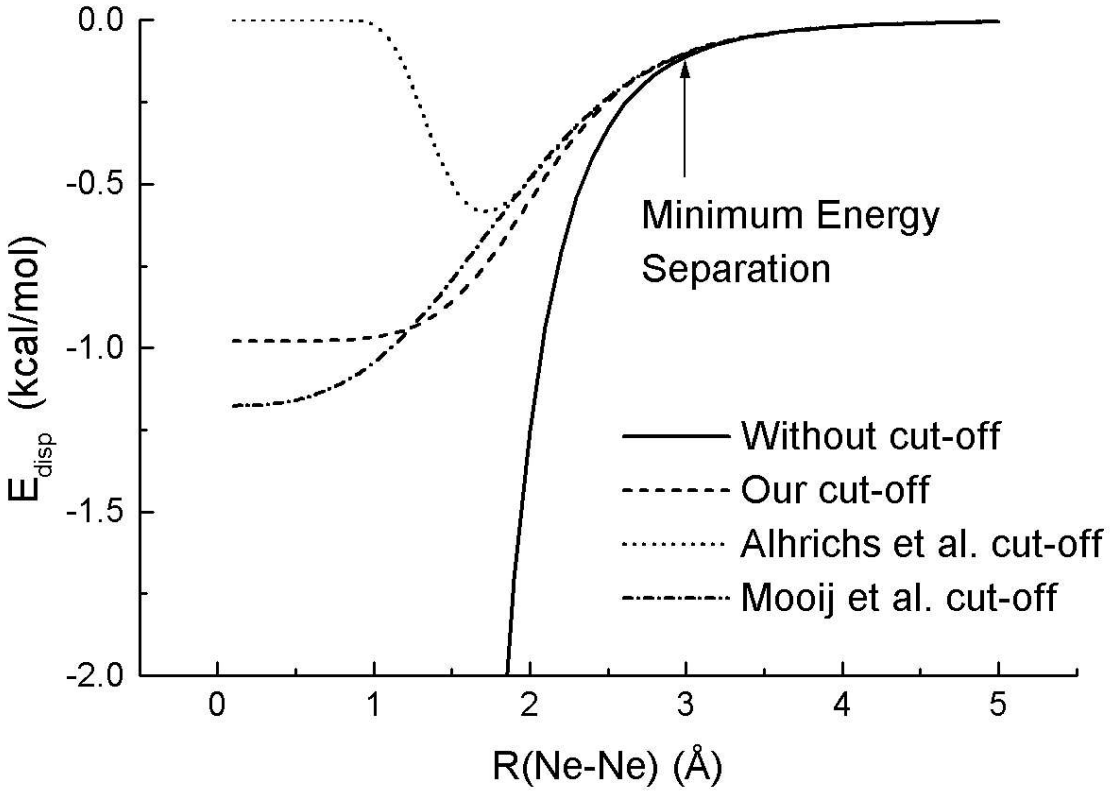

Figure 4.2: Conformations and optimized CCSD(T) intermolecular separations (in Å) of selected complexes. The optimized separations were obtained from basis-set extrapolated, counterpoise corrected CCSD(T) calculations as described in Section 4.3.2, except for silane-methane where results were obtained from Ref. [92]. CM refers to the intramolecular center of mass.

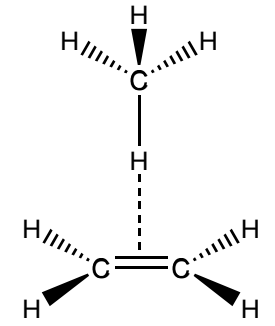

R(C-CM)=4.2Å

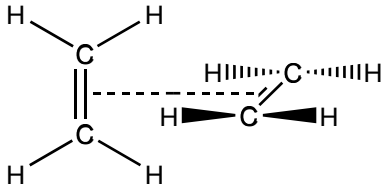

R(CM-CM)=3.7Å

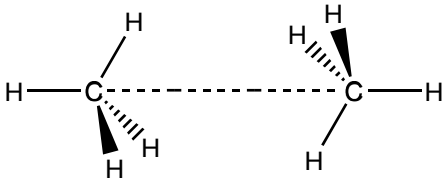

R(C-C)=3.6Å

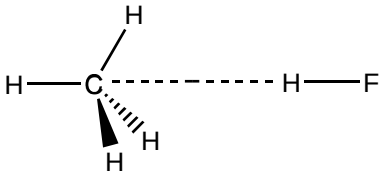

R(C-H)=2.3Å

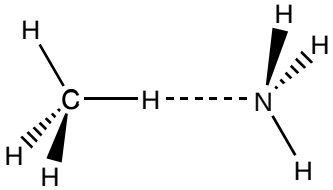

R(C-N)=3.9Å

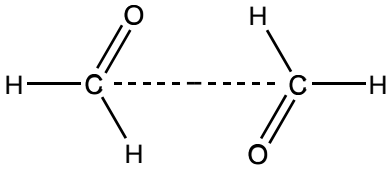

R(C-C)=3.7Å

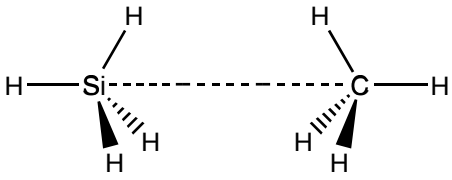

R(Si-C)=3.8Å

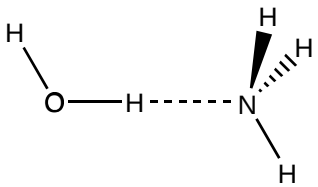

R(O-N)=3.0Å

Figure 4.3: Calculated potential energy surfaces for the methane dimer. E_{disp} was calculated using $\kappa = 500$.

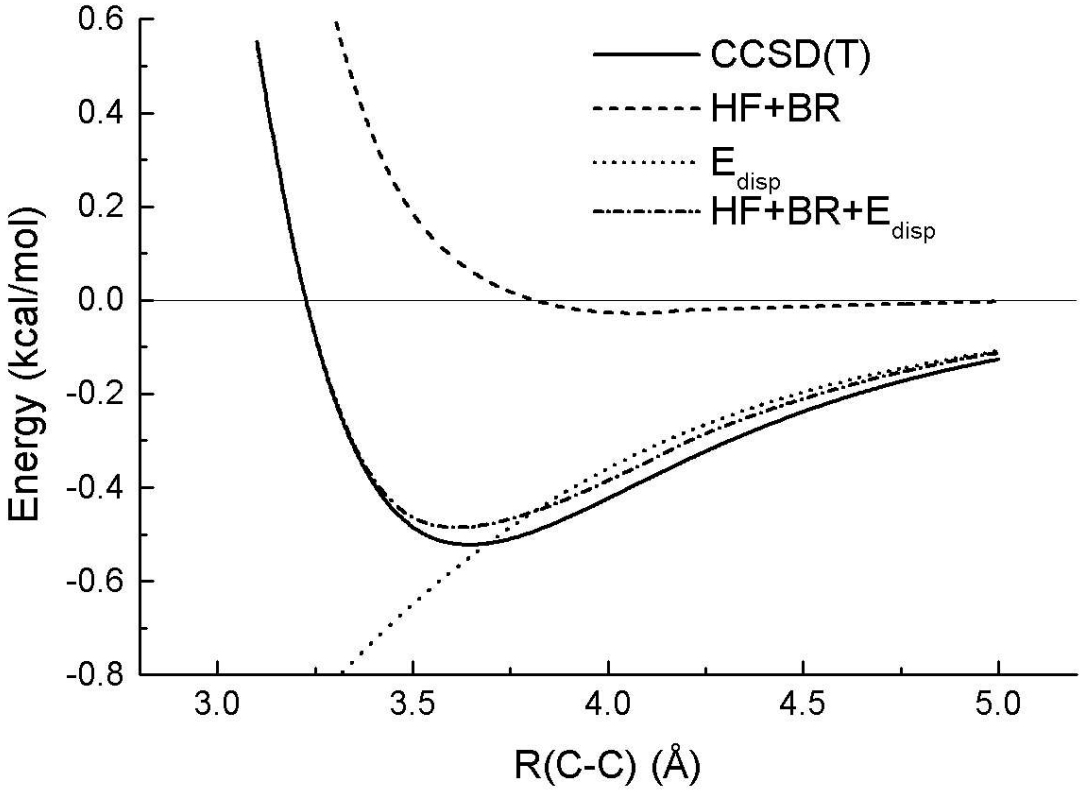

Chapter 5

A Density-Functional Model of the Dispersion Interaction

Original reference: A. D. Becke and E. R. Johnson, J. Chem. Phys. **123**, 154101 (2005).

Abstract

We have recently introduced [84] a simple parameter-free model of the dispersion interaction based on the instantaneous, in space, dipole moment of the exchange hole. The model generates remarkably accurate interatomic and intermolecular C_6 dispersion coefficients, and geometries and binding energies of intermolecular complexes. The model involves, in its original form, occupied Hartree-Fock or Kohn-Sham orbitals. Here we present a density-functional reformulation depending only on total density, the gradient and laplacian of the density, and the kinetic energy density. This density-functional model performs as well as the explicitly orbital-dependent model, yet offers obvious computational advantages.

5.1 Introduction

In Ref. [84], a simple model of the dispersion interaction was introduced which proposed that its source is the position-dependent dipole moment of the exchange hole. The idea underpinning this model is that a dipole moment instantaneous in *real space*, rather than instantaneous in virtual configuration space or in time, might be responsible for dispersion.

The exchange-hole dipole moment at any given point in a system A is assumed to induce an instantaneous dipole moment in another system B at separation R from A. The resulting potential energy of interaction, at large R, after angular averaging and density-weighted integration over all points in A, is given by

$$U^{AB}_{dip-dip} = -2 < d^2_X >_A \alpha_B / R^6 \tag{5.1}$$

and the reverse interaction is similarly given by

$$U^{BA}_{dip-dip} = -2 < d^2_X >_B \alpha_A / R^6. \tag{5.2}$$

In these expressions, α_A and α_B are the isotropic polarizabilities of A and B, and $< d^2_X >$ is the following integral:

$$< d^2_X >= \int \rho_\alpha(\mathbf{r}) d^2_{X\alpha}(\mathbf{r}) d^3\mathbf{r} + \int \rho_\beta(\mathbf{r}) d^2_{X\beta}(\mathbf{r}) d^3\mathbf{r}, \tag{5.3}$$

where ρ_α and ρ_β are up and down spin densities, and $d^2_{X\sigma}(\mathbf{r})$ is the squared exchange-hole dipole moment of the σ-spin electrons at point $\mathbf{r}$.

It was argued in Ref. [84], using 2nd-order perturbation theory, that the appropriate combination of Eqs. (5.1) and (5.2) for the total A-B dispersion energy at long

range, including kinetic and charge rearrangement effects, is

$$E_{disp} = -\frac{C_6}{R^6}, \tag{5.4}$$

$$C_6 = \frac{< d_X^2 >_A < d_X^2 >_B \alpha_A \alpha_B}{< d_X^2 >_A \alpha_B + < d_X^2 >_B \alpha_A}. \tag{5.5}$$

Thus the computation of isotropic intermolecular C_6 dispersion coefficients involves a simple integration, Eq. (5.3), over the position-dependent $d_{X\sigma}^2(\mathbf{r})$ of the systems involved, and knowledge of their isotropic polarizabilities.

The exchange-hole dipole moment $\mathbf{d}_{X\sigma}(\mathbf{r})$, for which expressions are given in the following section, depends only on time independent, occupied, Hartree-Fock or Kohn-Sham orbitals. No time dependence, virtual orbitals, or correlation (in the usual sense of the word) are involved. If polarizabilities are taken from tables, or otherwise calculated, then intermolecular C_6's can be easily and elegantly computed in a post-Hartree-Fock or post-Kohn-Sham manner from Eq. (5.5). Though not exact, C_6's from Eq. (5.5) are remarkably good considering the simplicity of the model. On a test set of 178 accurate interatomic and intermolecular data [99], this model has a mean absolute error of only 11.1 percent.

Furthermore, we derived in Ref. [99] an algebraic decomposition of Eq. (5.5) for an intermolecular C_6 into interatomic pair terms:

$$C_6 = \sum_{ij} C_{6,ij}, \tag{5.6}$$

where i refers to an atom in system A and j to an atom in system B, positing the

dispersion energy expression

$$E_{disp} = -\sum_{ij} \frac{C_{6,ij}}{R_{ij}^6}. \tag{5.7}$$

With suitable damping of each term at small R_{ij}, a post-Hartree-Fock model of intermolecular interactions was tested on geometries and binding energies of 20 intermolecular complexes with very encouraging results [99].

In the present work we derive an approximate formula for the exchange-hole dipole moment, $\mathbf{d}_{X\sigma}(\mathbf{r})$, depending only on the local spin density, its gradient and laplacian, and the local kinetic energy density. Thus we obtain a *density-functional* model of intermolecular dispersion interactions. In contemporary DFT (density-functional theory) language, this is called a "meta-GGA" (meta generalized gradient approximation) for the dispersion interaction.

In Section 5.2, the underlying model of Ref. [84] is briefly reviewed. In Section 5.3, its density-functional reformulation is introduced and tested on interatomic and intermolecular C_6's. The exchange-hole model of Becke and Roussel [43] (to be denoted BR) is the key. The BR model was the first exchange meta-GGA in the literature and has been fruitful in many contexts. It has been generalized to include current-density dependence [100], thereby solving a longstanding problem in the density-functional theory of open-shell atomic states [101]. It is the basis of a promising new approach to the molecular nondynamical correlation problem [15, 25]. Here we exploit a further property of the Becke-Roussel exchange hole, namely that the BR hole has non-zero *dipole moment*.

In Section 5.4, our decomposition of intermolecular dispersion energy into interatomic pair terms [99] is reviewed and recast into the present BR framework. In Section 5.5, the test set of 20 intermolecular geometries and binding energies employed in Ref. [99] is expanded to 41 complexes, and our original and the present

dispersion models are assessed on these complexes in a post-Hartree-Fock manner. Finally, concluding remarks and a preview of future work are offered in Section 5.6.

5.2 The Basic Model

We refer the reader to Ref. [84] for a complete account of the present model. A summary of the underlying theory is provided here to set the stage for its density-functional reformulation in the next section.

Consider an electron of σ spin in an atomic or molecular system. As it moves through the system it is accompanied by an exchange (or Fermi) hole whose shape depends on the electron's instantaneous position $\mathbf{r}$. The hole is given by the expression

$$h_{X\sigma}(\mathbf{r},\mathbf{r}') = -\frac{1}{\rho_\sigma(\mathbf{r})}\sum_{ij}\psi_{i\sigma}(\mathbf{r})\psi_{j\sigma}(\mathbf{r})\psi_{i\sigma}(\mathbf{r}')\psi_{j\sigma}(\mathbf{r}'), \tag{5.8}$$

where $\mathbf{r}'$ defines the shape of the hole and $\mathbf{r}$ is called the "reference" point. Summation is over all orbitals of σ spin (Hartree-Fock or Kohn-Sham, and assumed in this paper to be real) and ρ_σ is the total σ-spin electron density.

When an electron is at $\mathbf{r}$, the hole measures the depletion of probability, with respect to the total electron density ρ, of finding another same-spin electron at $\mathbf{r}'$. Several important and well-known properties of the hole are easily deduced from Eq. (5.8). The probability of finding another same-spin electron at $\mathbf{r}' = \mathbf{r}$ is completely extinguished,

$$h_{X\sigma}(\mathbf{r},\mathbf{r}) = -\rho_\sigma(\mathbf{r}), \tag{5.9}$$

as required by the Pauli exclusion principle. The hole is always negative, as can be

seen by rewriting Eq. (5.8) as

$$h_{X\sigma}(\mathbf{r},\mathbf{r}') = -\frac{1}{\rho_\sigma(\mathbf{r})}\left[\sum_i \psi_{i\sigma}(\mathbf{r})\psi_{i\sigma}(\mathbf{r}')\right]^2 \tag{5.10}$$

and the hole always contains exactly (minus) one electron:

$$\int h_{X\sigma}(\mathbf{r},\mathbf{r}')d^3\mathbf{r}' = -1. \tag{5.11}$$

The electron plus its hole, therefore, always has zero overall charge.

Useful information on the behaviour of the hole *near* the reference point can be obtained from a Taylor expansion of the spherical average of $h_{X\sigma}(\mathbf{r},\mathbf{r}')$ around $\mathbf{r}$. To second order in the interelectronic distance s, we have,

$$h_{X\sigma}(\mathbf{r},\mathbf{r}+s) = -\rho_\sigma - Q_\sigma s^2 + \ldots, \tag{5.12}$$

where

$$Q_\sigma = \frac{1}{6}\left[\nabla^2\rho_\sigma - 2\tau_\sigma + \frac{1}{2}\frac{(\nabla\rho_\sigma)^2}{\rho_\sigma}\right] \tag{5.13}$$

and where

$$\tau_\sigma = \sum_i (\nabla\psi_{i\sigma})^2 \tag{5.14}$$

is the "kinetic energy" density (without a factor of 1/2). This short-range information is an important ingredient in the BR model [43]. It is through Eqs. (5.12) to (5.14) that local density gradients enter.

The hole is generally not spherically symmetric around $\mathbf{r}$. Only in a uniform electron gas does it have spherical symmetry. Even in systems with spherically symmetric

densities, the hole is nonspherical unless $\mathbf{r}$ is at the center of the system. Thus the electron plus its exchange hole generally has a *non-zero dipole moment*, given by a simple integration over $\mathbf{r}'$ in Eq. (5.8):

$$\mathbf{d}_{X\sigma}(\mathbf{r}) = \left[\frac{1}{\rho_\sigma(\mathbf{r})}\sum_{ij}\mathbf{r}_{ij\sigma}\psi_{i\sigma}(\mathbf{r})\psi_{j\sigma}(\mathbf{r})\right] - \mathbf{r}, \tag{5.15}$$

where

$$\mathbf{r}_{ij\sigma} = \int \mathbf{r}'\psi_{i\sigma}(\mathbf{r}')\psi_{j\sigma}(\mathbf{r}')d^3\mathbf{r}' \tag{5.16}$$

and only the occupied orbitals are involved.

If this *instantaneous in space* non-zero dipole moment $\mathbf{d}_{X\sigma}(\mathbf{r})$ in a system A is allowed to *induce* a dipole moment in another system B, far from A, then simple electrostatics, angular averaging, and a density-weighted $\mathbf{r}$ integration lead to the formulas in Section 5.1 for the isotropic C_6 of an A-B dispersion interaction [84]. The integrations required in Eqs. (5.3) and (5.16) may be carried out numerically [77], or analytically in the case of Eq. (5.16).

Eqs. (5.15) and (5.16) for $\mathbf{d}_{X\sigma}(\mathbf{r})$ are exact, and the computation of the $< d_X^2 >$ expectation value of Eq. (5.3) is an order N^3 task. Though of relatively minor cost compared to computation of the orbitals themselves, a linear scaling $< d_X^2 >$ procedure would be highly desirable in the wake of rapid ongoing advances in linear scaling Hartree-Fock, density-functional, and density matrix technologies. The Becke-Roussel meta-GGA model of the exchange hole [43] allows such a linearization.

5.3 Density-Functional Reformulation

The BR model [43] places a normalized, off-center, exponential function

$$-\frac{a^3}{8\pi}e^{-ar}, \tag{5.17}$$

at a distance b from the reference position $\mathbf{r}$ of a σ-spin electron. Enforcing Eq. (5.9), that the value of the hole at the reference point is $-\rho_\sigma$, gives the equation

$$\rho_\sigma = \frac{a^3}{8\pi}e^{-ab}. \tag{5.18}$$

Requiring, also, that the model hole have the same quadratic short-range behaviour near $\mathbf{r}$ as the exact hole gives a second equation,

$$Q_\sigma = \frac{\rho_\sigma}{6b}\left(a^2 b - 2a\right), \tag{5.19}$$

where Q_σ is given by Eqs. (5.13) and (5.14). Then, setting $x = ab$, simultaneous solution of Eqs. (5.18) and (5.19) is achieved by solving the nonlinear problem

$$\frac{xe^{-2x/3}}{(x-2)} = \frac{2}{3}\pi^{2/3}\frac{\rho_\sigma^{5/3}}{Q_\sigma}, \tag{5.20}$$

following which b is obtained from

$$b^3 = \frac{x^3 e^{-x}}{8\pi\rho_\sigma} \tag{5.21}$$

and finally $a = x/b$. Eq. (5.20) is easily solved, for all possible ρ_σ and Q_σ, by the Newton-Raphson method [102].

The BR model was motivated [43] by the hydrogenic atom as a prototype system. It reproduces, by construction, the *exact* exchange hole of a *hydrogenic atom* at any

reference point. In any other system, it is an approximation to the exact hole that has correct normalization, Eq. (5.11), and correct short-range behaviour, Eq. (5.12), at all reference points. Comparative plots of the spherically averaged BR hole may be found in Ref. [43]. The model is sufficiently flexible to accommodate positive or negative curvatures Q_σ, and even *infinitely negative* Q_σ as occurs at every nuclear cusp (see Ref. [43]).

For the present purposes, notice that the BR model hole, like the exact hole, is *not spherically symmetric* around $\mathbf{r}$ and has a *non-zero dipole moment.* Indeed, the (squared) dipole moment of the electron plus its BR hole is given by

$$d^2_{\mathrm{BRX}\sigma}(\mathbf{r}) = b^2, \tag{5.22}$$

where b is determined by the local density and curvature, $\rho_\sigma(\mathbf{r})$ and $Q_\sigma(\mathbf{r})$, through Eqs. (5.20) and (5.21). All the C_6 formulas of Section 5.1, therefore, may be cast into density-functional form simply by replacing $< d^2_X >$ of Eq. (5.3) by the following Becke-Roussel analog:

$$< d^2_{\mathrm{BRX}} >= \int \rho_\alpha(\mathbf{r}) d^2_{\mathrm{BRX}\alpha}(\mathbf{r}) d^3\mathbf{r} + \int \rho_\beta(\mathbf{r}) d^2_{\mathrm{BRX}\beta}(\mathbf{r}) d^3\mathbf{r}, \tag{5.23}$$

whose computational cost scales linearly with system size.

This BR analog of our original theory has been tested on accurate C_6 data, compiled in Ref. [99], for 178 atom and molecule pairs. The mean absolute percent error (MAPE) is 15.0%, only slightly worse than the MAPE of 11.1% for the exact-exchange-based theory.

In the next section, we review our dispersion energy decomposition scheme of Ref. [99], and Eq. (5.7), in preparation for an assessment of this BR model on geometries and binding energies of intermolecular complexes in Section 5.5.

5.4 Interatomic Decomposition

The fundamental quantity on which our model is based is the integrand of Eq. (5.3), the squared exchange-hole dipole moment density at $\mathbf{r}$:

$$d_X^2(\mathbf{r}) = \rho_\alpha(\mathbf{r}) d_{X\alpha}^2(\mathbf{r}) + \rho_\beta(\mathbf{r}) d_{X\beta}^2(\mathbf{r}), \tag{5.24}$$

or its BR analog from Eq. (5.23):

$$d_{\mathrm{BRX}}^2(\mathbf{r}) = \rho_\alpha(\mathbf{r}) d_{\mathrm{BRX}\alpha}^2(\mathbf{r}) + \rho_\beta(\mathbf{r}) d_{\mathrm{BRX}\beta}^2(\mathbf{r}), \tag{5.25}$$

We will refer to this quantity as the "dipole density" from now on. Being a local function of $\mathbf{r}$, the dipole density in a molecule may be easily partitioned into atomic components using any suitable real-space atomic partitioning scheme such as, eg., Bader partitioning [103], smoothed Voronoi partitioning [77], or Hirshfeld partitioning [88]. We used the Hirshfeld scheme in our earlier work, Ref. [99], and we use it in the present work as well.

An atomic weight function, $w_i(\mathbf{r})$, is constructed for each atom i in a molecule as follows:

$$w_i(\mathbf{r}) = \frac{\rho_i^{at}(\mathbf{r})}{\sum_n \rho_n^{at}(\mathbf{r})}, \tag{5.26}$$

where ρ^{at} is a free sphericalized atomic density placed at the appropriate nucleus, and the n summation is over all atoms in the molecule. Clearly, the weight functions sum to 1 everywhere,

$$\sum_n w_n(\mathbf{r}) = 1, \tag{5.27}$$

and $w_i(\mathbf{r})$ has value close to 1 at points in the vicinity of atom i and close to 0

everywhere else. The dipole density on atom i is thus given by

$$< d_X^2 >_i = \int w_i(\mathbf{r}) d_X^2(\mathbf{r}) d^3\mathbf{r} \tag{5.28}$$

or by its BR analog.

Polarizability is not related to a local function of $\mathbf{r}$, is not additive (i.e. molecular polarizabilities are not sums of free atomic polarizabilities), and is therefore not so easy to partition into atomic components. We suggested in Ref. [99] the following reasonable ansatz:

$$\alpha_i = \frac{< d_X^2 >_i}{< d_X^2 >} \alpha, \tag{5.29}$$

where α is the total polarizability of the molecule. In other words, the polarizability of atom i in the molecule is proportional to the fraction of the dipole density owned by the atom. In addition to being a reasonable ansatz, we discovered [99] that, *given* this definition, our model C_6 of Eq. (5.5) algebraically decomposes into a sum over atomic pair C_6's as in Eq. (5.6):

$$C_6 = \sum_i^A \sum_j^B C_{6,ij}, \tag{5.30}$$

where

$$C_{6,ij} = \frac{< d_X^2 >_i < d_X^2 >_j \alpha_i \alpha_j}{< d_X^2 >_i \alpha_j + < d_X^2 >_j \alpha_i} \tag{5.31}$$

and where we adopt the convention, here and in the rest of this section, that index i refers to an atom in system A and index j refers to an atom in B.

Eqs. (5.30) and (5.31) motivate the dispersion energy formula of Eq. (5.7), which requires damping of each term at small R_{ij}. In Ref. [99], a novel energy-based damp-

ing,

$$E_{disp} = -\sum_{ij} \frac{C_{6,ij}}{(\kappa C_{6,ij}/E_{C,ij}) + R_{ij}^6}, \tag{5.32}$$

was proposed in which $E_{C,ij}$ is the sum of the absolute values of the correlation energies of the free atoms i and j (with 21 mH, half the He value, taken for H) and κ is a universal parameter limiting the dispersion energy of each ij pair to $-E_{C,ij}/\kappa$ at small R_{ij}. This formula contains only one, universal, empirical parameter κ (with value of order 1000) and, unlike other formulas in the literature, requires no van der Waals radii.

Since free atomic correlation energies are well defined [96] the dispersion energy, Eq. (5.32), contains *no empirical parameters* except for κ. The interatomic $C_{6,ij}$ coefficients are computed from occupied molecular orbitals through the dipole density of Eq. (5.24) or (5.25), and the atomic partitionings of Eqs. (5.28) and (5.29), without any empiricism or fitting whatsoever. We test this dispersion energy formula on a variety of intermolecular complexes in the next section.

5.5 Computations and Assessment

In Ref. [99], tests were performed on 20 intermolecular complexes using Hartree-Fock orbitals from the basis-set-free NUMOL program [78, 79]. Since NUMOL Hartree-Fock calculations are practical on small systems only, we have developed a post-Gaussian 98 methodology for larger systems in the present work. We employ the Gaussian 98 program [49] to compute HF/aug-cc-pvtz orbitals using the keyword "output=wfn" to create a WFN file. Orbital information is read from the WFN file and all quantities needed in the present work, including density gradients, laplacians, and kinetic energy densities, are analytically evaluated at all points of a numerical

integration grid [77]. All integrations are then carried out on the numerical grid.

Intermolecular energies are strongly affected by dynamical correlation. It is not sufficient to add a dispersion correction such as Eq. (5.32) to the Hartree-Fock energy alone. A dynamical correlation term must be included as well. We choose the dynamical correlation functional of Becke [39], as modified in Ref. [47] to incorporate BR exchange. Denoting this functional as $E_C^{\rm BR}$, our target total energy is

$$E_{total} = E_{\rm HF} + E_C^{\rm BR} + E_{disp}. \tag{5.33}$$

The two variations of our theory, involving the dipole density of the exact exchange hole, Eq. (5.24), or the dipole density of the BR model hole, Eq. (5.25), will be denoted "XX" and "BR" respectively in this section. In either case, E_{total} is evaluated using Hartree-Fock orbitals and therefore the present work, as was the work of Ref. [99], is best described as post-Hartree-Fock.

We have applied the XX and BR post-Hartree-Fock methods to calculation of minimum-energy separations and binding energies for a test set of 41 van der Waals complexes involving dispersion, dipole-induced dipole, dipole-dipole, and hydrogen-bonding interactions. The conformations of these complexes are shown in Fig. 5.1. The geometries of all monomers were optimized using CCSD/aug-cc-pvtz [93], except for the benzene geometry which was taken from Ref. [104]. Counterpoise-corrected [94] HF/aug-cc-pvtz potential energy surfaces (PES) were then generated for each of the complexes by keeping the monomer geometries fixed and varying up to three intermonomer coordinates in increments of 0.1 Å or 5°. Post-HF evaluations of the dynamical BR correlation energy and both XX and BR dipole densities were performed on the complex at each point on the PES and on the separated monomers (not counterpoise corrected). Polarizabilities of all species were taken from Ref. [76], except for FCl for which no value was available. The polarizability of FCl was calculated

using HF/aug-cc-pvtz. The lowest-energy point on the resulting $E_{\rm HF} + E_C^{\rm BR} + E_{disp}$ PES was deemed the optimized geometry of the complex. Binding energies (BEs) were computed as the total energy difference between the optimized complex and the separated monomers.

Our calculated intermonomer separations and binding energies are listed in Table 5.1 and compared to high level reference data [13, 90, 91, 92, 99, 104, 105, 106, 107, 108, 109, 110, 111]. The reference geometries are also shown in Fig. 5.1. We divide the complexes into classes according to the type of van der Waals interaction involved, though in many cases the binding may involve several interaction types. An optimum value of $\kappa = 800$ was selected by minimizing the mean absolute percent error (MAPE) in the calculated BEs. The optimum κ is the same for both the XX and the BR models.

There is little difference between the results obtained from the XX or the BR dipole densities for this set of van der Waals complexes. The mean absolute error (MAE) for the intermonomer separations is identical for both XX and BR, and the MAPE in the binding energies differs by only 0.1% between the two approaches. It is gratifying that the more efficient BR approach is no less accurate than the exact-exchange approach of our earlier work [99].

The agreement between our calculated separations and the high level reference data is excellent, with a MAE of 0.08 Å. For the set of 41 complexes, our methods have maximum errors of 0.4 Å (XX) and 0.3 Å (BR), the worst cases being overestimation of the monomer separations in the parallel and slipped-parallel conformations of the benzene dimer. There is also good agreement with high level reference data for our calculated BEs, with MAPEs of 15.4% (XX) and 15.3% (BR). Our methods show similar mean errors for each class of van der Waals interactions. The parallel and slipped-parallel benzene dimers are again the worst cases, with MAPEs improving to 12.8% (XX) and 13.1% (BR) if these π-stacked complexes are omitted from the

statistics.

The π-stacked benzene dimer conformations are also a difficult case for MP2, which, with the aug-cc-pvqz basis set, overestimates the binding energies by 98.2% and 82.8% for the parallel and slipped-parallel conformations respectively [104]. Also, most "standard" DFTs predict a separation for the slipped-parallel benzene dimer that is far too long by ca. 2 Å, and fail to predict any binding for the parallel conformation [18]. Therefore the present methods, while having relatively large errors for the π-stacked benzene dimers as well, nevertheless represent major improvements over both MP2 and standard DFTs for which these are pathological cases.

To assess our results in the context of recent literature we compare with the work of Grimme [23], who added an empirical dispersion correction to the BLYP [42, 46] exchange-correlation functional and applied his method to a set of 28 van der Waals complexes. Grimme obtained C_6 coefficients from fits to experimental C_6 data and reported parameters for C, N, O, H, and halogen atoms. An additional global scaling parameter was used to improve the binding energies. This yielded a MAE of 0.09 Å for separations and a MAPE of 20.4% for binding energies. Our method has significantly lower binding energy errors, the more remarkable considering that our C_6 coefficients are completely free of empirical parametrization or fitting.

In a recent study of 28 van der Waals complexes [110], B971/6-311++G(3df,3pd) [53] was found to be the best standard DFT for structure prediction and, with counterpoise correction, was also the best for calculating binding energies. In Table 5.2, we present a direct comparison between our methods and B971/6-311++G(3df,3pd) for the 26 complexes common between this data set and the current work. The two complexes omitted are the parallel benzene dimer, which is predicted to be unbound by B971, and the formic acid dimer, in which there is significant monomer distortion in the dimer and thus our rigid monomer approach is not appropriate. Our methods perform far better than B971 for calculation of both optimized separations

and binding energies for dispersion-bound complexes and perform similarly for the other classes of van der Waals complexes. The high accuracy of our calculated geometries and binding energies, particularly in comparison with standard DFTs, is very promising for applications such as protein structure prediction in which van der Waals interactions are the primary determinants of structure and energetics.

5.6 Conclusions and Outlook

The present work introduces a density-functional model of the dispersion interaction with the *physics* of dispersion explicitly incorporated. The underlying idea [84], that the non-zero, instantaneous *in space*, dipole moment of the exchange hole is the source of induced dipole moments in far systems, is elegant and easy to implement. The exchange-hole dipole moment depends on local density, gradient and laplacian of the density, and the local kinetic energy density. The model predicts, without any empirical parameters whatsoever, intermolecular C_6 dispersion coefficients of very good accuracy.

With a previously derived [99] algebraic decomposition of our intermolecular C_6 formula into interatomic pair terms, and a novel energy-based damping [99] of each term at small R_{ij}, a density-functional theory of intermolecular interactions is obtained. Geometries and binding energies for a test set of 41 intermolecular complexes are predicted with remarkable accuracy invoking only one, universal, empirical parameter. The worst results occurred for the π-stacked conformations of the benzene dimer. We believe this will be rectified in future work by adding a C_8/R^8 term in the dispersion energy.

The model in its present form requires the polarizability of each monomer. Although polarizability data is readily available for numerous systems, this is inconvenient in general and is fundamentally problematic for *intra*molecular dispersion

interactions. In future work, therefore, we will also investigate how to remove molecular polarizability from the theory.

Table 5.1: Calculated intermonomer separations and binding energies (κ = 800). Mean absolute errors (MAE), relative to high level reference data, are shown for the separations and mean absolute percent errors (MAPE) are shown for the binding energies.

Complex	Separation (Å)			Binding Energy (kcal/mol)		
	XX	BR	High level	XX	BR	High Level
Dispersion						
He_2	3.0	2.9	3.0[d]	0.021	0.022	0.022[d]
He-Ne	2.9	2.9	3.0[d]	0.053	0.057	0.041[d]
He-Ar	3.4	3.4	3.5[d]	0.065	0.063	0.057[d]
Ne_2	2.9	2.9	3.1[d]	0.105	0.113	0.084[d]
Ne-Ar	3.4	3.4	3.5[d]	0.125	0.121	0.134[d]
Ar_2	3.8	3.8	3.8[d]	0.216	0.199	0.285[d]
He-N_2 Linear	3.9	3.9	3.9[e]	0.044	0.045	0.053[e]
He-N_2 Tshape	3.4	3.4	3.4[e]	0.062	0.063	0.066[e]
He-FCl	3.9	3.9	3.9[f]	0.082	0.087	0.097[f]
FCl-He	3.5	3.5	3.5[f]	0.185	0.182	0.182[f]
Ne-CH_4	3.3	3.3	3.5[g]	0.20	0.20	0.22[g]
Ne-C_6H_6	3.3	3.3	3.2[g]	0.35	0.39	0.47[g]
CH_4-C_2H_4	4.3	4.3	4.2[h]	0.44	0.45	0.50[h]
$(CH_4)_2$	3.7	3.7	3.6[g]	0.40	0.41	0.51[g]
$(CF_4)_2$	3.8	3.8	4.0[i]	0.76	0.92	0.78[i]
CH_4-SiH_4	3.8	3.8	3.8[j]	0.72	0.74	0.81[j]
CH_4-C_6H_6	4.0	4.0	3.8[k]	0.90	0.94	1.23[k]
$(C_2H_2)_2$	4.2	4.2	4.2[g]	1.52	1.51	1.34[g]
$(CO_2)_2$	3.6	3.6	3.6[l]	1.60	1.61	1.37[l]
$(OCS)_2$	3.8	3.8	3.8[m]	1.44	1.40	1.40[m]
$(C_2H_4)_2$	3.7	3.7	3.8[g]	1.37	1.39	1.42[g]
P-$(C_6H_6)_2$[a]	4.2	4.2	3.9[n]	0.34	0.48	1.70[n]
T-$(C_6H_6)_2$[b]	5.0	5.0	5.0[n]	2.26	2.43	2.61[n]
SP-$(C_6H_6)_2$[c]	4.3	4.2	3.9[n]	1.28	1.47	2.62[n]
MA(P)E	0.09	0.09	—	18.1	17.4	—
Dipole-Induced Dipole						
CH_4-NH_3	3.9	3.9	3.9[h]	0.72	0.73	0.73[h]
SiH_4-HF	3.2	3.2	3.3[o]	0.86	0.88	0.73[o]
CH_4-HF	2.3	2.3	2.3[h]	1.74	1.74	1.65[h]
NH_3-C_6H_6	3.8	3.8	3.6[p]	2.56	2.63	2.22[p]

continued on next page

Complex	Separation (Å)			Binding Energy (kcal/mol)		
	XX	BR	High level	XX	BR	High Level
H_2O-C_6H_6	3.3	3.3	3.4[p]	3.80	3.89	3.17[p]
C_2H_4-HF	2.1	2.1	2.2[o]	5.51	5.51	4.47[o]
MA(P)E	0.08	0.08	—	13.8	15.2	—
Dipole-Dipole						
$(H_2S)_2$	2.9	2.9	2.8[g]	1.67	1.63	1.66[g]
$(HCl)_2$	2.5	2.5	2.5[g]	2.04	1.99	2.01[g]
$(H_3CF)_2$	3.8	3.8	3.9[o]	2.76	2.82	2.33[o]
H_2S-HCl	2.5	2.5	2.5[g]	3.46	3.42	3.35[g]
$(H_2CO)_2$	3.6	3.6	3.6[h]	4.44	4.47	3.37[h]
$(H_3CCN)_2$	3.3	3.3	3.4[o]	6.46	6.49	6.16[o]
MA(P)E	0.06	0.06	—	10.1	10.6	—
Hydrogen bonded						
$(NH_3)_2$	3.3	3.3	3.3[g]	3.21	3.21	3.15[g]
$(HF)_2$	1.8	1.8	1.9[g]	5.45	5.46	4.57[g]
$(H_2O)_2$	1.9	1.9	2.0[g]	5.61	5.61	4.97[g]
H_2O-NH_3	2.9	2.9	3.0[g]	6.67	6.67	6.09[g]
HCN-HF	1.8	1.8	1.9[h]	8.05	8.06	7.30[h]
MA(P)E	0.07	0.07	—	10.8	10.9	—
Overall MA(P)E	0.08	0.08	—	15.4 (12.8)[q]	15.3 (13.1)[q]	—

[a]Parallel conformation. [b]T-shaped conformation. [c]Slipped-Parallel conformation. [d]Ref. [13]. [e]Ref. [90]. [f]Ref. [91]. [g]Ref. [105]. [h]Ref. [99]. [i]Ref. [106]. [j]Ref. [92]. [k]Ref. [107]. [l]Ref. [108]. [m]Ref. [109]. [n]Ref. [104]. [o]Ref. [110]. [p]Ref. [111]. [q]Values in parentheses are errors determined by omitting Parallel and Slipped-Parallel benzene dimer values.

Table 5.2: Mean absolute errors (MAE) in separations and mean absolute percent errors (MAPE) in binding energies for 26 van der Waals complexes. The B971 values in parentheses were not corrected for basis set superposition error. The B971 results were obtained from data in Ref. [110].

Interaction Type	MAE in Separation (Å)			MAPE in Binding Energy (%)		
	B971/ 6-311++G(3df,3pd)	XX	BR	B971/ 6-311++G(3df,3pd)	XX	BR
Dispersion	0.34 (0.30)	0.11	0.10	44.7 (50.1)	16.7	17.3
Dipole-Induced Dipole	0.09 (0.05)	0.08	0.08	16.9 (13.6)	13.8	15.2
Dipole-Dipole	0.04 (0.03)	0.06	0.06	13.1 (9.4)	18.4	19.7
Hydrogen bonded	0.07 (0.06)	0.07	0.07	3.4 (5.7)	8.7	8.7
Overall	0.20 (0.17)	0.09	0.09	28.2 (30.2)	15.0	15.8

Figure 5.1: Structures of van der Waals complexes and reference intermonomer separations obtained from high level theory. See Table 5.1 for references.

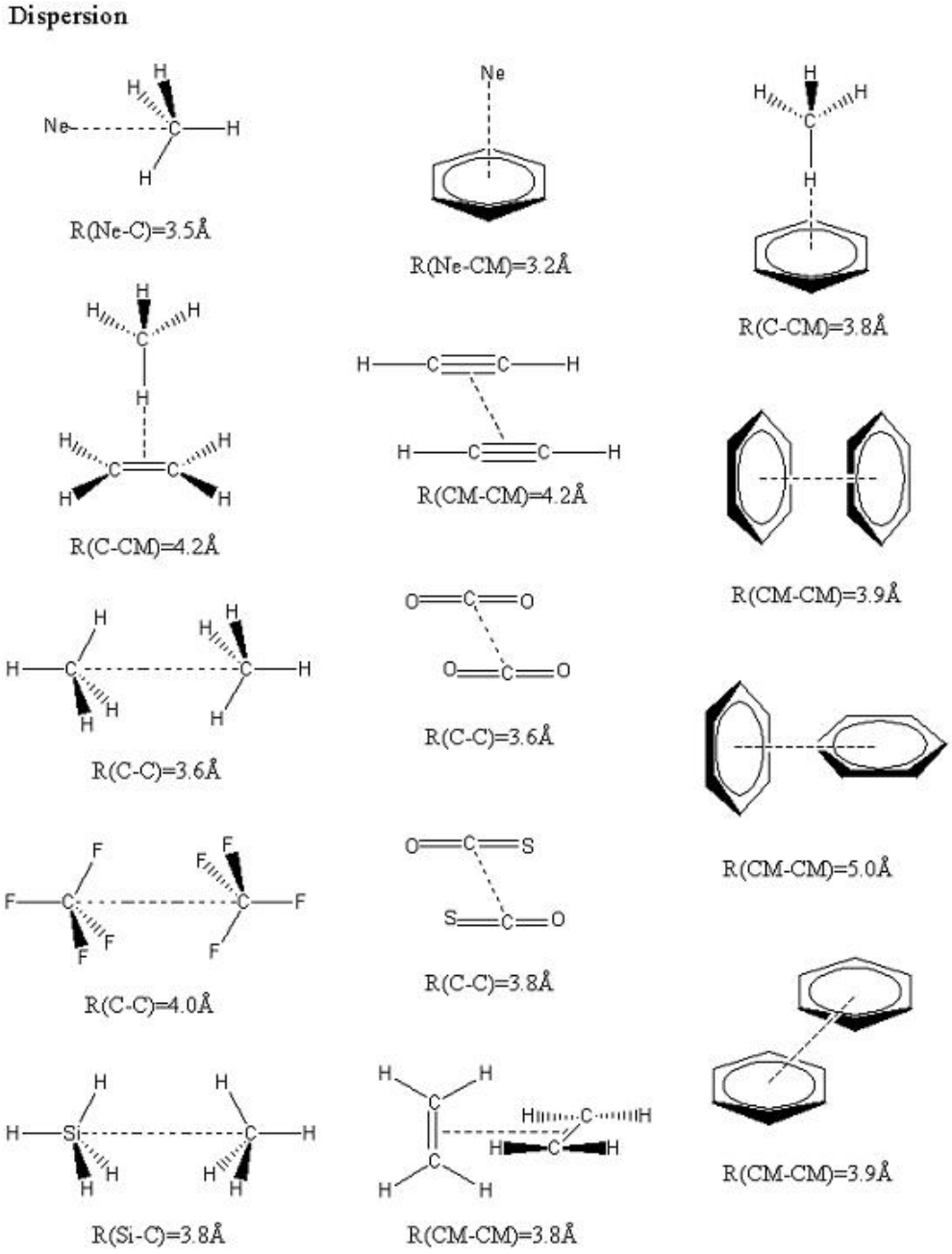

Dipole-Induced dipole

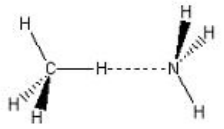

R(C-N)=3.9Å

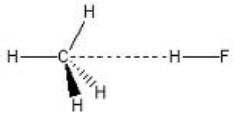

R(C-H)=2.3Å

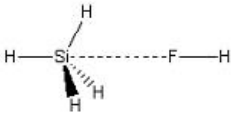

R(Si-F)=3.3Å

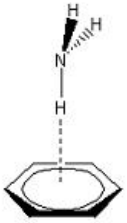

R(N-CM)=3.6Å

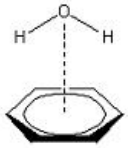

R(O-CM)=3.4Å

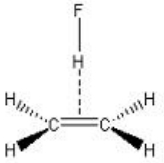

R(H-CM)=2.2Å

Dipole-Dipole

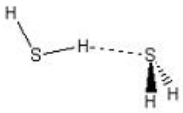

R(H-S)=2.8Å

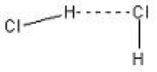

R(H-Cl)=2.5Å

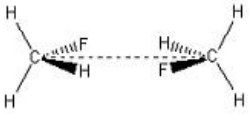

R(C-C)=3.9Å

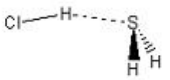

R(H-S)=2.5Å

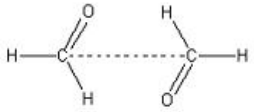

R(C-C)=3.6Å

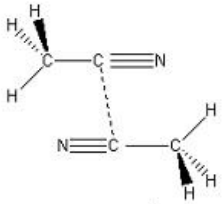

R(C-C)=3.4Å

H-Bond

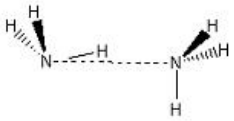

R(N-N)=3.3Å

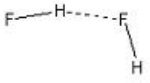

R(H-F)=1.9Å

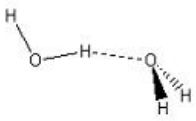

R(H-O)=2.0Å

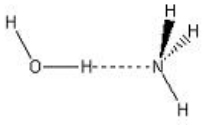

R(O-N)=3.0Å

R(N-H)=1.9Å

Chapter 6

Exchange-Hole Dipole Moment and the Dispersion Interaction: High Order Dispersion Coefficients

Original reference: A. D. Becke and E. R. Johnson, J. Chem. Phys. **124**, 014104 (2006).

Abstract

In recent publications [84, 99] we have demonstrated that the position-dependent dipole moment of the exchange hole can be used to generate dispersion interactions between closed-shell systems. Remarkably accurate C_6 coefficients and intermolecular potential energy surfaces can be obtained from Hartree-Fock occupied orbitals and polarizability data alone. In the present work, our model is extended to predict C_8 and C_{10} coefficients as well. These higher-order coefficients are obtained as easily as C_6 and with comparable accuracy.

6.1 Introduction

The "exchange" or "Fermi" hole is a representation of pair probability in a Slater determinant wavefunction that has tremendous interpretive power. The exchange energy of a Slater determinant may be written in the form

$$E_X = \sum_\sigma \frac{1}{2} \int \int \rho_\sigma(\mathbf{r}_1) \frac{h_{X\sigma}(\mathbf{r}_1, \mathbf{r}_2)}{r_{12}} d^3\mathbf{r}_2 d^3\mathbf{r}_1, \tag{6.1}$$

where σ denotes up or down electron spin, ρ_σ is the σ-spin density, and

$$h_{X\sigma}(\mathbf{r}_1, \mathbf{r}_2) = -\frac{1}{\rho_\sigma(\mathbf{r}_1)} \sum_{ij} \psi_{i\sigma}(\mathbf{r}_1)\psi_{j\sigma}(\mathbf{r}_1)\psi_{i\sigma}(\mathbf{r}_2)\psi_{j\sigma}(\mathbf{r}_2) \tag{6.2}$$

is the σ-spin exchange hole. The summation is over orbitals of σ spin, assumed to be real in the present work. Note that coordinates $\mathbf{r}_1$ and $\mathbf{r}_2$ are not equivalent in Eq. (6.2), and $\mathbf{r}_1$ will be called the "reference" point.

The exchange-hole definition allows us to *visualize* the effects of self-interaction-correction and exchange [72]. It is a conditional probability [112]. When a reference electron is at $\mathbf{r}_1$ the hole measures the depletion of probability, with respect to the total electron density ρ, of finding another same-spin electron at $\mathbf{r}_2$. The probability of finding another same-spin electron "on top" of the reference electron (i.e. at $\mathbf{r}_2 = \mathbf{r}_1$) is completely extinguished,

$$h_{X\sigma}(\mathbf{r}_1, \mathbf{r}_1) = -\rho_\sigma(\mathbf{r}_1), \tag{6.3}$$

in accordance with the Pauli exclusion principle. The hole is always negative, as can be seen by rewriting Eq. (6.2) as

$$h_{X\sigma}(\mathbf{r}_1, \mathbf{r}_2) = -\frac{1}{\rho_\sigma(\mathbf{r}_1)} \left[\sum_i \psi_{i\sigma}(\mathbf{r}_1)\psi_{i\sigma}(\mathbf{r}_2) \right]^2, \tag{6.4}$$

and the hole always contains exactly (minus) one electron:

$$\int h_{X\sigma}(\mathbf{r}_1, \mathbf{r}_2) d^3\mathbf{r}_2 = -1, \tag{6.5}$$

easily proved from Eq. (6.2) and the orthonormality of the orbitals $\psi_{i\sigma}$.

As an electron moves through a system, it is accompanied by this hole. Its shape, in terms of the variable $\mathbf{r}_2$, depends on the electrons instantaneous position $\mathbf{r}_1$. The electron plus its hole has *zero charge* overall [guaranteed by Eq. (6.5)] but a *nonzero dipole moment* in general [84]. Indeed, the dipole moment of the hole and its reference electron is easily obtained by integration over $\mathbf{r}_2$ in Eq. (6.2):

$$\mathbf{d}_{X\sigma}(\mathbf{r}_1) = \left[\frac{1}{\rho_\sigma(\mathbf{r}_1)} \sum_{ij} \mathbf{r}_{ij\sigma} \psi_{i\sigma}(\mathbf{r}_1) \psi_{j\sigma}(\mathbf{r}_1) \right] - \mathbf{r}_1, \tag{6.6}$$

$$\mathbf{r}_{ij\sigma} = \int \mathbf{r}_2 \psi_{i\sigma}(\mathbf{r}_2) \psi_{j\sigma}(\mathbf{r}_2) d^3\mathbf{r}_2. \tag{6.7}$$

Only in the uniform electron gas, or at centers of inversion symmetry in atoms and molecules, does the dipole moment vanish. We hypothesized in Ref. [84] that this *instantaneous in space* dipole moment could be used to generate a dispersion interaction by polarizing a far system according to its polarizability α. After angular integration of the resulting dipole-induced-dipole interaction, integration over reference points $\mathbf{r}_1$, and further heuristic arguments, we obtained a simple formula for the isotropic C_6 dispersion coefficient between systems A and B:

$$C_6 = \frac{< d_X^2 >_A < d_X^2 >_B \alpha_A \alpha_B}{< d_X^2 >_A \alpha_B + < d_X^2 >_B \alpha_A}, \tag{6.8}$$

with $< d_X^2 >$ defined by

$$< d_X^2 >= \sum_\sigma \int \rho_\sigma(\mathbf{r}_1) d_{X\sigma}^2(\mathbf{r}_1) d^3\mathbf{r}_1, \tag{6.9}$$

and the dipole moment $\mathbf{d}_{X\sigma}(\mathbf{r}_1)$ given by Eq. (6.6). These equations apply to atomic or molecular monomers A or B.

Post-Hartree-Fock C_6 coefficients from Eq. (6.8) agree remarkably well with accurate reference data [84, 99]. The somewhat heuristic derivation in Ref. [84], however, is not entirely satisfying. The present work introduces a more rigorous approach. We derive not only a formula for C_6, but formulas for the higher coefficients C_8 and C_{10} as well. We eliminate molecular polarizabilies from the model also. Free atomic polarizabilities of the constituent atoms are used instead. This greatly enhances its convenience and will allow application of the model to *intra*molecular interactions as well.

We begin with a review of the second-order perturbation theory of the dispersion interaction in Section 6.2. We then make approximations to the theory for the case of interatomic interactions in Section 6.3. In Section 6.4 the model is generalized to intermolecular interactions. Section 6.5 offers concluding remarks. The end result is a model of both interatomic and intermolecular C_6, C_8, and C_{10} dispersion coefficients requiring only Hartree-Fock occupied orbitals of the monomers and free atomic polarizabilities. Throughout this work, $\mathbf{d}_{X\sigma}(\mathbf{r}_1)$ is the central object. The model is computationally and conceptually elegant and it works quite well, as will be demonstrated on interatomic and intermolecular test sets in Sections 6.3 and 6.4.

6.2 Perturbation Theory of the Dispersion Interaction

The formulas in this section are from the review of Dalgarno and Davison [2] to which we refer the reader for background information. We restrict ourselves to atomic systems in this and the next Section.

For two non-overlapping atoms A and B, second-order perturbation theory gives the following dispersion energy of interaction:

$$E_{disp} = -\sum_{\ell_A=1}^{\infty}\sum_{\ell_B=1}^{\infty}\frac{\epsilon_2(\ell_A,\ell_B)}{R^{2(\ell_A+\ell_B+1)}}. \tag{6.10}$$

If the ground states of both atoms have zero angular momentum, and if both z-axes point along the internuclear vector, then

$$\epsilon_2(\ell_A,\ell_B) = \lambda(\ell_A,\ell_B)\sum_a\sum_b \frac{|<\psi_A^a|M_{\ell_A}|\psi_A^0>|^2|<\psi_B^b|M_{\ell_B}|\psi_B^0>|^2}{E_A^a+E_B^b-E_A^0-E_B^0}, \tag{6.11}$$

where a and b denote excited states of A and B respectively, M_ℓ denotes the $m=0$ component of the total ℓ-moment operator,

$$M_\ell = \sqrt{4\pi}\sum_i r_i^\ell Y_\ell^0(\Omega_i) \tag{6.12}$$

(with summation over all electrons in A or B as appropriate and with prefactor $\sqrt{4\pi}$ included in the definition for later convenience), and

$$\lambda(\ell_A,\ell_B) = \frac{(2\ell_A+2\ell_B)!}{(2\ell_A+1)(2\ell_B+1)(2\ell_A)!(2\ell_B)!}. \tag{6.13}$$

We now make a "closure" approximation, common in second-order perturbation theory [12], in order to eliminate the summations over excited states. If the denomi-

nator in Eq. (6.11) is replaced by an average excitation energy,

$$E_A^a + E_B^b - E_A^0 - E_B^0 \approx \Delta E_A + \Delta E_B, \tag{6.14}$$

then

$$\epsilon_2(\ell_A, \ell_B) \cong \frac{\lambda(\ell_A, \ell_B)}{\Delta E_A + \Delta E_B} \sum_a \sum_b | < \psi_A^a | M_{\ell_A} | \psi_A^0 > |^2 | < \psi_B^b | M_{\ell_B} | \psi_B^0 > |^2. \tag{6.15}$$

Noting that

$$< \psi_A^0 | M_{\ell_A} | \psi_A^0 > = < \psi_B^0 | M_{\ell_B} | \psi_B^0 > = 0, \tag{6.16}$$

by assumption (since atoms A and B have zero angular momentum and $\ell_A, \ell_B \geq 1$), the excited-state summations over a and b may be extended to include the ground states and, using completeness of the states ψ_A^a and ψ_B^b ($a = 0$ and $b = 0$ included), we get the approximate formula

$$\epsilon_2(\ell_A, \ell_B) \cong \lambda(\ell_A, \ell_B) \frac{< \psi_A^0 | M_{\ell_A}^2 | \psi_A^0 >< \psi_B^0 | M_{\ell_B}^2 | \psi_B^0 >}{\Delta E_A + \Delta E_B}, \tag{6.17}$$

involving ground-state expectation values of the *squared* total ℓ_A-pole and ℓ_B-pole operators in A and B.

The squared multipole operator,

$$M_\ell^2 = 4\pi \sum_i r_i^\ell Y_\ell^0(\Omega_i) \sum_j r_j^\ell Y_\ell^0(\Omega_j), \tag{6.18}$$

contains a one-body part from the diagonal terms and a *two*-body part from the cross terms. Though not problematic in atoms, the two-body part is not amenable to atomic decomposition as will later be required for *molecules* in Section 6.4. We there-

fore propose, in the next section, a simple and elegant *one-electron* approximation for the expectation value of M_ℓ^2 which will easily adapt itself to molecular systems in Section 6.4.

6.3 The Model

When an electron is at distance r from the center of a zero angular momentum (and hence spherically symmetric) atom, the exchange-hole dipole moment $\mathbf{d}_{X\sigma}$ is directed toward the nucleus. Viewed from afar, the dipole field is the same as the field of two unit point charges of opposite sign at distances r and $(r - d_{X\sigma})$ from the nucleus. This is illustrated in Fig. 6.1. The position of the inner positive charge is the mean position of the exchange hole. Notice that, with respect to the nucleus as origin, the point-charge dipole of Fig. 6.1 also has nonzero *quadrupole, octopole, etc.* multipole moments due to its displacement from the nucleus. The ℓ-pole moment of Eq. (6.12) is given by

$$M_\ell = -\sqrt{4\pi}\left[r^\ell - (r - d_{X\sigma})^\ell\right] Y_\ell^0(\Omega), \tag{6.19}$$

when the reference electron is at polar coordinates r and Ω.

Let us eliminate the Ω dependence by *angular averaging* the squared M_ℓ moment as follows:

$$M_\ell^2(\text{angular average}) = \left[r^\ell - (r - d_{X\sigma})^\ell\right]^2. \tag{6.20}$$

If we now assume that the *density-weighted integral*

$$< M_\ell^2 >= \sum_\sigma \int \rho_\sigma(\mathbf{r}) \left[r^\ell - (r - d_{X\sigma})^\ell\right]^2 d^3\mathbf{r} \tag{6.21}$$

is a reasonable substitute for the expectation values of M_ℓ^2 in Eq. (6.17), then a very simple perturbation-theory approximation is obtained:

$$\epsilon_2(\ell_A, \ell_B) \cong \lambda(\ell_A, \ell_B) \frac{< M_{\ell_A}^2 >_A < M_{\ell_B}^2 >_B}{\Delta E_A + \Delta E_B}, \tag{6.22}$$

involving only one-electron integrals in the numerator.

Using $\lambda(1,1) = 2/3$, $\lambda(1,2) = \lambda(2,1) = 1$, $\lambda(1,3) = \lambda(3,1) = 4/5$, and $\lambda(2,2) = 14/5$, and comparing Eq. (6.10) with

$$E_{disp} = -\frac{C_6}{R^6} - \frac{C_8}{R^8} - \frac{C_{10}}{R^{10}} - \dots, \tag{6.23}$$

we derive formulas for C_6, C_8, and C_{10}:

$$C_6 \cong \frac{2}{3} \frac{< M_1^2 >_A < M_1^2 >_B}{\Delta E_A + \Delta E_B}, \tag{6.24}$$

$$C_8 \cong \frac{< M_1^2 >_A < M_2^2 >_B + < M_2^2 >_A < M_1^2 >_B}{\Delta E_A + \Delta E_B}, \tag{6.25}$$

$$\begin{aligned} C_{10} \cong \frac{4}{5} & \frac{< M_1^2 >_A < M_3^2 >_B + < M_3^2 >_A < M_1^2 >_B}{\Delta E_A + \Delta E_B} \\ & + \frac{14}{5} \frac{< M_2^2 >_A < M_2^2 >_B}{\Delta E_A + \Delta E_B}. \end{aligned} \tag{6.26}$$

We stop at C_{10} because the next coefficient, C_{12}, involves fourth-order perturbation theory which will not be considered in this work.

Note that, even though Eqs. (6.24) to (6.26) contain dipole, quadrupole, and octopole moment integrals, only the magnitude of the exchange-hole *dipole* moment $d_{X\sigma}$ is actually needed. In practise, $d_{X\sigma}$ is precomputed at all points of a numerical integration grid using Eq. (6.6), and subsequent numerical evaluation of the multipole

moment integrals is very economical.

It remains to determine the effective atomic excitation energies ΔE_A and ΔE_B. These are hard to deduce from direct physical arguments. We think the best strategy is to extract effective excitation energies from second-order perturbation theory in some independent manner. The perturbation theory of polarizability will be used for this purpose.

For an atom (having zero permanent dipole moment) the second-order perturbation theory of dipole polarizability α gives, after making the same "average excitation energy" approximation as in Section 6.2,

$$\alpha = \frac{2 < \mu^2 >}{3\Delta E}, \tag{6.27}$$

where μ^2 is the square of the total dipole moment operator. See Ref. [12] for a thorough and comprehensible derivation. If the atom is spherically symmetric, then

$$< \mu^2 >=< M_1^2 >, \tag{6.28}$$

where the moment operator is as defined in Eq. (6.12). Solving for ΔE, we obtain

$$\Delta E = \frac{2 < M_1^2 >}{3\alpha}. \tag{6.29}$$

This is what we use for ΔE_A and ΔE_B in Eqs. (6.24) to (6.26), with the approximate one-electron integral of Eq. (6.21) for $< M_1^2 >$. Atomic polarizabilities are taken from readily available tabulations such as Ref. [76].

C_6, C_8, and C_{10} dispersion coefficients for all combinations of the atoms H, He, Ne, Ar, Kr, and Xe have been computed from Hartree-Fock orbitals and compared with accurate reference data in Table 6.1. Orbitals were computed with the fully numerical NUMOL program [78, 79] and all integrations required by the model were

performed "post-Hartree-Fock" on NUMOL numerical grids [77].

There is an abundance of highly accurate C_6 data available in the literature, but few sources of accurate C_8's and C_{10}'s. Very accurate coefficients are known for the H-H and H-He systems [80]. The remainder of the reference data is from many-body perturbation theory calculations (MBPT) with dispersion coefficients obtained from frequency dependent polarizabilities [113, 114].

Our model performs quite well on the 21 interatomic C_6's in Table 6.1, with a mean absolute percent error (MAPE) of 3.4%. For C_8 the model shows good performance, but with a larger MAPE of 21.5%. The MAPE for C_{10} is 8.4%. We cannot rationalize the somewhat larger MAPE for the C_8's compared to the C_6's and the C_{10}'s at this time. Our model is based on several approximations and does not incorporate dynamical correlation effects in the hole. The agreement between our calculated dispersion coefficients and the MBPT results is therefore very encouraging considering the simplicity and the minimal computational cost of our method, a negligible fraction of the cost of the Hartree-Fock orbital calculations.

In the next section, the model is extended from atomic to molecular systems.

6.4 From Atoms to Molecules

We have so far assumed that A and B are zero-angular-momentum, spherically symmetric atoms. Since the multipole integrals of Eq. (6.21) depend on origin for $\ell \geq 2$, it is not immediately clear how to generalize the model to multinuclear systems. We propose a logical method in this section for constructing C_6, C_8 and C_{10} coefficients in intermolecular cases from approximate *interatomic* coefficients.

We assume that, for each of $m = 6$, 8, and 10, an intermolecular C_m can be

written as a sum over interatomic coefficients $C_{m,ij}$:

$$C_m = \sum_i^A \sum_j^B C_{m,ij}. \tag{6.30}$$

Now and hereafter, A and B denote *molecules*, with i referring to an atom in molecule A and j referring to an atom in molecule B. Molecule A (and similarly molecule B) will be partitioned into atoms by Hirshfeld atomic weight functions [88]:

$$w_i(\mathbf{r}) = \frac{\rho_i^{at}(\mathbf{r})}{\sum_n \rho_n^{at}(\mathbf{r})}, \tag{6.31}$$

where ρ^{at} is a sphericalized free atomic density placed at the appropriate nucleus, and the n summation is over all atoms in the molecule. Weight function $w_i(\mathbf{r})$ has value close to 1 at points in the vicinity of nucleus i and close to 0 everywhere else. Moreover, the $w_i(\mathbf{r})$ sum to 1 everywhere:

$$\sum_i w_i(\mathbf{r}) = 1. \tag{6.32}$$

Other partitioning schemes are possible. The Hirshfeld scheme has been used in our previous work [99] and we continue to use it here.

We generalize Eqs. (6.24) to (6.26) to *atoms in molecules* by replacing subscripts A and B with i and j:

$$C_{6,ij} = \frac{2}{3} \frac{< M_1^2 >_i < M_1^2 >_j}{\Delta E_i + \Delta E_j}, \tag{6.33}$$

$$C_{8,ij} \cong \frac{< M_1^2 >_i < M_2^2 >_j + < M_2^2 >_i < M_1^2 >_j}{\Delta E_i + \Delta E_j}, \tag{6.34}$$

$$C_{10,ij} \cong \frac{4}{5}\frac{< M_1^2 >_i < M_3^2 >_j + < M_3^2 >_i < M_1^2 >_j}{\Delta E_i + \Delta E_j} + \frac{14}{5}\frac{< M_2^2 >_i < M_2^2 >_j}{\Delta E_i + \Delta E_j}, \tag{6.35}$$

where $< M_\ell^2 >_i$ is defined by

$$< M_\ell^2 >_i = \sum_\sigma \int w_i(\mathbf{r})\rho_\sigma(\mathbf{r}) \left[r^\ell - (r - d_{X\sigma})^\ell\right]^2 d^3\mathbf{r} \tag{6.36}$$

[i.e. Eq. (6.21) with the atomic partitioning function $w_i(\mathbf{r})$ inserted in the integrand] with a similar formula for atoms j in B. The energy ΔE_i, and similarly ΔE_j, is given by the following generalization of Eq. (6.29):

$$\Delta E_i = \frac{2 < M_1^2 >_i}{3\alpha_i}, \tag{6.37}$$

where α_i is the *effective* polarizability of atom i in molecule A.

For α_i we propose the approximation

$$\alpha_i = \frac{< r^3 >_i}{< r^3 >_{i,free}} \alpha_{i,free}, \tag{6.38}$$

where $< r^3 >_i$ is the integral

$$< r^3 >_i = \int r^3 w_i(\mathbf{r})\rho(\mathbf{r}) d^3\mathbf{r}, \tag{6.39}$$

and $< r^3 >_{i,free}$ is the analogous integral

$$< r^3 >_{i,free} = \int r^3 \rho_{i,free}(\mathbf{r}) d^3\mathbf{r}, \tag{6.40}$$

for the *free* atom i. This approximation is motivated by the qualitative, if not quantitative, general relationship between polarizability and volume. We expound on this

relationship in the Appendix rather than digressing here. We note, however, that this is not the same definition of α_i as in Ref. [99]. Our previous definition [99] involved *molecular* polarizabilities. The new definition, Eq. (6.38), involves only free atomic polarizabilities. We return to this point at the end of the section.

The origin with respect to which r and $(r - d_{X\sigma})$ are defined in Eqs. (6.36) and (6.39) is the position of nucleus i. In Eq. (6.36) we furthermore assume, as in Fig. 6.1, that $\mathbf{d}_{X\sigma}$ is *directed toward nucleus i* when evaluating $< M_\ell^2 >_i$. Since the direction of the exchange-hole dipole moment at any given point in a molecule is surely toward the nearest nucleus, this is physically reasonable. Hirshfeld atoms in molecules are not perfectly spherically symmetric, however, and $\mathbf{d}_{X\sigma}$ is not directed exactly toward nucleus i. Fig. 6.1 is thus an approximation for an atom in a molecule. Its validity will be assessed by looking at computed data.

In Table 6.2, we report C_6, C_8, and C_{10} coefficients for a test set of 18 molecule-atom and molecule-molecule pairs. As in Section 6.3, fully numerical Hartree-Fock computations were carried out on the monomers with the NUMOL program [78, 79] and all moment integrations were performed on NUMOL numerical grids [77]. Free atomic polarizabilities for the effective excitation energies ΔE_i and ΔE_j are from Ref. [76]. The MBPT literature data is from Refs. [113], [114], and [115]. Literature data was unavailable for the C_{10} coefficients of the Cl_2-atom complexes and for H_2-N_2 and N_2-N_2.

Mean absolute percent errors (MAPEs) are 12.7% for C_6, 16.5% for C_8, and 21.2% for C_{10}. These errors are of the same order as the atom-atom pair errors in Section 6.3, thus validating the assumptions and approximations of this section. Again the agreement with accurate data is very encouraging for such a simple and computationally inexpensive method.

On the much more extensive test set of 178 intermolecular C_6's compiled in Ref. [99], we obtain a MAPE of 9.1% compared to the MAPE of 11.1% we previously

obtained [99] using molecular polarizabilities in Eq. (6.8). This is a significant advance, since we now require free atomic polarizabilities only [i.e. see Eq.(6.38)] and no molecular polarizabilities at all.

6.5 Summary and Outlook

The idea, introduced in Ref. [84], that the position-dependent dipole moment of an electron plus its exchange hole can be used to generate C_6 dispersion coefficients, has been extended in this work to C_8 and C_{10} coefficients. A point-charge dipole *at a nonzero distance* from a nucleus (see Fig. 6.1) has quadrupole, octopole, and higher moments as well with respect to that nucleus. This model can be used to estimate, by simple one-electron integrations, total multipole moment expectation values that occur in the perturbation theory of the dispersion interaction. Approximate formulas for C_6, C_8 and C_{10} are thereby derived.

In Ref. [116], we showed how the C_6 model of Refs. [84] and [99] can be transformed into a *density functional* model depending on local density, the local gradient and Laplacian of the density, and the local kinetic energy density. This is possible because $d_{X\sigma}$ can be estimated, at any given point in an atom or molecule, using these local densities [116]. The present $C_6/C_8/C_{10}$ model is similarly transcribable into density functional form. The overall MAPEs for all test systems in Tables 6.1 and 6.2 are, for the orbital-dependent $d_{X\sigma}$ of Eq. (6.6), 7.7% for C_6, 19.2% for C_8, and 12.8% for C_{10}. The analogous MAPEs for the density functional approximation to $d_{X\sigma}$ are 10.9% for C_6, 16.3% for C_8, and 13.3% for C_{10}. We see that the density functional model works about as well as the explictly orbital dependent model.

Given the tremendous simplicity and economy of the model, it is very gratifying that its results compare well with accurate reference data. In future work, C_8 and C_{10} will be incorporated into modelling of intermolecular potential energy surfaces. We

have already developed a post-Hartree-Fock approach to intermolecular interactions [99, 116] that works remarkably well using C_6. The π-stacked conformations of the benzene dimer stand out, however, as the poorest cases [116]. Addition of C_8 and C_{10} terms may offer improvement. Future applications of the model to intramolecular dispersion energies are also planned.

6.6 Appendix: Atomic Polarizability and Volume

In Section 6.4, the effective polarizability α_i of an atom in a molecule is related to its free polarizability $\alpha_{i,free}$ by Eq. (6.38):

$$\alpha_i = \frac{< r^3 >_i}{< r^3 >_{i,free}} \alpha_{i,free}, \tag{6.41}$$

where $< r^3 >_i$ and $< r^3 >_{i,free}$ are the density-weighted integrals of r^3 over the Hirshfeld atom-in-the-molecule density and the free-atom density respectively. The density-weighted r^3 integration is a simple, parameter-free, numerical measure of atomic "volume", which is in turn related to polarizability.

Polarizability has the same dimensionality as volume. Classical models of polarizability, such as the conducting sphere model [117] or the uniform-density sphere model [118], yield a polarizability equal to R^3 where R is the radius of the sphere. For real chemical systems, strong linear correlations between polarizability and volume have been empirically demonstrated [119]. It is therefore reasonable to propose, as in Eq. (6.38), that the ratio of the polarizability of a Hirshfeld atom in a molecule to its free polarizability is equal to the ratio of its Hirshfeld *volume* to its free *volume*. Considering that Hirshfeld atomic densities are only slightly perturbed from free densities, this would seem to be a sound proposition.

Table 6.1: C_6, C_8, and C_{10} coefficients for atomic pairs (atomic units)

Pair	C_6 calc.	C_6 lit.	C_8 calc.	C_8 lit.	C_{10} calc.	C_{10} lit.
H-H[a]	6.75	6.49	152.0	124.4	3299	3286
H-He[a]	2.98	2.82	48.25	41.75	760.9	858.7
H-Ne[b]	5.69	5.69	111.6	97.8	1969	2221
H-Ar[b]	20.12	19.86	560.4	442.1	12703	12617
H-Kr[b]	29.43	29.15	920.2	732.2	22743	23441
H-Xe[b]	45.12	44.14	1687	1357	47273	51088
He-He[c]	1.64	1.46	16.10	14.11	157.7	183.2
He-Ne[b]	3.09	3.07	40.96	36.18	453.2	545.1
He-Ar[b]	9.79	9.57	210.8	167.5	3277	3701
He-Kr[b]	14.05	13.65	350.3	280.0	6122	7257
He-Xe[b]	20.86	19.92	647.8	525.0	13316	16674
Ne-Ne[b]	5.83	6.55	97.32	90.34	1277	1536
Ne-Ar[b]	18.60	19.75	464.0	390.1	8551	9335
Ne-Kr[b]	26.70	28.01	757.4	638.1	15563	17658
Ne-Xe[b]	39.71	40.52	1370	1162	32748	38978
Ar-Ar[b]	62.74	64.54	2082	1623	51891	49063
Ar-Kr[b]	90.95	93.16	3329	2617	91195	88260
Ar-Xe[b]	137.4	138.0	5871	4669	183934	184250
Kr-Kr[b]	132.1	135.1	5286	4187	158503	155450
Kr-Xe[b]	200.1	201.3	9234	7389	315196	316030
Xe-Xe[b]	304.7	302.3	15924	12807	615431	619840
MAPE[d]	3.4	–	21.5	–	8.4	–

[a]Ref. [80]. [b]Ref. [113]. [c]Ref. [114]. [d]MAPE: mean absolute percent error.

Table 6.2: C_6, C_8, and C_{10} coefficients for molecule-atom and molecule-molecule pairs (atomic units).

Pair	C_6 calc.	C_6 lit.	C_8 calc.	C_8 lit.	C_{10} calc.	C_{10} lit.
H_2-He[a]	4.78	4.05	59.03	55.43	780	1005
H_2-Ne[b]	9.08	8.19	143.3	130.0	2086	2611
H_2-Ar[b]	31.24	27.76	750.9	588.8	14254	15539
H_2-Kr[b]	45.48	40.41	910.2	975.5	26081	29289
H_2-Xe[b]	69.15	60.54	2321	1808	55646	64764
N_2-He[c]	10.84	9.76	202.5	219.2	3046	5184
N_2-Ne[c]	20.61	20.23	455.8	497.6	8000	12842
N_2-Ar[c]	71.77	65.52	2179	1982	51103	64192
N_2-Kr[c]	104.71	94.40	3537	3139	91053	112990
N_2-Xe[c]	159.8	139.5	6375	5452	187446	229260
Cl_2-He[c]	21.64	23.48	508.1	810.3	–	–
Cl_2-Ne[c]	41.14	47.98	1107	1770	–	–
Cl_2-Ar[c]	142.9	161.5	5022	6765	–	–
Cl_2-Kr[c]	208.3	234.8	8034	10505	–	–
Cl_2-Xe[c]	317.5	351.2	14190	17688	–	–
H_2-H_2[a]	15.70	12.15	233.5	212.6	3799	4741
H_2-N_2[a]	36.24	30.54	768.5	771.7	–	–
N_2-N_2[a]	83.89	75.63	2310	2489	–	–
MAPE[d]	12.7	–	16.5	–	21.2	–

[a]Ref. [114]. [b]Ref. [113]. [c]Ref. [115]. [d]MAPE: mean absolute percent error.

Figure 6.1: Exchange-hole dipole geometry (e^- is the reference position of a σ-spin electron and h^+ is the mean position of its exchange hole).

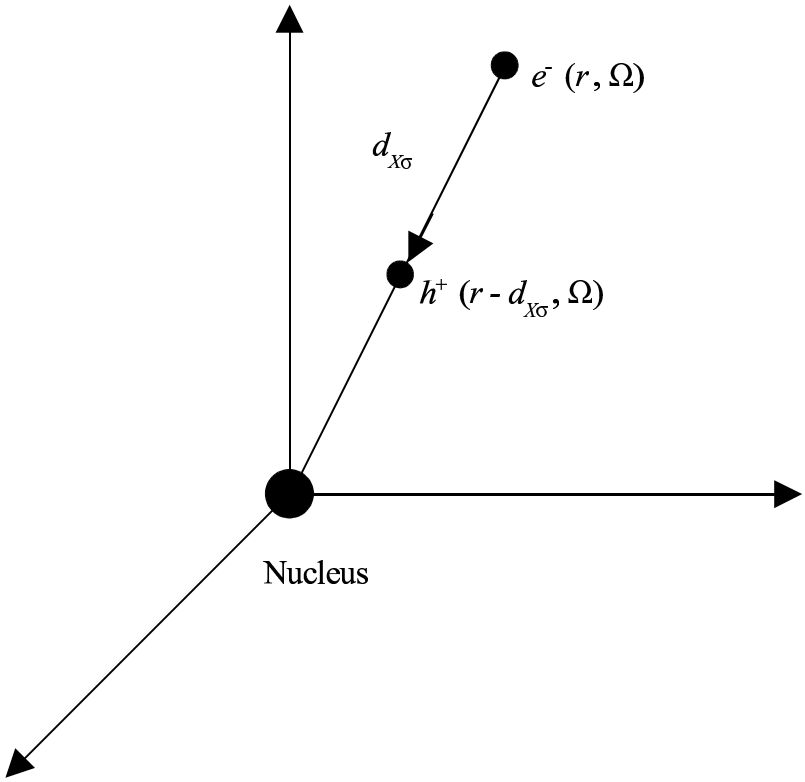

Chapter 7

A Post-Hartree-Fock Model of Intermolecular Interactions: Inclusion of Higher-Order Corrections

Original reference: E. R. Johnson and A. D. Becke, J. Chem. Phys. **124**, 174104 (2006).

Abstract

We have previously demonstrated that the dipole moment of the exchange hole can be used to derive intermolecular C_6 dispersion coefficients [84]. This was subsequently the basis for a novel post-Hartree-Fock model of intermolecular interactions [99]. In the present work, the model is extended to include higher-order dispersion coefficients C_8 and C_{10}. The extended model performs very well for prediction of intermonomer separations and binding energies of 45 van der Waals complexes. In particular, it performs twice as well as basis-set extrapolated MP2 theory for dispersion-bound

complexes, with minimal computational cost.

7.1 Introduction

Satisfactory treatment of the London dispersion interaction is a long-standing problem in computational chemistry. While correlated *ab initio* methods with large basis sets can accurately model this interaction, Hartree-Fock (HF) and contemporary functionals in Density Functional Theory (DFT) do not contain the physics of dispersion. DFT treatments that do include dispersion are either too computationally expensive to be practical in large chemical systems [59, 61, 21] or require extensive parameterization [120].

A promising alternative is to add the following explicit dispersion energy correction to the HF or DFT energy [22, 23, 63, 64, 65, 66].

$$E_{disp} = -\sum_{i>j} \frac{C_{6,ij}}{R_{ij}^6}. \tag{7.1}$$

The summation is over all atom pairs in the system and a suitable cut-off is also required to prevent a divergent dispersion energy at small internuclear separations R_{ij}. The values of the C_6 dispersion coefficients are typically determined [22, 23, 63, 64, 65, 66] by fitting to experimental data and their use is therefore limited to atom types included in the fit sets.

In previous work, we have developed a theoretical model that allows accurate calculation of dispersion coefficients based on the exchange-hole dipole moment [84]. The model has been tested on C_6 dispersion coefficients, intermonomer separations, and binding energies of a variety of van der Waals (vdW) complexes [99, 116]. It performs significantly better than contemporary DFTs on dispersion-bound systems, but yields large errors in the binding energies of π-stacked complexes. We believe that

this failure is due to neglect of higher-order terms, involving C_8 and C_{10} coefficients, in the dispersion energy expansion [116].

Our original C_6 theory has recently been generalized to include higher-order dispersion coefficients and also to eliminate the need for molecular polarizability information [121]. In the present work, an improved post-Hartree-Fock model of intermolecular interactions involving C_6, C_8, and C_{10} terms is proposed. The following formula, suitably cut off at small internuclear separations, is used for the dispersion energy [63]:

$$E_{disp} = -\sum_{i>j} \left(\frac{C_{6,ij}}{R_{ij}^6} + \frac{C_{8,ij}}{R_{ij}^8} + \frac{C_{10,ij}}{R_{ij}^{10}} \right). \tag{7.2}$$

The model is calibrated on the binding energies and minimum-energy separations of a test set of 45 vdW complexes.

7.2 The Present Model

7.2.1 Dispersion Coefficients

In this section, we review our exchange-hole-based theory of dispersion coefficients. Consider an electron of σ spin at reference position $\mathbf{r}_1$ in an atom or molecule. The electron's exchange or Fermi hole, $h_{X\sigma}(\mathbf{r}_1, \mathbf{r}_2)$, measures the depletion of probability, with respect to the total σ-spin electron density ρ_σ, of finding another same-spin electron at position $\mathbf{r}_2$:

$$h_{X\sigma}(\mathbf{r}_1, \mathbf{r}_2) = -\frac{1}{\rho_\sigma(\mathbf{r}_1)} \sum_{ij} \psi_{i\sigma}(\mathbf{r}_1)\psi_{j\sigma}(\mathbf{r}_1)\psi_{i\sigma}(\mathbf{r}_2)\psi_{j\sigma}(\mathbf{r}_2). \tag{7.3}$$

The $\psi_{i\sigma}$ are real, occupied, Hartree-Fock or Kohn-Sham orbitals. The electron plus its hole always has zero net charge, but generally a *non-zero dipole moment*. The

dipole moment $\mathbf{d}_{X\sigma}(\mathbf{r}_1)$ of a reference electron and its associated exchange hole is obtained from Eq. (7.3) by integration over $\mathbf{r}_2$:

$$\mathbf{d}_{X\sigma}(\mathbf{r}_1) = \left[\frac{1}{\rho(\mathbf{r}_1)}\sum_{ij}\psi_{i\sigma}(\mathbf{r}_1)\psi_{j\sigma}(\mathbf{r}_1)\int \mathbf{r}_2\psi_{i\sigma}(\mathbf{r}_2)\psi_{j\sigma}(\mathbf{r}_2)d^3\mathbf{r}_2\right] - \mathbf{r}_1. \tag{7.4}$$

We proposed [84] on heuristic grounds that this position-dependent dipole moment could be used to generate a dispersion interaction by polarizing neighboring atoms or molecules. Second-order perturbation theory [2] was then used in Ref. [121] to obtain a more general formula for dispersion coefficients of high order. We will summarize the resulting equations here and direct interested readers to Ref. [121] for a complete derivation.

From second-order perturbation theory [2, 121], one obtains the following approximate dispersion energy for two non-overlapping, zero angular momentum atoms A and B:

$$E_{disp} = -\sum_{\ell_A=1}^{\infty}\sum_{\ell_B=1}^{\infty}\frac{\epsilon_2(\ell_A,\ell_B)}{R^{2(\ell_A+\ell_B+1)}}, \tag{7.5}$$

$$\epsilon_2(\ell_A,\ell_B) = \lambda(\ell_A,\ell_B)\frac{<\Psi_A^0|M_{\ell_A}^2|\Psi_A^0><\Psi_B^0|M_{\ell_B}^2|\Psi_B^0>}{\Delta E_A + \Delta E_B}, \tag{7.6a}$$

$$\lambda(\ell_A,\ell_B) = \frac{(2\ell_A+2\ell_B)!}{(2\ell_A+1)(2\ell_B+1)(2\ell_A)!(2\ell_B)!}, \tag{7.6b}$$

where ΔE is an "average" atomic excitation energy and Ψ^0 is a ground-state atomic wavefunction. This expression involves ground-state expectation values of the squared

total multipole operator

$$M_\ell^2 = 4\pi \sum_i r_i^\ell Y_\ell^0(\Omega_i) \sum_j r_j^\ell Y_\ell^0(\Omega_j), \tag{7.7}$$

where i and j are electron labels and Y_ℓ^0 are spherical harmonics. Its ground-state expectation value is approximated in Ref. [121] by a simple integration over the position-dependent multipole moments of the electron and its exchange hole.

When an electron is at a distance r from the nucleus of an atom, the exchange-hole dipole moment is directed toward the nucleus. The electron and the *mean* position of its exchange hole can be viewed as a pair of point charges at points $e^- = (r, \Omega)$ and $h^+ = (r - d_{X\sigma}, \Omega)$, where $d_{X\sigma}$ is the magnitude of the exchange-hole dipole moment of Eq. (7.4). This pair of point charges has non-zero quadrupole, octopole, and higher-order multipole moments with respect to the nucleus as well, given by

$$M_\ell = -\sqrt{4\pi} \left[r^\ell - (r - d_{X\sigma})^\ell \right] Y_\ell^0(\Omega). \tag{7.8}$$

We approximate the expectation value of M_ℓ^2 by the following density-weighted integral:

$$< M_\ell^2 >= \sum_\sigma \int \rho_\sigma(\mathbf{r}) \left[r^\ell - (r - d_{X\sigma})^\ell \right]^2 d^3\mathbf{r}. \tag{7.9}$$

For an atom i *within a molecule*, this is generalized by inserting a Hirshfeld atomic partitioning weight, $w_i(\mathbf{r})$, into the integrand:

$$< M_\ell^2 >_i= \sum_\sigma \int w_i(\mathbf{r}) \rho_\sigma(\mathbf{r}) \left[r^\ell - (r - d_{X\sigma})^\ell \right]^2 d^3\mathbf{r}. \tag{7.10}$$

The Hirshfeld atomic partitioning weight [88] is defined by

$$w_i(\mathbf{r}) = \frac{\rho_i^{at}(\mathbf{r})}{\sum_n \rho_n^{at}(\mathbf{r})}, \tag{7.11}$$

where ρ_i^{at} is a sphericalized free atomic density placed at nucleus i and the n summation is over all atoms in the system. By construction, $w_i(\mathbf{r})$ approaches 1 near nucleus i and approaches 0 everywhere else, and the weights sum to 1 at every point in the system.

For the "average" atomic excitation energy, ΔE, we use the second-order perturbation theory of polarizability [12]:

$$\Delta E = \frac{2 < M_1^2 >}{3\alpha}. \tag{7.12}$$

The dispersion coefficients in Eq. (7.2) are then obtained from Eqs. (7.5) and (7.6), and the expectation value approximation of Eq. (7.10), as follows:

$$C_{6,ij} = \frac{\alpha_i \alpha_j < M_1^2 >_i < M_1^2 >_j}{< M_1^2 >_i \alpha_j + < M_1^2 >_j \alpha_i}, \tag{7.13}$$

$$C_{8,ij} = \frac{3}{2} \frac{\alpha_i \alpha_j \left(< M_1^2 >_i < M_2^2 >_j + < M_2^2 >_i < M_1^2 >_j\right)}{< M_1^2 >_i \alpha_j + < M_1^2 >_j \alpha_i}, \tag{7.14}$$

$$C_{10,ij} = \frac{6}{5} \frac{\alpha_i \alpha_j \left(< M_1^2 >_i < M_3^2 >_j + < M_3^2 >_i < M_1^2 >_j\right)}{< M_1^2 >_i \alpha_j + < M_1^2 >_j \alpha_i} + \frac{21}{5} \frac{\alpha_i \alpha_j < M_2^2 >_i < M_2^2 >_j}{< M_1^2 >_i \alpha_j + < M_1^2 >_j \alpha_i}, \tag{7.15}$$

where α_i is the effective *atom-in-molecule* polarizability of atom i. We estimate this effective polarizability by exploiting the well-known empirical relationship between

polarizability and volume [117, 118, 119]. Thus, for α_i, we make the approximation

$$\alpha_i = \frac{< r^3 >_i}{< r^3 >_{i,free}} \alpha_{i,free}, \tag{7.16}$$

where $\alpha_{i,free}$ is the *free* atomic polarizability, taken from readily available tabulations [76], and the expectation value $< r^3 >_i$ is assumed to be a measure of effective volume. For atom i in the molecule,

$$< r^3 >_i = \int r^3 w_i(\mathbf{r}) \rho(\mathbf{r}) d^3\mathbf{r}, \tag{7.17}$$

and for the free atom i,

$$< r^3 >_{i,free} = \int r^3 \rho_{i,free}(\mathbf{r}) d^3\mathbf{r}. \tag{7.18}$$

This simple theory of dispersion coefficients only requires time-independent *occupied* HF orbitals, and free atomic polarizabilities. Nevertheless, it gives accurate interatomic and intermolecular C_6, C_8, and C_{10} values compared to many-body perturbation theory results [121].

7.2.2 Damped Dispersion Energy

The dispersion coefficients of the previous section will be used in Eq. (7.2) for the dispersion energy. However, Eq. (7.2) must be modified to prevent negatively infinite value if any internuclear separation approaches zero. In our previous work [99, 116], we introduced an energy-based C_6 cut-off of the form

$$E_{disp} = -\sum_{i>j} \frac{C_{6,ij}}{(\kappa C_{6,ij}/E_{C,ij}) + R_{ij}^6}, \tag{7.19}$$

where $E_{C,ij}$ is the sum of the free atomic correlation energies of atoms i and j, and κ is a universal parameter of order ca. 1000. It is not clear how to generalize this energy-based C_6 cut-off to C_8 and C_{10} terms, since we do not know the relative energy contributions of these three terms in the limit of small internuclear separations.

Here we consider cut-offs depending on *separation* rather than energy. Many separation-dependent cut-off formulae have been proposed [22, 63, 86] based on vdW radii which are empirical and not well defined for all atom types. Knowledge of higher-order dispersion coefficients, however, allows us to determine effective vdW radii non-empirically.

At large internuclear separations, the dispersion energy terms decrease in magnitude as the order of the terms increases. As R_{ij} approaches zero, however, the higher-order terms diverge faster than the lower-order terms and the ordering reverses. This is illustrated for the neon dimer in Fig. 7.1, which plots the C_6, C_8, and C_{10} dispersion terms as a function of internuclear separation. The terms cross on the steep portion of the curve where the dispersion energy is rapidly changing with separation. There is therefore a "critical" interatomic separation $R_{c,ij}$ where the three dispersion terms are roughly equal in magnitude.

$$\frac{C_{6,ij}}{R_{c,ij}^6} \approx \frac{C_{8ij}}{R_{c,ij}^8} \approx \frac{C_{10,ij}}{R_{c,ij}^{10}}. \tag{7.20}$$

For interatomic separations near $R_{c,ij}$, Eq. (7.2) for the asymptotic series expansion of the dispersion energy is no longer valid and the series must be significantly damped.

Solving for the critical separation yields three possible definitions,

$$R_{c,ij} \approx \left(\frac{C_{8,ij}}{C_{6,ij}}\right)^{1/2} \approx \left(\frac{C_{10,ij}}{C_{6,ij}}\right)^{1/4} \approx \left(\frac{C_{10,ij}}{C_{8,ij}}\right)^{1/2}. \tag{7.21}$$

The first of these has been suggested previously [122] as an approximate measure of

atomic size. Here we have two more possibilities. The critical atomic radius, $\frac{1}{2}R_{c,ii}$, obtained from each of these definitions is shown in Table 7.1 for the homonuclear free atom pairs of H, He, C, N, O, F, Ne, Si, P, S, Cl, and Ar. The three values of $\frac{1}{2}R_{c,ii}$ for each homonuclear pair differ slightly and span a range of 0.2 Å or less, with $(C_{8,ii}/C_{6,ii})^{1/2} > (C_{10,ii}/C_{6,ii})^{1/4} > (C_{10,ii}/C_{8,ii})^{1/2}$. In the remainder of this work, we take $R_{c,ij}$ to be the *average* of these three values.

We propose the following very simple expression for the damped dispersion energy:

$$E_{disp} = -\sum_{i>j}\left(\frac{C_{6,ij}}{R_{vdW,ij}^6 + R_{ij}^6} + \frac{C_{8,ij}}{R_{vdW,ij}^8 + R_{ij}^8} + \frac{C_{10,ij}}{R_{vdW,ij}^{10} + R_{ij}^{10}}\right), \tag{7.22}$$

where $R_{vdW,ij}$ is a sum of effective vdW radii of atoms i and j which will be related to our non-empirical $R_{c,ij}$. The dispersion energy is damped by a factor of 2 when $R_{ij} = R_{vdW,ij}$. When $R_{ij} >> R_{vdW,ij}$ the dispersion energy approaches the proper limiting form of Eq. (7.2). As R_{ij} approaches zero, the dispersion energy approaches a constant.

To ensure that the dispersion energy is sufficiently damped near the critical separation, $R_{vdW,ij}$ should be larger than $R_{c,ij}$. We assume a linear relationship as in Ref. [59]:

$$R_{vdW,ij} = a_1 R_{c,ij} + a_2, \tag{7.23}$$

where a_1 and a_2 are universal (i.e. atom independent) parameters determined in Section 7.4 by minimizing the root-mean-square percent error in the binding energies of 45 intermolecular complexes. The best-fit values are $a_1 = 0.83$ and $a_2 = 1.55$Å. The resulting vdW atomic radii ($\frac{1}{2}R_{vdW,ii}$) of selected homonuclear atom pairs are shown in Table 7.1 and in Fig. 7.2.

Fig. 7.2 reveals a strong linear correlation between $\frac{1}{2}R_{vdW,ii}$ and the *atomic* radii

of Clementi *et al.* [123] ($R^2 = 0.984$). While linearly related to the atomic radius for *free* atomic pairs, the vdW radius defined here is a more flexible quantity since it is a function of interatomic dispersion coefficients for atoms *within a molecule*. For example, the electron density of the hydrogen atom is more compact in the H_2 molecule than in the free atom. Thus, the effective vdW radius of hydrogen should be significantly less in H_2. Our calculated values indeed reflect this expectation, with $\frac{1}{2}R_{vdW,\mathrm{HH}} = 1.81$Å for the free H atom and $\frac{1}{2}R_{vdW,\mathrm{HH}} = 1.64$Å for H in H_2.

Note that Eq. (7.22) for the damped dispersion energy implies that the C_6, C_8, and C_{10} terms are all damped by the same 1/2 factor at $R_{ij} = R_{vdW,ij}$. It has been demonstrated for some simple systems, in Ref. [122], that the C_{10} term is in fact damped faster than the C_8 term, which is in turn damped faster than the C_6 term. Despite its simplicity, Eq. (7.22) yields *total* dispersion energy curves in good agreement with those obtained in Ref. [122]. It is apparently not necessary to complicate our model by using a different R_{vdW} for each dispersion term. The component terms of our damped dispersion energy are shown in Fig. 7.3 for the neon dimer.

The damped dispersion energy of Eq. (7.22), the dispersion coefficients of Eqs. (7.13)-(7.15), and Eqs. (7.21) and (7.23) for the effective vdW separations, comprise our dispersion model. The dispersion coefficients and critical separations of Eq. (7.21) are parameter free. Only two *universal* parameters, a_1 and a_2, are needed in Eq. (7.23). The dispersion energy is obtained from time-independent, occupied HF orbitals and free atomic polarizabilities. The computational cost is much less than that required to compute the HF orbitals themselves.

7.3 Method of Calculation

The present dispersion model has been calibrated on a test set of minimum-energy intermolecular separations and binding energies (BEs) of 45 vdW complexes. The

test set is the same as in Ref. [116], with the addition of the four naphthalene dimer conformations [124] shown in Fig. 7.4.

It is not sufficient to add a dispersion correction to the Hartree-Fock energy alone. Intermolecular interaction energies are also strongly affected by dynamical correlation. As in our previous work [99, 116], we use the Becke-Roussel modification [47] of the dynamical correlation functional of Becke [39] to obtain the dynamical correlation energy. This will be denoted E_C^{BR}. BEs are thus obtained from differences in the following total energy,

$$E_{total} = E_{\mathrm{HF}} + E_C^{\mathrm{BR}} + E_{disp}. \tag{7.24}$$

All calculations use the post-Hartree-Fock methodology described in our previous work [116]. HF/aug-cc-pvtz calculations were performed on all species using the Gaussian 98 program [49] to obtain the HF orbitals. The E_C^{BR} dynamical correlation energy and all expectation values required for the dispersion coefficients were then obtained from the HF orbitals by numerical integrations [77].

The geometries of all monomers except benzene and naphthalene were optimized using CCSD/aug-cc-pvtz. The geometry of benzene was taken from Ref. [104]. The naphthalene geometry was optimized using MP2/6-31G* [124]. Counterpoise [94] corrected HF/aug-cc-pvtz potential energy surfaces (PES) were generated for each of the complexes by keeping the monomer geometries fixed and varying up to three intermonomer coordinates in increments of 0.1 Å or 5°. Post-HF evaluations of $E_{\mathrm{C}}^{\mathrm{BR}}$ and E_{disp} were performed for the complex at each point on the PES and on the separated monomers (not counterpoise corrected). The point on the PES with the lowest total energy was deemed the optimized geometry of the complex. BEs were computed as the total energy difference between the optimized complex and the separated monomers. The values of a_1 and a_2 in Eq. (7.23) were fit to minimize the

root-mean-square percent error in the calculated BEs. Their optimum values are $a_1 = 0.83$ and $a_2 = 1.55$ Å.

7.4 Results and Discussion

Table 7.2 lists the optimized intermonomer separations and BEs obtained with our model compared to high level reference data [13, 90, 91, 92, 97, 99, 104, 105, 106, 107, 108, 109, 110, 111, 124, 125], generally from CCSD(T) or W1 theory [126]. BEs from the MP2 method extrapolated to the basis-set limit, or from calculations using basis sets of at least triple-zeta quality where extrapolated data was unavailable, are also shown. See Table 7.2 for individual references. The complexes are divided into classes according to the dominant type of vdW interaction involved, though in many cases the binding may involve several interaction types.

The agreement between our calculated intermonomer separations and the high-level reference data is excellent, with a mean absolute error (MAE) of 0.06 Å and a maximum error of only 0.3 Å (for the slipped-parallel conformation of the benzene dimer). On BEs, our model performs twice as well as MP2 for dispersion-bound complexes and performs similarly for dipole-induced-dipole and dipole-dipole interactions. MP2 performs somewhat better, however, for H-bonded complexes. Overall, our model gives a more balanced treatment of intermolecular interactions than MP2. Our mean absolute percent error (MAPE) in binding energies is 14.1% and maximum error is -37% (for tetrafluoromethane dimer), compared to the MP2 MAPE of 24.1% and maximum error of 110% (for the parallel conformation of the naphthalene dimer).

The present work is a major improvement over our earlier work [99, 116]. We no longer require molecular polarizability data, and the earlier severe underestimation of the BEs of π-stacked complexes is largely overcome. Although some underestimation does remain in the parallel conformation of the benzene dimer (-31%, the third largest

BE error in our test set) the present method outperforms both conventional DFTs and MP2. This can be seen in Fig. 7.5, which shows PESs of the parallel benzene dimer from several levels of theory. The CCSD(T) and MP2 curves were obtained from the work of Sherrill [104]. B971 is chosen as representative of "standard" DFTs because it was found to be the best standard DFT for calculation of BEs of vdW complexes in Ref. [110]. HF and B971 give qualitatively incorrect behaviour, showing no binding and a repulsive PES at large separations. Conversely, MP2 drastically overbinds by a factor of 2. The present method gives a PES that best resembles the CCSD(T) result. This is particularly impressive considering that our method has virtually no cost beyond a standard HF or DFT calculation and is therefore significantly more practical than MP2 for large systems.

Since our model involves C_6, C_8, and C_{10} terms, it is interesting to analyse their relative contributions to the dispersion energy. Table 7.3 gives a breakdown of the dispersion energy into its components for each complex at its optimum geometry. We see that C_8 and C_{10} terms have large effects on the binding energies. On average, the contributions to the dispersion energy are 58% from C_6, 29% from C_8, and 13% from C_{10}. This emphasizes the importance of including these higher-order terms in dispersion models.

Examination of Table 7.3 also explains the failure of our previous C_6-based model for π-stacked systems [116]. For the majority of the dispersion bound complexes considered here, the dispersion energy is approximately equal to the binding energy at the minimum-energy separation. However, for the π-stacked complexes, P-$(C_6H_6)_2$, SP-$(C_6H_6)_2$, P-$(C_{10}H_8)_2$, and PC-$(C_{10}H_8)_2$, there is significant intermonomer Hartree-Fock repulsion at the minimum-energy separation which is compensated by a dispersion energy relatively larger than the binding energy. Though C_8 and C_{10} terms typically account for only 40% of the dispersion energy, BEs near zero would be given by our model for π-stacked dimers if these terms were omitted. Consider, for ex-

ample, the methane dimer and the P-benzene dimer. The dispersion energy for the methane dimer is 0.68 kcal/mol compared to a BE of 0.63 kcal/mol. Thus, neglect of higher-order terms would reduce both the dispersion energy and the BE by about 40%. For P-benzene, however, the dispersion energy is 2.40 kcal/mol compared to a BE of 1.17 kcal/mol. Neglect of higher-order terms in this case would reduce the dispersion energy again by about 40%, but would reduce the BE by an enormous 85%.

7.5 Conclusions and Future Work

The present post-Hartree-Fock dispersion model gives an excellent treatment of vdW interactions, with a MAE of 0.06Å for intermonomer separations and a MAPE of 14.1% for BEs in a 45-complex test set. Unlike popular existing DFTs, it gives the correct attractive asymptotic dispersion energy behaviour. The model also outperforms MP2 theory on dispersion-bound complexes by a factor of roughly 2. The inclusion of higher-order dispersion coefficients overcomes the deficiencies in our previous C_6-only model for π-stacked complexes.

Unlike our previous model, the present model does not rely on molecular polarizability data. It therefore might be very useful in protein modeling and in other biological applications. In future work, the model will be applied to cases where intramolecular vdW interactions may have an important effect on conformational energies. Also, we plan to combine the present dispersion model with the real-space non-dynamical correlation model of Becke [25] to obtain a density-functional theory robust enough to handle all correlation types encountered in chemistry.

Table 7.1: Calculated critical and vdW radii and Clementi atomic radii R_A from Ref. [123]. All values are in Å.

Atom	$\frac{1}{2}(C_8/C_6)^{1/2}$	$\frac{1}{2}(C_{10}/C_6)^{1/4}$	$\frac{1}{2}(C_{10}/C_8)^{1/2}$	Average	$\frac{1}{2}R_{vdW}$	R_A
H	1.26	1.24	1.23	1.24	1.81	0.53
He	0.83	0.83	0.82	0.83	1.46	0.31
C	1.48	1.41	1.35	1.42	1.95	0.67
N	1.33	1.27	1.20	1.27	1.83	0.56
O	1.25	1.19	1.13	1.19	1.76	0.48
F	1.16	1.09	1.03	1.10	1.68	0.42
Ne	1.08	1.01	0.95	1.01	1.62	0.38
Si	2.02	1.92	1.82	1.92	2.37	1.11
P	1.84	1.74	1.63	1.74	2.22	0.98
S	1.73	1.63	1.53	1.63	2.13	0.88
Cl	1.62	1.52	1.41	1.52	2.04	0.79
Ar	1.52	1.42	1.32	1.42	1.95	0.71

Table 7.2: Minimum-energy separations and binding energies of vdW complexes. Mean absolute errors (MAE) in Å are shown for separations and mean absolute percent errors (MAPE) are shown for binding energies.

Complex	Separation (Å)		Binding Energy (kcal/mol)		
	This work	High level	This work	MP2	High level
Dispersion					
He_2	3.0	3.0[a]	0.023	0.013[b]	0.022[a]
He-Ne	3.0	3.0[a]	0.042	0.023[b]	0.041[a]
He-Ar	3.5	3.5[a]	0.063	0.043[b]	0.057[a]
Ne_2	3.0	3.1[a]	0.076	0.042[b]	0.084[a]
Ne-Ar	3.5	3.5[a]	0.116	0.092[b]	0.134[a]
Ar_2	3.9	3.8[a]	0.240	0.277[b]	0.285[a]
L-He-N_2 [c]	3.9	3.9[d]	0.051	0.038[e]	0.053[d]
T-He-N_2 [f]	3.4	3.4[d]	0.073	0.055[e]	0.066[d]
He-FCl	4.0	3.9[g]	0.066	0.075[e]	0.097[g]
FCl-He	3.6	3.5[g]	0.137	0.144[e]	0.182[g]
Ne-CH_4	3.4	3.5[h]	0.17	0.13[e]	0.22[h]
Ne-C_6H_6	3.4	3.2[h]	0.35	0.43[e]	0.47[h]
CH_4-C_2H_4	4.2	4.2[i]	0.61	0.54[b]	0.50[i]
$(CH_4)_2$	3.7	3.6[h]	0.63	0.48[b]	0.51[h]
$(CF_4)_2$	4.0	4.0[j]	0.49	0.65[j]	0.78[j]
SiH_4-CH_4	3.8	3.8[k]	0.90	0.76[b]	0.81[k]
CH_4-C_6H_6	3.8	3.8[l]	1.50	1.74[l]	1.23[l]
$(C_2H_2)_2$	4.2	4.2[h]	1.70	1.50[e]	1.34[h]
$(CO_2)_2$	3.6	3.6[m]	1.50	1.36[m]	1.37[m]
$(OCS)_2$	3.9	3.8[n]	1.46	1.40[n]	1.40[n]
$(C_2H_4)_2$	3.8	3.8[h]	1.63	1.56[b]	1.42[h]
P-$(C_6H_6)_2$ [o]	4.1	3.9[p]	1.17	3.44[p]	1.70[p]
T-$(C_6H_6)_2$ [f]	5.0	5.0[p]	2.70	3.60[p]	2.61[p]
SP-$(C_6H_6)_2$ [q]	4.2	3.9[p]	2.10	4.87[p]	2.62[p]
P-$(C_{10}H_8)_2$ [o]	4.0	3.8[r]	2.71	7.93[r]	3.78[r]
PC-$(C_{10}H_8)_2$ [s]	3.8	3.6[r]	3.96	10.45[r]	5.28[r]
T-$(C_{10}H_8)_2$ [f]	5.1	5.0[r]	4.80	6.56[r]	4.34[r]
TC-$(C_{10}H_8)_2$ [t]	5.3	5.2[r]	3.33	4.68[r]	3.09[r]
MA(P)E	0.07	–	16.9	34.7	–
Dipole-induced dipole					
NH_3-CH_4	3.9	3.9[i]	0.83	0.66[b]	0.73[i]
Complex	Separation (Å)		Binding Energy (kcal/mol)		

continued on next page

	This work	High level	This work	MP2	High level
SiH_4-HF	3.3	3.3[b]	0.77	0.67[b]	0.73[b]
CH_4-HF	2.3	2.3[i]	1.66	1.56[b]	1.65[i]
NH_3-C_6H_6	3.6	3.6[u]	2.47	2.55[u]	2.22[u]
H_2O-C_6H_6	3.4	3.4[u]	3.60	3.46[u]	3.17[u]
C_2H_4-HF	2.1	2.2[b]	5.35	4.65[b]	4.47[b]
MA(P)E	0.02	–	10.7	8.5	–
Dipole-Dipole					
$(H_2S)_2$	2.9	2.8[h]	1.70	1.85[e]	1.66[h]
$(HCl)_2$	2.6	2.5[h]	1.92	2.17[e]	2.01[h]
$(CFH_3)_2$	3.8	3.9[b]	2.61	2.18[b]	2.33[b]
HCl-H_2S	2.5	2.5[h]	3.34	3.74[e]	3.35[h]
$(CH_2O)_2$	3.6	3.6[i]	4.28	3.14[b]	3.37[i]
$(H_3CCN)_2$	3.3	3.4[b]	6.60	6.50[b]	6.16[b]
MA(P)E	0.07	–	8.9	8.3	–
Hydrogen Bonded					
$(NH_3)_2$	3.3	3.3[h]	3.25	3.03[v]	3.15[h]
$(HF)_2$	1.8	1.9[h]	5.20	4.35[e]	4.57[h]
$(H_2O)_2$	1.9	2.0[h]	5.45	4.92[w]	4.97[h]
H_2O-NH_3	2.9	3.0[h]	6.59	6.05[b]	6.09[h]
HCN-HF	1.8	1.9[i]	7.90	7.44[b]	7.3[i]
MA(P)E	0.07	–	8.6	2.4	–
Overall MA(P)E	0.06	–	14.1	24.1	–
Overall M(P)E	0.03	–	1.1	5.9	–
Overall Max(P)E	0.2	–	-36.9	109.8	–

[a]Ref. [13], [b]Ref. [110], [c]Linear conformation, [d]Ref. [90], [e]This work, obtained from basis set extrapolation [95] of the CP-corrected aug-cc-pvdz and aug-cc-pvtz energies [49]. [f]T-shaped conformation, [g]Ref. [91], [h]Ref. [105], [i]Ref. [99], [j]Ref. [106], [k]Ref. [92], [l]Ref. [107], [m]Ref. [108], [n]Ref. [109], [o]Parallel conformation, [p]Ref. [104], [q]Slipped-parallel conformation, [r]Ref. [124], [s]Parallel crossed conformation, [t]T-shaped crossed conformation, [u]Ref. [111], [v]Ref. [97], [w]Ref. [125].

Table 7.3: Calculated dispersion energies at the optimum intermonomer separation, in kcal/mol. The percent contributions from the component terms in the dispersion energy are also shown.

Complex	BE	E_{disp}	% C_6	% C_8	% C_{10}
Dispersion					
He_2	0.023	0.023	70.8	22.2	6.9
He-Ne	0.042	0.041	65.2	26.1	8.7
He-Ar	0.063	0.065	59.4	29.8	10.8
Ne_2	0.076	0.070	60.9	28.6	10.5
Ne-Ar	0.116	0.115	56.1	31.2	12.7
Ar_2	0.240	0.227	53.0	32.3	14.7
L-He-N_2	0.051	0.054	63.6	26.9	9.5
T-He-N_2	0.073	0.077	61.9	28.0	10.2
He-FCl	0.066	0.068	64.7	26.4	8.9
FCl-He	0.137	0.098	56.5	30.9	12.6
Ne-CH_4	0.17	0.18	60.5	27.8	11.7
Ne-C_6H_6	0.35	0.32	58.3	29.1	12.6
CH_4-C_2H_4	0.61	0.53	61.0	27.4	11.7
$(CH_4)_2$	0.63	0.68	59.0	28.0	13.1
$(CF_4)_2$	0.49	0.70	59.2	28.9	11.9
SiH_4-CH_4	0.90	0.84	55.9	29.6	14.5
CH_4-C_6H_6	1.50	1.27	57.7	29.0	13.3
$(C_2H_2)_2$	1.70	0.71	54.1	30.6	15.3
$(CO_2)_2$	1.50	0.66	55.2	30.8	14.1
$(OCS)_2$	1.46	1.15	50.6	32.7	16.8
$(C_2H_4)_2$	1.63	1.17	55.9	29.5	14.6
P-$(C_6H_6)_2$	1.17	2.40	58.7	28.7	12.6
T-$(C_6H_6)_2$	2.70	1.99	57.7	28.8	13.4
SP-$(C_6H_6)_2$	2.10	2.67	57.1	29.3	13.6
P-$(C_{10}H_8)_2$	2.71	4.68	58.2	28.9	13.0
PC-$(C_{10}H_8)_2$	3.96	5.28	57.1	29.3	13.6
T-$(C_{10}H_8)_2$	4.80	3.53	58.0	28.7	13.3
TC-$(C_{10}H_8)_2$	3.33	2.86	59.7	27.9	12.3
Dipole-induced Dipole					
NH_3-CH_4	0.83	0.38	62.1	27.2	10.8
SiH_4-HF	0.77	0.38	57.5	29.2	13.3
CH_4-HF	1.66	0.43	58.1	28.7	13.2
Complex	BE	E_{disp}	% C_6	% C_8	% C_{10}

continued on next page

NH_3-C_6H_6	2.47	1.29	56.4	29.5	14.1
H_2O-C_6H_6	3.60	1.29	55.2	30.0	14.8
C_2H_4-HF	5.35	0.58	56.4	29.7	14.0
Dipole-Dipole					
$(H_2S)_2$	1.70	0.63	54.1	30.9	15.0
$(HCl)_2$	1.92	0.55	52.2	32.0	15.8
$(CFH_3)_2$	2.61	0.70	62.9	25.3	11.8
HCl-H_2S	3.34	0.67	52.4	31.7	15.9
$(CH_2O)_2$	4.28	0.78	55.8	30.0	14.1
$(H_3CCN)_2$	6.60	1.38	54.8	30.5	14.7
Hydrogen Bonded					
$(NH_3)_2$	3.25	0.52	58.5	28.4	13.0
$(HF)_2$	5.20	0.22	58.7	29.0	12.3
$(H_2O)_2$	5.45	0.41	58.1	28.9	13.0
H_2O-NH_3	6.59	0.53	57.8	28.9	13.3
HCN-HF	7.90	0.33	55.7	30.4	13.8
Average			58.1	29.1	12.9

Figure 7.1: Plot of the component terms of the dispersion energy for the neon dimer as a function of internuclear separation.

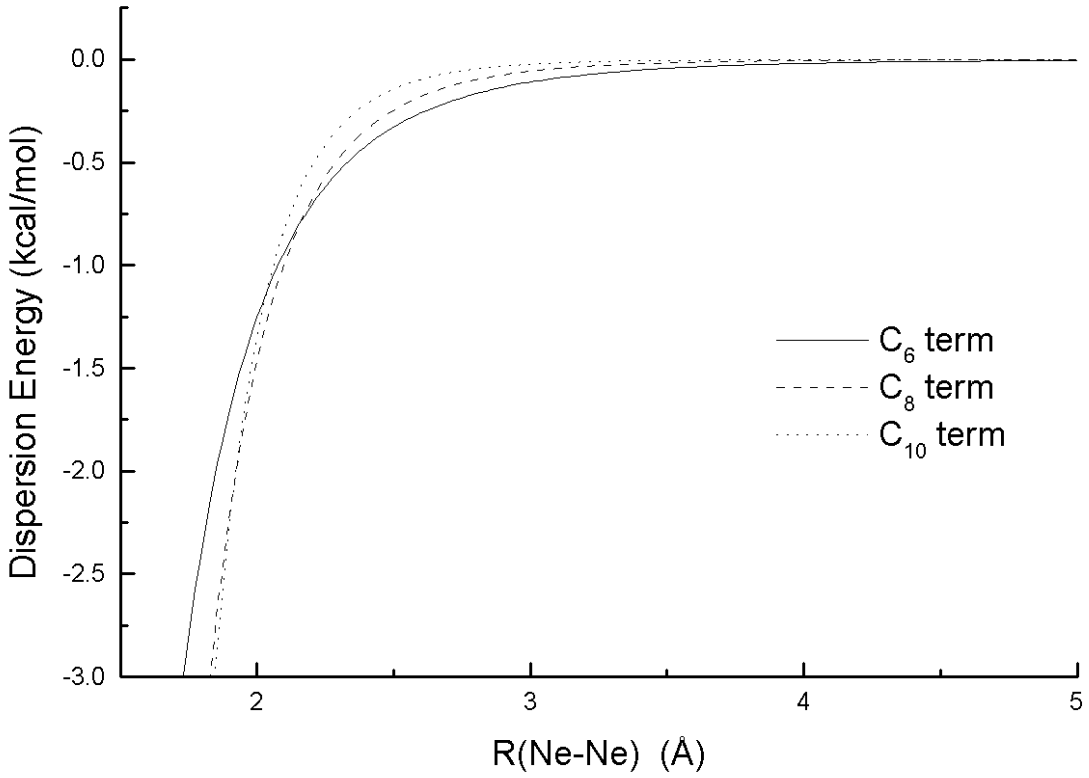

Figure 7.2: Linear correlation of calculated $\frac{1}{2}R_{vdW,ii}$ values with Clementi atomic radii [123]. All values are in Å.

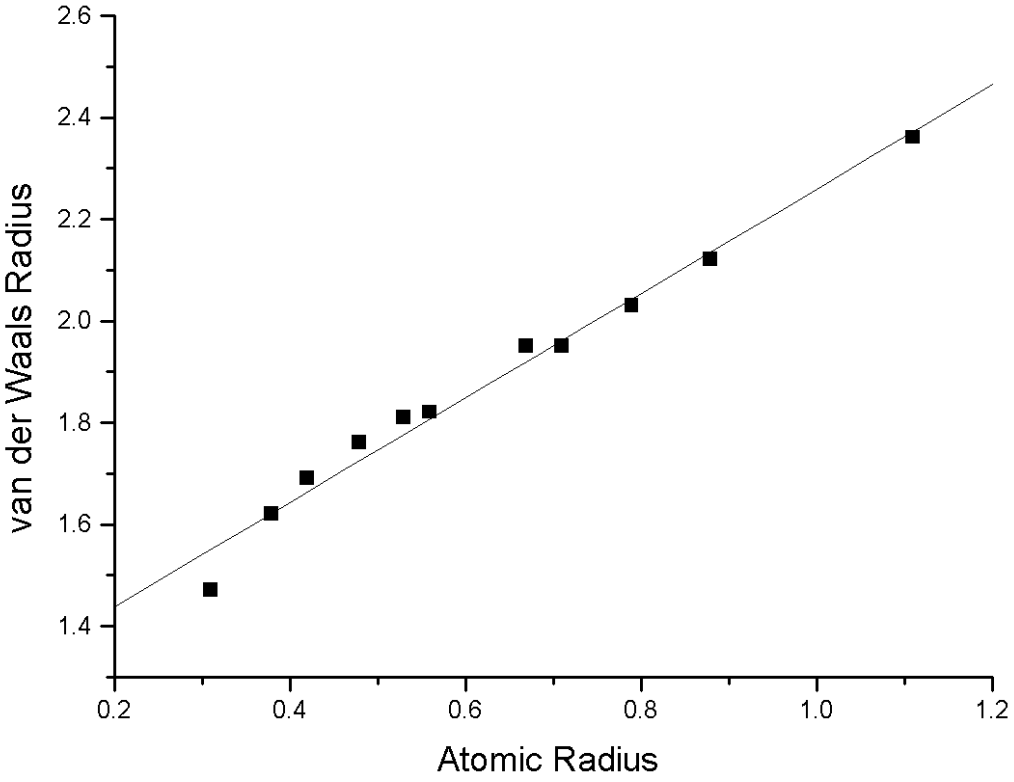

Figure 7.3: Plot of the component terms of the damped dispersion energy for the neon dimer as a function of internuclear separation.

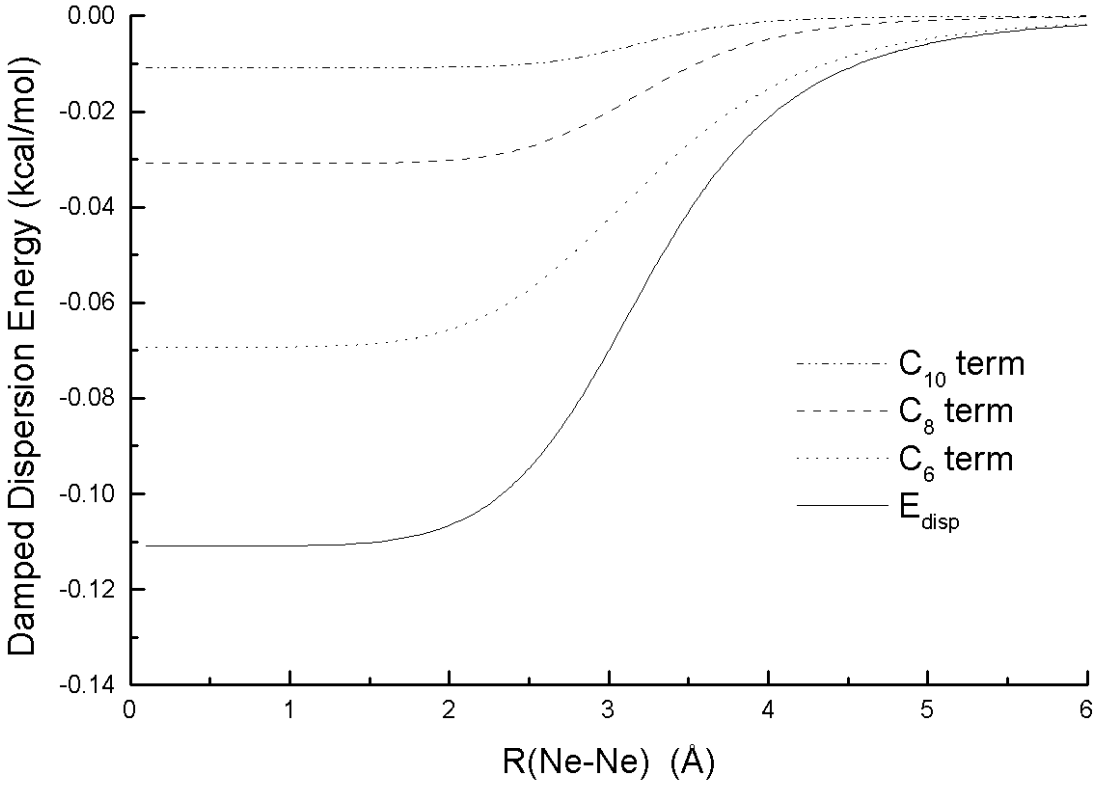

Figure 7.4: Conformations of the naphthalene dimer and minimum-energy center-of-mass separations from high-level theory [124]. Conformations are, in clockwise order: Parallel (P), Parallel Crossed (PC), T-Shaped Crossed (TC), and T-Shaped (T).

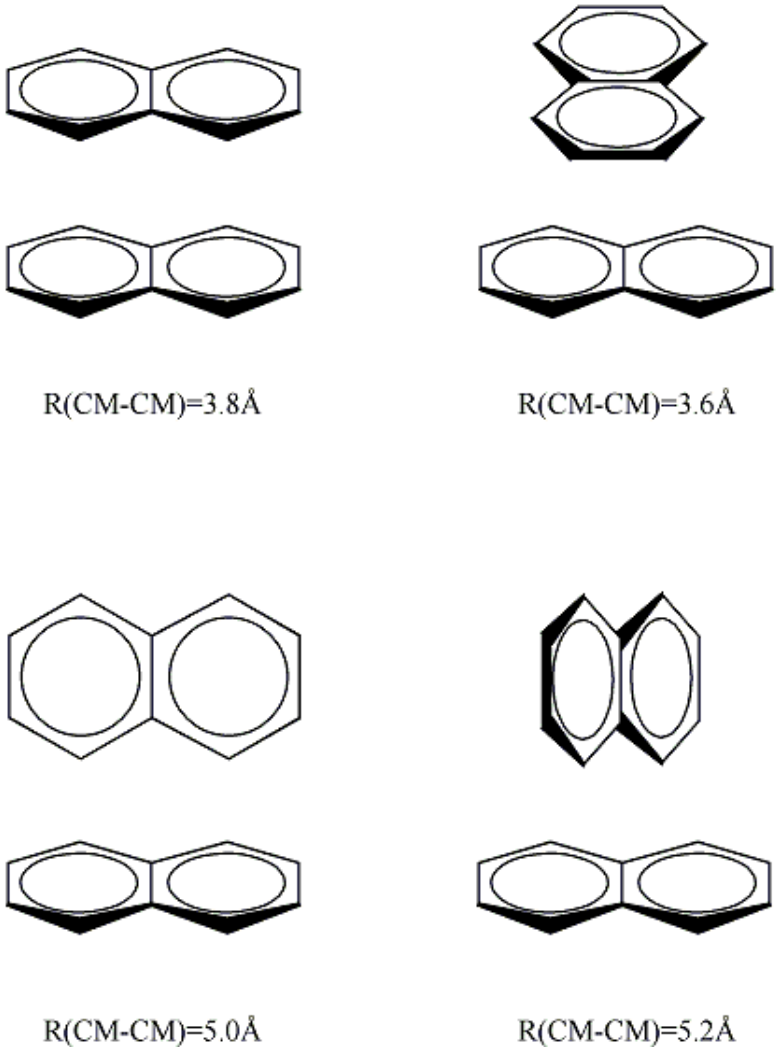

Figure 7.5: Potential energy curves for the parallel conformation of the benzene dimer from various levels of theory (counterpoise corrected). The MP2 and CCSD(T) curves are from Ref. [104].

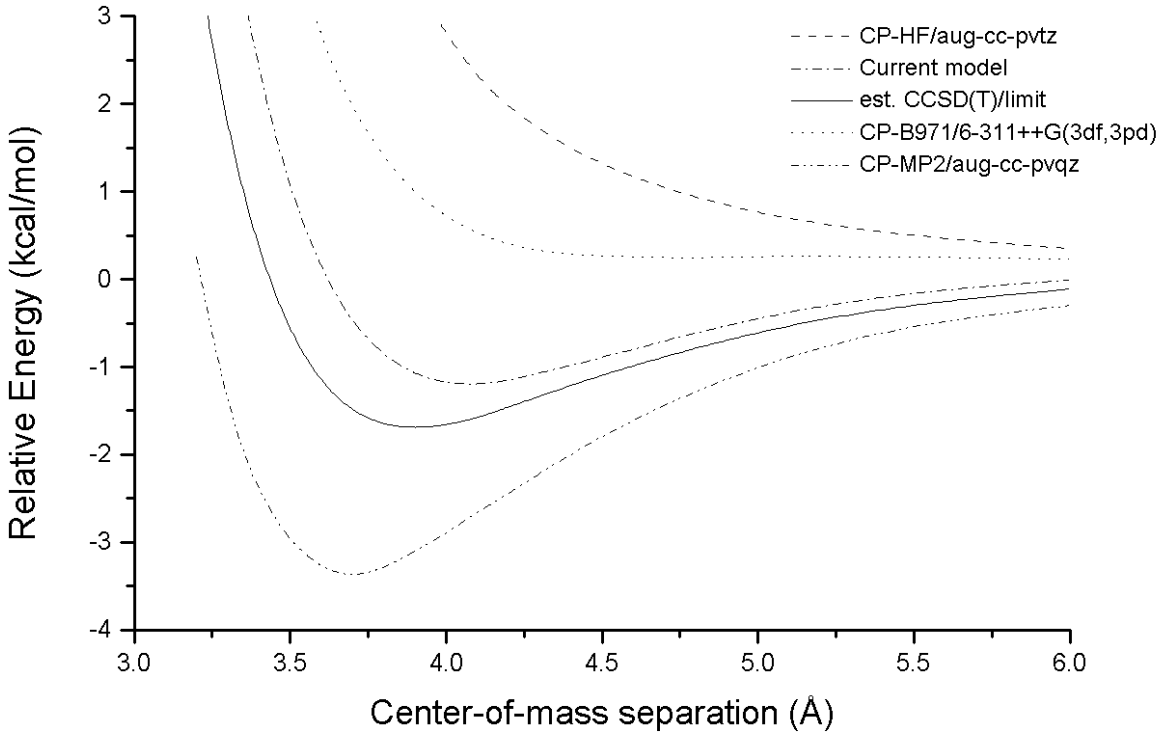

Chapter 8

Van der Waals Interactions from the Exchange Hole Dipole Moment: Application to Bio-organic Benchmark Systems

Original reference: E. R. Johnson and A. D. Becke, Chem. Phys. Lett. **432**, 600 (2006).

Abstract

We have recently completed the development of a simple model of the dispersion interaction based on the dipole moment of the exchange hole [127]. The model generates remarkably accurate dispersion coefficients, geometries, and binding energies of intermolecular complexes. In this work, the model is tested on three biochemical benchmark systems: binding energies of nucleobase pairs, relative conformational energies of the alanine dipeptide, and the anomeric effect from conformational energies of substituted tetrahydropyrans and cyclohexanes. The model gives binding energies

and conformational energies in good agreement with correlated *ab initio* reference data.

8.1 Introduction

Satisfactory treatment of the London dispersion interaction is a long-standing problem in computational chemistry. Correlated *ab initio* methods with large basis sets can accurately model this interaction, but are too computationally expensive for application to large systems. More efficient methods such as Hartree-Fock (HF) and Density-Functional Theory (DFT) do not contain the physics of dispersion. This can result in qualitatively incorrect descriptions of chemistry in applications where dispersion interactions are important, such as π stacking [18].

We have recently developed a model which uses the position-dependent dipole moment of the exchange hole to generate dispersion interactions [127]. We will refer to this model as the exchange-hole dipole moment (XDM) model in this work. The XDM model generates excellent C_6 dispersion coefficients, with a mean absolute percent error of 9.1% for a set of 178 intermolecular complexes [121]. The model also generates the higher-order dispersion coefficients C_8 and C_{10} with mean absolute percent errors of 19.2% and 12.8% percent for smaller test sets of 39 and 32 complexes, respectively [121]. When combined with Hartree-Fock theory and the Becke-Roussel (BR) dynamical correlation functional [39, 47], the XDM method provides accurate treatment of intermolecular van der Waals potential energy surfaces, having a mean absolute error of 0.06 Å in the minimum-energy separations and a mean absolute percent error of 14.1% in the binding energies of 45 bimolecular complexes [127]. For dispersion-bound complexes, the HFBR-XDM method is twice as accurate as MP2 in binding energy calculations. This level of accuracy is particularly impressive given that the computational cost of the XDM method is negligible compared to the cal-

culation of the HF orbitals themselves. In this work, we assess the performance of the HFBR-XDM model in applications spanning three major classes of biomolecules: DNA, amino acids, and carbohydrates.

The interactions between DNA nucleotides are controlled by van der Waals interactions, specifically hydrogen bonding between deoxyadenosine and deoxythymidine and between deoxycytidine and deoxyguanosine. Full nucleotide pairs are too large to treat with correlated ab initio methods. However, interactions between the nucleobase pairs have been the subject of an extensive theoretical study [128]. It was shown by correlated *ab initio* calculations that π-stacking energies between the nucleobase pairs are of similar magnitude as the H-bond strengths [128]. Predicting accurate binding energies for both H-bonded and π-stacked conformations of the nucleobase pairs is a challenging test for DFT methods. In particular, the X3LYP modification [129] of the B3LYP [46, 48] functional, with the cc-pvtz basis set and counterpoise (CP) correction [94], severely underestimates the binding of the stacked conformations of adenine-thymine (A-T) and cytosine-guanine (C-G) [130]. In the present work, the HFBR-XDM approach will be applied to the H-bonded and π-stacked conformations of the A-T and C-G pairs.

To date, HFBR-XDM has been applied only to intermolecular interactions. In this work we also consider intramolecular van der Waals interactions, as measured by relative conformational energies. An efficient methodology for computation of accurate conformational energies of proteins would be extremely valuable in protein folding studies. The alanine dipeptide is the prototypical model system for protein structure prediction, and HFBR-XDM and correlated *ab initio* results [131] for the relative energies of six conformations of this dipeptide will be compared.

Another instance where intramolecular van der Waals interactions affect structure is the anomeric effect in carbohydrate chemistry. The anomeric effect refers to the energetic preference for axial conformations of 2-substituted tetrahydropyrans, as op-

posed to the equatorial conformations preferred by substituted cyclohexanes. HFBR-XDM relative energies of the axial and equatorial conformations of four substituted cyclohexanes and tetrahydropyrans will be computed and the results compared to correlated ab initio reference data [132].

These three applications will serve as tests of the ability of the HFBR-XDM model to predict accurate binding or conformational energies of biologically relevant systems.

8.2 Methodology

Our exchange-hole-based dispersion model is fully described elsewhere [127], but will be briefly reviewed here. In our HFBR-XDM approach, we add an explicit dispersion energy term to the Hartree-Fock energy and the Becke-Roussel modification [47] of the dynamical correlation functional of Becke [39]. Thus, the total HFBR-XDM energy is given by

$$E_{\text{HFBR-XDM}} = E_{\text{HF}} + E_C^{\text{BR}} + E_{disp}. \tag{8.1}$$

The dispersion energy is a summation over all pairs of atoms i and j of C_6, C_8, and C_{10} terms, damped to prevent singularities at small interatomic separations:

$$E_{disp} = -\sum_{i>j} \left(\frac{C_{6,ij}}{R_{vdW,ij}^6 + R_{ij}^6} + \frac{C_{8,ij}}{R_{vdW,ij}^8 + R_{ij}^8} + \frac{C_{10,ij}}{R_{vdW,ij}^{10} + R_{ij}^{10}} \right). \tag{8.2}$$

$R_{vdW,ij}$ is an effective van der Waals interatomic separation, linearly related to a "critical" interatomic separation $R_{c,ij}$ by

$$R_{vdW,ij} = a_1 R_{c,ij} + a_2, \tag{8.3}$$

with the critical separation $R_{c,ij}$ given by the average of $(C_{8,ij}/C_{6,ij})^{1/2}$, $(C_{10,ij}/C_{6,ij})^{1/4}$,

and $(C_{10,ij}/C_{8,ij})^{1/2}$. The atom-independent parameters $a_1 = 0.83$ and $a_2 = 1.55$ Å were determined by least squares fitting to the binding energies of 45 intermolecular complexes [127].

The dispersion coefficients are completely non-empirical and are given by

$$C_{6,ij} = \frac{\alpha_i \alpha_j < M_1^2 >_i < M_1^2 >_j}{< M_1^2 >_i \alpha_j + < M_1^2 >_j \alpha_i}, \tag{8.4}$$

$$C_{8,ij} = \frac{3}{2} \frac{\alpha_i \alpha_j (< M_1^2 >_i < M_2^2 >_j + < M_2^2 >_i < M_1^2 >_j)}{< M_1^2 >_i \alpha_j + < M_1^2 >_j \alpha_i}, \tag{8.5}$$

$$\begin{aligned} C_{10,ij} = \frac{6}{5} \frac{\alpha_i \alpha_j (< M_1^2 >_i < M_3^2 >_j + < M_3^2 >_i < M_1^2 >_j)}{< M_1^2 >_i \alpha_j + < M_1^2 >_j \alpha_i} \\ + \frac{21}{5} \frac{\alpha_i \alpha_j < M_2^2 >_i < M_2^2 >_j}{< M_1^2 >_i \alpha_j + < M_1^2 >_j \alpha_i}, \end{aligned} \tag{8.6}$$

where α_i is the effective atom-in-molecule polarizability of atom i. We estimate this effective polarizability by exploiting the well-known proportionality between polarizability and volume [119]. Thus, for α_i, we take

$$\alpha_i = \left(\frac{< r^3 >_i}{< r^3 >_{i,free}} \right) \alpha_{i,free} = \left(\frac{\int r^3 w_i(\mathbf{r}) \rho(\mathbf{r}) d^3\mathbf{r}}{\int r^3 \rho_{i,free}(\mathbf{r}) d^3\mathbf{r}} \right) \alpha_{i,free}, \tag{8.7}$$

where $\alpha_{i,free}$ is the free atomic polarizability, taken from readily available tabulations [76], and the expectation value $< r^3 >_i$ is assumed to be a measure of effective volume. $w_i(\mathbf{r})$ is the Hirshfeld atomic partitioning weight [88] defined by

$$w_i(\mathbf{r}) = \frac{\rho_i^{at}(\mathbf{r})}{\sum_n \rho_n^{at}(\mathbf{r})}, \tag{8.8}$$

where ρ_i^{at} is a sphericalized free atomic density on nucleus i and the n summation is over all atoms in the system. By construction, $w_i(\mathbf{r})$ approaches 1 near nucleus i and

approaches 0 everywhere else, and the weights sum to 1 at every point in the system.

Finally, Eqs. (8.4) - (8.6) for the dispersion coefficients involve atomic expectation values $< M_\ell^2 >_i$ of squared multipole operators:

$$< M_\ell^2 >_i = \sum_\sigma \int w_i(\mathbf{r}) \rho_\sigma(\mathbf{r}) \left[r^\ell - (r - d_{X\sigma})^\ell \right]^2 d^3\mathbf{r}, \tag{8.9}$$

where $d_{X\sigma}$ is the magnitude of the dipole moment of a σ-spin electron and its exchange hole at point $\mathbf{r}_1$:

$$\mathbf{d}_{X\sigma}(\mathbf{r}_1) = \left[\frac{1}{\rho(\mathbf{r}_1)} \sum_{kl} \psi_{k\sigma}(\mathbf{r}_1) \psi_{l\sigma}(\mathbf{r}_1) \int \mathbf{r}_2 \psi_{k\sigma}(\mathbf{r}_2) \psi_{l\sigma}(\mathbf{r}_2) d^3\mathbf{r}_2 \right] - \mathbf{r}_1 \tag{8.10}$$

and r is the distance from nucleus i. The double summation in Eq. (8.10) is over the Hartree-Fock orbitals.

All calculations are post-Hartree-Fock as described in our previous work [127]. HF/aug-cc-pvtz calculations were performed on all species using the Gaussian 98 program [49]. The $E_{\mathrm{C}}^{\mathrm{BR}}$ dynamical correlation energy and all expectation values required for the dispersion energy were then obtained from the HF orbitals by numerical integrations [77].

The geometries of all species were obtained from Refs, [131], [132], and [133]. Single-point HFBR-XDM energy calculations were performed to obtain relative conformational energies. Although only single-point calculations were performed here for expediency, the extensive optimization tests of Ref. [127] suggest that full optimization would have negligible effect on the present results. For the nucleobase pairs, post-HF evaluations of $E_{\mathrm{C}}^{\mathrm{BR}}$ and E_{disp} were carried out for the complex and the separated monomers and were added to the counterpoise-corrected [94] HF/aug-cc-pvtz energies. BEs were computed as the total energy difference between the complex and the separated monomers. Calculations were also performed on all species with

B971/6-311++G(3df,3pd) [53] for comparison, since we believe it to be the best "conventional" DFT for intermolecular van der Waals interactions [110].

8.3 Results and Discussion

8.3.1 Nucleobase Pairs

The calculated HFBR-XDM and B971 binding energies of the four nucleobase pairs are compared to correlated *ab initio* reference data in Table 8.1. We expect B971 to predict little or no binding for the π-stacked conformations of the nucleobase pairs, though it should give accurate binding energies for the hydrogen-bonded conformations [110]. These expectations are confirmed by the results in the Table.

The HFBR-XDM results reflect the trends in our previous work [127] on the fit set of 45 bimolecular complexes. The binding energies of the H-bonded complexes in Ref. [127] had a mean absolute percent error (MAPE) of 8.6% and were slightly overbound, while the π-stacked complexes were underbound with a MAPE of 26.1%. Similar underbinding of the π-stacked cases is seen in Table 8.1. Unlike B971, however, the performance of HFBR-XDM is qualitatively correct for both hydrogen-bonded and π-stacked cases. Overall, the mean absolute error is 2.6 kcal/mol or 17.6% for these four complexes. This is particularly impressive considering the much lower computational cost and improved scaling of HFBR-XDM compared to MP2 or coupled-cluster methods. The cost of our post-HF approach is essentially the cost of the HF computation itself.

8.3.2 Alanine Dipeptide

For alanine dipeptide in the gas phase, the $C7_{eq}$ conformation is the most stable of 6 local minimum-energy structures according to basis-set extrapolated MP2 theory

[131]. The conformational energies of the dipeptide, relative to the $C7_{eq}$ conformation, are shown in Table 8.2 for HFBR-XDM, B971, and MP2.

The conformational energies are dominated by intramolecular H-bonding and popular DFTs and MP2 perform well for H-bonded interactions. Thus, we expect that both B971 and HFBR-XDM will yield accurate conformational energies for alanine dipeptide. B971 has a mean absolute error (MAE) of 0.28 kcal/mol and HFBR-XDM has a similar MAE of 0.31 kcal/mol. While there is no advantage to HFBR-XDM over B971 in this case, it is reassuring that our model performs as well for intramolecular interactions as intermolecular interactions in H-bonding cases. For larger polypeptides, steric and π-stacking interactions will become important factors in structure prediction. It is in these cases, where dispersion interactions come into play, that our model will be superior to existing DFTs.

8.3.3 The Anomeric Effect

The energies of the equatorial conformations, relative to the axial forms, of four 2-substituted tetrahydropyrans and cyclohexanes are shown in Table 8.3 for HFBR-XDM and B971. Estimated basis-set limit CCSD(T) values are shown for comparison.

Weldon *et al.* [132] showed that HF and B3LYP both underestimate the stabilization of the axial form relative to the equatorial conformation of substituted cyclohexanes and tetrahydropyrans, with MAEs of 0.99 kcal/mol (HF) and 0.73 kcal/mol (B3LYP). It is likely that at least part of this error is due to neglect of dispersion, since a greater intramolecular dispersion interaction is expected between the substituent and the ring in the axial conformation. While none of HF, B3LYP, or B971 include the proper physics of dispersion, the data in Table 8.3 show that B971 is an improvement over B3LYP (MAE of 0.44 kcal/mol). However, HFBR-XDM is much better still with a MAE of only 0.17 kcal/mol, in excellent agreement with the CCSD(T) basis-set limit estimates. While the magnitude of the intramolecular dispersion inter-

action is relatively small in these systems, neglect of this interaction by conventional DFTs could result in incorrect prediction of the more stable conformer in more highly substituted tetrahydropyrans, or in other sterically crowded systems. HFBR-XDM would evidently be much more reliable.

8.4 Conclusions

In this work, we have tested our HFBR-XDM method of Ref. [127] on three diverse applications in organic and bio-organic chemistry. Calculation of binding energies of both hydrogen-bonded and π-stacked conformations of nucleobase pairs serves as a test of the model's applicability to DNA chemistry. Calculation of the relative conformational energies of alanine dipeptide tests the model's performance on intramolecular interactions in protein chemistry. The final application, another intramolecular interaction test, was the anomeric effect in carbohydrate chemistry. For each of these applications, our model is in good agreement with correlated *ab initio* reference calculations, with mean absolute errors of 2.6 kcal/mol for the four nucleobase binding energies and 0.22 kcal/mol for the conformational energies of Sections 8.3.2 and 8.3.3. Our model is a dramatic improvement over popular existing DFTs, as represented by the B971 functional, since it gives a balanced treatment of all van der Waals interactions while B971 does not. It promises to be widely useful in biochemical applications where MP2 or coupled-cluster calculations are impractical.

While the present work is post Hartree-Fock, we will examine in future work the effect of other potentials on our vdW potential energy surfaces.

Table 8.1: Calculated CP-corrected HFBR-XDM and B971/6-311++G(3df,3pd) binding energies for the nucleobase pairs, in kcal/mol. Errors are relative to the estimated basis set limit CCSD(T) values from Ref. [128].

Dimer	HFBR-XDM	B971	Ref. [128]
A-T H-bond	14.5	12.8	15.4
A-T stack	7.2	-0.2	11.6
C-G H-bond	30.0	25.5	28.8
C-G stack	13.2	5.2	16.9
MAE	2.6	7.4	–
ME	-2.0	-7.4	–
MaxE	-4.4	-11.8	–

A-T: adenine-thymine, C-G: cytosine-guanine, MAE: mean absolute error, ME: mean error, MaxE: maximum error.

Table 8.2: Relative energies of 6 conformations of the alanine dipeptide, in kcal/mol, calculated with HFBR-XDM and B971/6-311++G(3df,3pd). Errors are relative to the estimated basis set limit MP2 values from Ref. [131].

Conformation	HFBR-XDM	B971	Ref. [131]
$C7_{eq}$	0.00	0.00	0.00
C5	0.85	0.96	1.39
$C7_{ax}$	3.04	2.52	2.66
β_2	3.52	3.29	3.35
α_L	5.50	5.67	5.19
α'	6.95	6.51	6.80
MAE	0.31	0.28	–
ME	0.09	-0.09	–
MaxE	-0.54	0.48	–

Table 8.3: Relative equatorial-axial conformational energies of 2-substituted tetrahydropyrans and cyclohexanes, in kcal/mol, calculated with HFBR-XDM and B971/6-311++G(3df,3pd). Errors are relative to the estimated basis set limit CCSD(T) values from Ref. [132].

Substituent	HFBR-XDM	B971	Ref. [132]
Cyclohexanes			
methyl	-1.9	-2.12	-1.75
fluoro	-0.18	-0.49	-0.2
methoxy	-0.33	-0.91	-0.21
hydroxy	-0.58	-0.98	-0.56
Tetrahydropyrans			
2-methyl	-2.96	-3.09	-2.82
2-fluoro	2.18	2.22	2.45
2-methoxy	0.94	0.52	1.27
2-hydroxy	0.57	0.38	0.86
MAE	0.17	0.44	–
ME	-0.16	-0.44	–
MaxE	-0.33	-0.75	–

Chapter 9

A Unified Density-Functional Treatment of Dynamical, Nondynamical, and Dispersion Correlations

Original reference: A. D. Becke and E. R. Johnson, J. Chem. Phys. **127**, 124108 (2007).

Abstract

In previous work we have introduced exact-exchange-based density-functional models for all of dynamical, nondynamical, and dispersion correlations. We have not yet, however, been able to combine these models into a single energy functional. The problem is that interaction curves in van der Waals complexes are too repulsive. A simple solution is proposed in the present work resulting in an exact-exchange-based energy functional for all chemical interactions, from the weakest (dispersion), to the strongest (molecular bonds).

9.1 Introduction

In recent publications [84, 99, 116, 121, 127, 134], we have developed a model of van der Waals interactions based on the position-dependent dipole moment of the exchange hole. We obtain remarkably good interatomic C_6, C_8, and C_{10} dispersion coefficients for atoms in molecules without any fitted parameters whatsoever [121]. Intermolecular potential energy surfaces are then obtained by introducing two universal fitted parameters into a simple attenuated dispersion energy formula [127].

The method as developed so far [84, 99, 116, 121, 127, 134] is post-Hartree-Fock and is applicable to intermolecular or intramolecular interactions [134] of van der Waals type. The total energy

$$E_{total} = E_{\rm HF} + E_{\rm DC}^{\rm BR} + E_{disp}, \tag{9.1}$$

consists of the Hartree-Fock energy $E_{\rm HF}$, the dynamical correlation energy $E_{\rm DC}^{\rm BR}$ of Becke and Roussel [39, 47] and the dispersion energy E_{disp}. By using Hartree-Fock as our reference, the repulsive part of intermolecular energy curves is treated exactly. This has allowed us to assess the dispersion and dynamical correlation contributions to vdW interactions without extraneous Pauli repulsion errors.

Eq. (9.1), however, poorly handles intramolecular *bonding* interactions because *nondynamical* correlation is absent. The usual inadequacies of Hartree-Fock theory in describing chemical bonds and transition states remain. Eq. (9.1) is not a "universal" energy functional applicable to all of chemistry. The objective of the present work is to find an accurate universal functional.

Becke has reported [15, 25] a nondynamical correlation model which, when partnered with exact exchange and $E_{\rm DC}^{\rm BR}$ dynamical correlation, gives excellent molecular atomization energies [25] and reaction barriers [57]. Adding Becke's nondynamical correlation energy to Eq. (9.1) should yield the desired universal functional. However,

this turns out not to be as straightforward as expected.

For subtle reasons, uncovered in Section 9.2, the problem resides in the repulsive part of vdW energy curves. A solution is proposed in Section 9.3 which also offers the great computational advantage that LDA (local density approximation) or other DFT (density-functional theory) orbitals can be used instead of Hartree-Fock orbitals. The result is a unified density-functional treatment of dynamical, nondynamical, and dispersion correlations that can be fine tuned to any convenient input orbital type. We call the method DF07. In Section 9.4 we assess a post-LDA realization of DF07 on a joint test set comprised of the G3/99 heats of formation of Curtiss, *et al.* [40] and 45 intermolecular complexes used in our previous dispersion studies [127].

In order to avoid long digressions, our previous correlation and dispersion models will be reviewed in three Appendices. Since DF07 combines such a large body of earlier work, it is useful to collect all relevant ideas and formulas here. Correlation formulas are reviewed in Appendices 1 and 2 and dispersion formulas in Appendix 3. The "B86" and "B88" exchange functionals [41, 42] also play a major role in DF07. These are reviewed in Appendix 4.

9.2 Repulsion in vdW Curves

In this section Becke's nondynamical correlation energy will be denoted $E^{B}_{\rm NDC}$ [see Appendix 2, Eq. (9.39)]. We have found in preliminary trials that Eq. (9.1) appended by $E^{\rm B}_{\rm NDC}$,

$$E_{total} = E_{\rm HF} + E^{\rm B}_{\rm NDC} + E^{\rm BR}_{\rm DC} + E_{disp}, \tag{9.2}$$

yields very poor, overly repulsive, intermolecular interactions. Nondynamical correlation should not, in principle, affect vdW curves. This is therefore a disappointing

result. The source of the error is uncovered below.

In Fig. 9.1 we plot He_2 energy curves for various pure exchange theories. The Hartree-Fock curve is strictly repulsive, a well-known property of exact exchange in closed-shell interactions. Also plotted in Fig. 9.1 are curves, all computed post-Hartree-Fock, for the density-functional exchange approximations B86 [41], B88 [42], and Becke-Roussel [43] (hereafter referred to as BR). Exchange approximations with a $-1/r$ asymptotic exchange-hole potential, such as B88 and BR, give repulsive vdW curves [19]. Indeed the B88 and BR curves are significantly more repulsive than Hartree-Fock. B86 shows *spurious binding*, however, as is typical [19] of functionals with an asymptotic exchange-hole potential weaker than $-1/r$. The wide variability of these pure "exchange" curves demonstrates that obtaining a good balance between Pauli repulsion and correlation in vdW interactions will be difficult.

Also plotted in Fig. 9.1 is the curve for $E_X^{exact} + E_{\rm NDC}^{\rm B}$, denoted HF+NDC in the figure. HF+NDC should reproduce Hartree-Fock if there is no nondynamical correlation in vdW interactions. Yet its curve lies closer to the BR curve than to the HF curve. What is wrong?

$E_{\rm NDC}^{\rm B}$ is based on a localized effective Becke-Roussel exchange hole (see Appendices 1 and 2) determined by first- and second-order local density gradients, local kinetic-energy density, and the exact exchange-hole potential, whose normalization is not fixed *a priori* and is not necessarily equal to 1. Normalization less than 1 indicates exchange-hole delocalization to other centers and hence the onset of nondynamical correlation. On the other hand, normalization equal to 1 means no nondynamical correlation.

In free atoms and in interactions between closed-shell systems, where no nondynamical correlation is expected, the effective BR normalization should everywhere equal 1. Because the BR model is not exact, however (except for hydrogenic atoms), slight variations from 1 occur in practice in these cases and artifactual non-zero val-

ues of $E^{\mathrm{B}}_{\mathrm{NDC}}$ thus arise. Data for the free atoms H through Ar is shown in Table 9.1. Notice that $E^{\mathrm{B}}_{\mathrm{NDC}}$ is not negligible in free atoms even though it should, in principle, be close to zero. Indeed, $E^{\mathrm{B}}_{\mathrm{NDC}}$ may even have *positive* value as, eg., in the atoms P through Ar. For the computation of chemical energy differences such as atomization energies [25] or reaction barriers [57] this is evidently not a problem thanks to cancellation of errors. For the extremely small energy differences in vdW interactions, however, Fig. 9.1 reveals that errors in $E^{\mathrm{B}}_{\mathrm{NDC}}$ are critical.

We note an interesting trend in Table 9.1. The energies $E_X^{exact} + E^{\mathrm{B}}_{\mathrm{NDC}}$ are much closer to E_X^{BR} than to E_X^{exact}. The effect of the "reverse BR" algorithm underlying $E^{\mathrm{B}}_{\mathrm{NDC}}$ (see Appendices 1 and 2) is to push the exact exchange energies in free atoms towards BR exchange energies. This is graphically illustrated in Fig. 9.2. All this explains why the HF+NDC curve in Fig. 9.1 lies closer to the BR curve than to the Hartree-Fock curve, and why intermolecular interactions from Eq. (9.2) are too repulsive. In the following section we propose a scheme to shift HF+NDC back towards Hartree-Fock.

9.3 Fine Tuning of Pauli Repulsion

All generalized gradient approximations (GGAs), because they share the same implicit assumption of a locally normalized exchange-correlation hole, give very similar thermochemistry. In Fig. 9.3, for example, we see that B86 and B88 dissociation curves for H_2 are virtually identical. The BR curve differs slightly from the B86/B88 curve because BR is not a GGA. With this in mind, we wonder if an appropriate multiple of the *difference* curve, B86-B88, might suitably lower the HF+NDC vdW curve in Fig. 9.1 *without deleteriously affecting ordinary thermochemistry.* We have found this strategy to be surprisingly successful.

The total energy is thus given by

$$E_{total} = E_X^{exact} + a_{\rm NDC}^{opp} E_{\rm NDC}^{opp} + a_{\rm NDC}^{par} E_{\rm NDC}^{par} + a_{\rm DC}^{opp} E_{\rm DC}^{opp} + a_{\rm DC}^{par} E_{\rm DC}^{par} + E_{disp} + a_{\rm RC} \left(E_X^{\rm B86} - E_X^{\rm B88} \right), \tag{9.3}$$

with the exact exchange energy E_X^{exact} as the leading term, followed by opposite- and parallel-spin components $E_{\rm NDC}^{opp}$ and $E_{\rm NDC}^{par}$ of the nondynamical correlation energy and opposite- and parallel-spin components $E_{\rm DC}^{opp}$ and $E_{\rm DC}^{par}$ of the dynamical correlation energy (see Appendix 2). The dispersion energy E_{disp} is given by the formulas of Appendix 3. The final term, $E_X^{\rm B86} - E_X^{\rm B88}$, might aptly be called a repulsion "fine tuning" correction. The "a" prefactors in Eq. (9.3) are linear fit parameters.

We will refer to Eq. (9.3) as "DF07". Noting that there are two nonlinear parameters in E_{disp}, we have seven parameters altogether in DF07. These will be fit to a combined test set of thermochemical and vdW data in Section 9.4.

Our dispersion model, E_{disp}, can be implemented in two ways (see Appendix 3). Its fundamental quantity, the position-dependent dipole moment $\mathbf{d}_{X\sigma}(\mathbf{r})$ of the exchange hole and its reference electron, can be computed using occupied orbitals as follows:

$$\mathbf{d}_{X\sigma}(\mathbf{r}) = \left[\frac{1}{\rho_\sigma(\mathbf{r})} \sum_{kl} \psi_{k\sigma}(\mathbf{r}) \psi_{l\sigma}(\mathbf{r}) \int \mathbf{r}' \psi_{k\sigma}(\mathbf{r}') \psi_{l\sigma}(\mathbf{r}') d^3\mathbf{r}' \right] - \mathbf{r}. \tag{9.4}$$

Alternatively, its magnitude $d_{X\sigma}(\mathbf{r})$ may be approximated using local densities and the Becke-Roussel exchange model:

$$d_{X\sigma}(\mathbf{r}) = b, \tag{9.5}$$

where b is the displacement from the reference point of the mean position of the BR model hole (see Appendix 1). The first approach, to be denoted XX, and the second approach, to be denoted BR, give very similar results [116, 121]. Both will be tested

in the fits of the next section.

9.4 Calibration on Thermochemical and vdW Data

Pauli repulsion depends not only on the energy functional, but also on the input orbitals. We propose that the DF07 Pauli-repulsion correction, $a_{\rm RC}(E_X^{\rm B86} - E_X^{\rm B88})$, compensate for *both*. The use of *any convenient orbitals, not necessarily Hartree-Fock orbitals*, may therefore be entertained. This is a great advantage in codes that can economically compute LDA or GGA orbitals, but not Hartree-Fock orbitals.

We have calibrated DF07 with our basis-set-free NUMOL code [78], *using LDA orbitals* [38], on a data set consisting of 222 molecular atomization energies and 45 intermolecular vdW complexes. The atomization energies are from the G3/99 thermochemical benchmark set of Curtiss, *et al.* [40]. We use B3LYP/6-31G(2df,p) geometries as recommended in their G3X procedure [135]. The vdW complexes are from our own previous work [127] and include key benchmark systems such as the benzene and naphthalene dimers. Geometries of the intermolecular complexes are determined by minimum-energy scans as described below.

The fits are challenging for several reasons. We have nonlinear as well as linear parameters. There is a huge disparity in binding energy magnitudes between the G3 and the vdW sets. Moreover, the geometries of the vdW complexes are not fixed, but are the minimum-energy geometries *for each given set of trial parameter values*. The following self-consistent procedure was adopted.

1. Starting values of the correlation parameters $a_{\rm NDC}^{opp}$, $a_{\rm NDC}^{par}$, $a_{\rm DC}^{opp}$, and $a_{\rm DC}^{par}$ were chosen from Ref. [25].

2. With correlation parameters $a_{\rm NDC}^{opp}$, $a_{\rm NDC}^{par}$, $a_{\rm DC}^{opp}$, and $a_{\rm DC}^{par}$ fixed, a 3D search is carried out for optimum dispersion parameters a_1, a_2, and $a_{\rm RC}$. The 3D search

is over a cubic grid of trial a_1, a_2, and $a_{\rm RC}$ values. For each set of trial values, the minimum-energy geometry of each of the 45 vdW test complexes is obtained (assuming rigid monomers) and its binding energy (BE) then computed. The optimum parameter values are those that minimize the rms deviation from accurate reference BE data [127]. This tedious process has been automated for the most part.

3. Now the optimum a_1, a_2, and $a_{\rm RC}$ dispersion parameters are fixed and a least-squares fit of the $a_{\rm NDC}^{opp}$, $a_{\rm NDC}^{par}$, $a_{\rm DC}^{opp}$, and $a_{\rm DC}^{par}$ correlation parameters to the heats of formation of the G3 molecules is performed [at their B3LYP/6-31G(2df,p) geometries].

4. With the new correlation parameters, return to step 2. Convergence is achieved in a few iterations.

In Table 9.2 we report optimum parameter values for the XX and BR variants of DF07. All calculations were performed by the NUMOL program with radial grids of 80 points for H-He, 120 for Li-Ne, 160 for Na-Ar, and angular grids of 302 points on all atoms.

The repulsion-correction coefficient $a_{\rm RC}$ has a relatively small value of 0.25 for DF07-XX and 0.27 for DF07-BR. When B86 is used in this way, it does *not* contribute *any* physical binding to our vdW complexes! The binding observed for B86 in vdW interactions in, eg., Ref. [19] or in Fig. 9.1, is spurious. The physics of dispersion is not contained in B86 or in any other exchange GGA. Its purpose in DF07 is to shift the HF+NDC curve down to the *repulsive* HF curve. The binding in all our dispersion-bound complexes arises entirely from the dynamical correlation and dispersion terms as it should.

The four correlation parameters $a_{\rm NDC}^{opp}$, $a_{\rm NDC}^{par}$, $a_{\rm DC}^{opp}$, and $a_{\rm DC}^{par}$ have values similar to those in Ref. [25]. The dispersion parameters a_1 and a_2 are similar to those in Ref.

[127]. Thus the repulsion-correction term joins these independent theories together without significantly altering either one.

The statistics in Table 9.2 are very good. Mean absolute errors (MAEs) are 2.9 kcal/mol (XX) and 2.8 kcal/mol (BR) for the G3/99 heats of formation. Mean absolute percent errors (MAPEs) are 12.0% (XX) and 7.9% (BR) for the vdW complexes. These MAPEs are even smaller than the 14.1% obtained by our post-Hartree-Fock method in Ref. [127]. For the geometries of the vdW complexes, the mean absolute error in the intermonomer separations is 0.11 Å (XX) and 0.12 Å (BR). The maximum errors are 0.3 Å for both.

DF07-BR performs somewhat better than DF07-XX on the vdW interactions, particularly in the important case of $\pi - \pi$ interactions. For the three conformations of the benzene dimer and the four conformations of the naphthalene dimer in our test set, the MAPEs are 23.9% and 7.3% for XX and BR respectively. The mean (percent) errors are -23.9% and 4.7%. XX clearly underbinds $\pi - \pi$ systems. BR is a significant improvement having a slight overbinding tendency.

9.5 Discussion and Conclusions

DF07 is a unified methodology for computing exact-exchange-based total electronic energies in chemical systems. Dynamical, nondynamical, and dispersion correlations are treated in a balanced manner. We have here presented DF07 parametrizations *for LDA input orbitals*. Mean absolute heat-of-formation error on the G3/99 thermochemical data set is below 3.0 kcal/mol, and mean absolute percent error on a test set of 45 intermolecular binding energies is of order 10 percent.

The seven parameters in DF07 might be discomforting to some. Let us point out, however, that each parameter is connected to a well-defined physical effect and that each parameter's value concurs with physical intuition. We feel, therefore, that

these fits are rational and justified. Pragmatic fitting of parameters is today quite acceptable in the design of accurate thermochemical procedures (see, eg., Ref. [40]).

DF07 compares favourably with the universal DFTs of Grimme [60] which combine various GGAs with *scaled* empirical dispersion. Grimme's most recent functional [60], containing 13 parameters, is called "B97-D". On 148 atomization energies, the MAE for DF07-BR is 2.5 kcal/mol compared to 3.8 kcal/mol for B97-D [60]. The MAPE for DF07-BR on our 45-complex vdW test set [127] is 7.9% compared to 17.3% for B97-D on a different 40-complex set [60]. B97-D is a simple GGA, however, compared to the much more complicated DF07. DF07 and B97-D use occupied orbitals only. Using virtual orbitals as well in an MP2-like manner, Grimme obtains a "double" hybrid theory with even better performance [136].

Extensive tests of DF07 on a wide variety of benchmark sets comprised of reaction barriers, bond energies, charge-transfer complexes, ionization potentials, electron affinities, proton affinities, etc. are under way and will be reported in a later communication.

Obtaining forces from DF07 will be difficult due to the complicated nature of the nondynamical correlation expressions (see Appendix 2). The possibility that useful geometries can be obtained from simplifications of DF07 will also be explored in future work.

9.6 Appendix 1: the Becke-Roussel Exchange-Hole Model

Our nondynamical and dynamical correlation theories, and the BR variant of our dispersion theory as well, rely on the Becke-Roussel model of the exchange hole [43]. Our correlation review must therefore begin with a review of the BR model.

Most exchange-hole models in the DFT literature are based on the uniform electron gas as the reference system. The Becke-Roussel model on the other hand, is inspired by the hydrogen atom. The BR model recovers the exact exchange hole at any reference point in any hydrogenic atom. In other systems it is an excellent approximation.

At any given reference point in an atom or molecule, the BR model hole is the spherical average of a simple exponential function

$$-Ae^{-ar} \tag{9.6}$$

centered at a distance b from the reference point. The three parameters in the model (A, a, and b) are determined by applying three constraints. The Taylor expansion of the model hole around the reference point $\mathbf{r}$, to second order in the interelectronic separation s, is given by

$$h_{X\sigma}^{\mathrm{BR}}(\mathbf{r}, s) = -Ae^{-x} - \frac{Aa^2}{6}\left(1 - \frac{2}{x}\right)e^{-x}s^2 + \dots , \tag{9.7}$$

where $x = ab$. Assuming real orbitals (see Refs. [100, 101, 137] for the generalization to complex orbitals and nonzero current densities) the Taylor expansion of the *exact* hole is

$$h_{X\sigma}^{exact}(\mathbf{r}, s) = -\rho_\sigma - Q_\sigma s^2 + \dots , \tag{9.8}$$

where

$$Q_\sigma = \frac{1}{6}\left(\nabla^2\rho_\sigma - 2D_\sigma\right) \tag{9.9}$$

and

$$D_\sigma = \tau_\sigma - \frac{1}{4}\frac{(\nabla\rho_\sigma)^2}{\rho_\sigma} \tag{9.10}$$

and τ_σ is the following kinetic-energy density:

$$\tau_\sigma = \sum_i (\nabla\psi_{i\sigma})^2. \tag{9.11}$$

Equating the Taylor expansions, Eqs. (9.7) and (9.8), gives two constraints. Normalizing the model hole to unit charge gives the third:

$$\frac{8\pi A}{a^3} = 1. \tag{9.12}$$

Solution of these constraints is simple. The end result is the following nonlinear equation for the variable x:

$$\frac{xe^{-2x/3}}{x-2} = \frac{2}{3}\pi^{2/3}\frac{\rho_\sigma^{5/3}}{Q_\sigma}, \tag{9.13}$$

which is efficiently solved by, eg., the Newton-Raphson method.

After the root of Eq. (9.13) is obtained, b is given by

$$b^3 = \frac{x^3 e^{-x}}{8\pi\rho_\sigma} \tag{9.14}$$

and the Coulomb potential of the BR hole at its reference point, $U_{X\sigma}^{\mathrm{BR}}(\mathbf{r})$, is then given by

$$U_{X\sigma}^{\mathrm{BR}} = -\frac{1}{b}\left(1 - e^{-x} - \frac{1}{2}xe^{-x}\right). \tag{9.15}$$

The total σ-spin exchange energy is

$$E_{X\sigma}^{\mathrm{BR}} = \frac{1}{2}\int \rho_\sigma U_{X\sigma}^{\mathrm{BR}} d^3\mathbf{r}. \tag{9.16}$$

Complete details, atomic benchmark data, and informative plots may be found in Ref. [43].

9.7 Appendix 2: Nondynamical and Dynamical Correlations

In this section, the nature of both "nondynamical" and "dynamical" correlations and our previously published models for each are reviewed.

Nondynamical correlation is also referred to as "static" correlation or "left-right" correlation. In real space it is multicentered in range. In configuration space it involves mixing of low-lying nearly-degenerate configurations. The multicenter nature of nondynamical correlation is the working definition of our model [15, 25].

If the extent of the (exact) exchange hole is localized to roughly atomic size, as it is in free atoms or in closed-shell interactions, there is no nondynamical correlation. In chemically bonded systems, however, the exchange hole is delocalized (or "nonlocal") and extends over more than one center. The Becke-Roussel exchange-hole model can be used to sense the nonlocality of the exact exchange hole. For this purpose, the procedure in Appendix 1 is "reversed".

As in Appendix 1, we equate the Taylor expansions of Eqs. (9.7) and (9.8) giving two constraints. Now, however, instead of using hole normalization as the third

constraint, we require that the Coulomb potential of the *exact* exchange hole,

$$U_{X\sigma}^{exact}(\mathbf{r}) = -\frac{1}{\rho_\sigma(\mathbf{r})}\sum_{kl}\psi_{k\sigma}(\mathbf{r})\psi_{l\sigma}(\mathbf{r})\int\frac{\psi_{k\sigma}(\mathbf{r}')\psi_{l\sigma}(\mathbf{r}')}{|\mathbf{r}-\mathbf{r}'|}d^3\mathbf{r}' \tag{9.17}$$

equal the Coulomb potential of the model hole:

$$-\frac{8\pi A}{a^2 x}\left(1-e^{-x}-\frac{1}{2}xe^{-x}\right), \tag{9.18}$$

where $x = ab$ as in Appendix 1. Solution of these constraints gives the nonlinear equation

$$\frac{x-2}{x^2}\left(e^x-1-\frac{x}{2}\right) = -\frac{3}{4\pi}\frac{Q_\sigma}{\rho_\sigma^2}U_{X\sigma}^{exact} \tag{9.19}$$

for the variable x, following which A and a are given by

$$A = \rho_\sigma e^x, \tag{9.20}$$

$$a^2 = \frac{6Q_\sigma}{\rho_\sigma}\frac{x}{x-2}. \tag{9.21}$$

The *normalization* of the BR hole is *not fixed* in this scheme. Instead, the normalization is given by

$$N_{X\sigma}^{\text{eff}} = \frac{8\pi A}{a^3} \tag{9.22}$$

and may be less than or equal to 1. This "effective" local normalization is a measure of the multicenter nonlocality of the exact hole. A value of $N_{X\sigma}^{\text{eff}}$ less than 1 signifies *hole delocalization to other centers.*

In practice, values slightly greater than 1 may occur since the BR model is not

exact (except in hydrogenic atoms). The consequences of this are discussed in Section 9.2 and, indeed, are the primary concern of this paper.

The model hole above is *not* the same hole as in Appendix 1. Both are based on the BR off-center exponential analytical form, but are subject to different constraints and are used for different purposes. The above hole will be designated $h^{\rm eff}_{X\sigma}$ (localized "effective" exchange hole) to distinguish it from $h^{\rm BR}_{X\sigma}$ of Appendix 1.

When $N^{\rm eff}_{X\sigma} < 1$, we model nondynamical correlation by *adding* to the effective σ-spin hole a fraction f of the effective hole of the *opposite*-spin electrons,

$$h_{{\rm XNDC}\alpha} = h^{\rm eff}_{X\alpha} + f h^{\rm eff}_{X\beta} \tag{9.23a}$$

$$h_{{\rm XNDC}\beta} = h^{\rm eff}_{X\beta} + f h^{\rm eff}_{X\alpha} \tag{9.23b}$$

such that these "exchange plus nondynamical correlation" (XNDC) holes are normalized:

$$f = \min\left(\frac{1 - N^{\rm eff}_{X\alpha}}{N^{\rm eff}_{X\beta}}, \frac{1 - N^{\rm eff}_{X\beta}}{N^{\rm eff}_{X\alpha}}, 1\right). \tag{9.24}$$

The first argument is the value of f which normalizes $h_{{\rm XNDC}\alpha}$ to 1. The second normalizes $h_{{\rm XNDC}\beta}$ to 1. The third argument $f = 1$ corresponds to maximum depletion of the opposite-spin hole. The "min" is required to ensure that neither XNDC hole contains *more* than 1 electron. The resulting nondynamical potential energy of correlation is

$$U^{opp}_{\rm NDC} = \frac{1}{2}\int f\rho_\alpha U^{exact}_{X\beta} d^3\mathbf{r} + \frac{1}{2}\int f\rho_\beta U^{exact}_{X\alpha} d^3\mathbf{r}, \tag{9.25}$$

where, for greater clarity, we adopt a slightly different notation than in Ref. [25].

In spin-neutral systems, both holes of Eqs. (9.23) are normalized. In spin-polarized systems, however, only one can be normalized and the other necessarily contains less than 1 electron. If either of the XNDC holes has less than 1 electron, a *parallel*-spin nondynamical correlation hole,

$$h_{\mathrm{NDC}\sigma\sigma} = A_{\sigma\sigma} s^2 h^{\mathrm{eff}}_{X\sigma} \tag{9.26}$$

is further added [25]. It vanishes quadratically at $s = 0$ because the parallel-spin pair density itself vanishes quadratically. The $A_{\sigma\sigma}$ prefactor is given by

$$A_{\sigma\sigma} = \min\left(\frac{1 - N^{\mathrm{eff}}_{X\sigma} - f N^{\mathrm{eff}}_{X\sigma'}}{M^{(2)}_{\sigma}}, \frac{D_\sigma}{3\rho_\sigma}\right), \tag{9.27}$$

where the first argument normalizes the total σ-spin XNDC hole (note that the σ' subscript refers to the *spin opposite to* σ), and the second argument corresponds to maximum depletion of *parallel* spin density. D_σ is defined in Appendix 1, Eq. (9.10), and $M^{(n)}_\sigma$ is the n^{th} moment of the effective BR hole:

$$M^{(n)}_\sigma = 4\pi \int_0^\infty s^{n+2} |h^{\mathrm{eff}}_{X\sigma}| ds. \tag{9.28}$$

The Coulomb potential of the hole $h_{\mathrm{NDC}\sigma\sigma}$ is

$$U_{\mathrm{NDC}\sigma\sigma} = -A_{\sigma\sigma} M^{(1)}_\sigma \tag{9.29}$$

and the total parallel-spin nondynamical potential energy of correlation is

$$U^{par}_{\mathrm{NDC}} = \frac{1}{2}\int \rho_\alpha U_{\mathrm{NDC}\alpha\alpha} d^3\mathbf{r} + \frac{1}{2}\int \rho_\beta U_{\mathrm{NDC}\beta\beta} d^3\mathbf{r}. \tag{9.30}$$

The BR hole moments $M_\sigma^{(1)}$ and $M_\sigma^{(2)}$ are given by

$$M_\sigma^{(1)} = N_{X\sigma}^{\text{eff}} \frac{x}{a} \left[1 + \frac{4}{x^2} - \left(1 + \frac{4}{x} \right) \frac{e^{-x}}{x} \right], \tag{9.31}$$

$$M_\sigma^{(2)} = N_{X\sigma}^{\text{eff}} \frac{x^2}{a^2} \left[1 + \frac{12}{x} \right], \tag{9.32}$$

where x, a, and $N_{X\sigma}^{\text{eff}}$ are given by Eqs. (9.19), (9.21), and (9.22).

Dynamical correlation must also be considered. This is a *local* correlation of shorter range than nondynamical correlation, acting over interelectronic distances of atomic size or less. In real space it arises, in part, from interelectronic cusp conditions [39]. In configuration space it is due to mixing of higher-energy excited configurations. Electron-gas-like dynamical correlation approximations have a long history in the DFT literature.

We use Becke's dynamical correlation model [39] with the BR modifications of Ref. [47]. For opposite spins,

$$E_{\text{DC}}^{opp} = -0.8 \int \rho_\alpha \rho_\beta z_{\alpha\beta}^2 \left[1 - \frac{\ln(1 + z_{\alpha\beta})}{z_{\alpha\beta}} \right] d^3\mathbf{r} \tag{9.33}$$

and for parallel spins,

$$E_{\text{DC}}^{par} = \sum_\sigma E_{\text{DC}}^{\sigma\sigma}, \tag{9.34}$$

$$E_{\text{DC}}^{\sigma\sigma} = -0.01 \int \rho_\sigma D_\sigma z_{\sigma\sigma}^4 \left[1 - \frac{2}{z_{\sigma\sigma}} \ln \left(1 + \frac{z_{\sigma\sigma}}{2} \right) \right] d^3\mathbf{r}, \tag{9.35}$$

where $z_{\alpha\beta}$ and $z_{\sigma\sigma}$ are correlation lengths characterizing the sizes of the opposite- and parallel-spin dynamical correlation holes respectively. These are related to the BR

exchange-hole potentials of Appendix 1, Eq. (9.15), by

$$z_{\sigma\sigma'} = c_{\sigma\sigma'} \left(|U_{X\sigma}^{\mathrm{BR}}|^{-1} + |U_{X\sigma'}^{\mathrm{BR}}|^{-1} \right), \tag{9.36}$$

with parameter values $c_{\alpha\beta} = 0.63$ and $c_{\sigma\sigma} = 0.88$ determined from fits to free atomic correlation energies [47].

The sum of the opposite- and parallel-spin components is denoted

$$E_{\mathrm{DC}}^{opp} + E_{\mathrm{DC}}^{par} = E_{\mathrm{DC}}^{\mathrm{BR}} \tag{9.37}$$

at various points in this paper.

If all four nondynamical and dynamical correlation terms with a linear prefactor for each are fit to thermochemical benchmark data, the following optimum total exchange-correlation energy is obtained [25]:

$$E_{\mathrm{XC}} = E_X^{exact} + a_{\mathrm{NDC}}^{opp} U_{\mathrm{NDC}}^{opp} + a_{\mathrm{NDC}}^{par} U_{\mathrm{NDC}}^{par} + a_{\mathrm{DC}}^{opp} U_{\mathrm{DC}}^{opp} + a_{\mathrm{DC}}^{par} U_{\mathrm{DC}}^{par}, \tag{9.38}$$

with parameter values $a_{\mathrm{NDC}}^{opp} = 0.514$ and $a_{\mathrm{NDC}}^{par} = 0.651$ for the nondynamical correlation terms, and $a_{\mathrm{DC}}^{opp} = 1.075$ and $a_{\mathrm{DC}}^{par} = 1.113$ for the dynamical correlation terms. Note that the NDC terms are *potential* energies of correlation. Thus the NDC parameter values, of order 1/2, are logical in view of the virial theorem. The DC parameters on the other hand, are of order 1 since Becke's dynamical correlation model includes kinetic-energy effects through a coupling-constant integration [39].

For notational convenience, the nondynamical correlation part is denoted

$$a_{\mathrm{NDC}}^{opp} U_{\mathrm{NDC}}^{opp} + a_{\mathrm{NDC}}^{par} U_{\mathrm{NDC}}^{par} = E_{\mathrm{NDC}}^{\mathrm{B}} \tag{9.39}$$

in Section 9.2.

9.8 Appendix 3: the Dispersion Model

Our dispersion energy is a sum over all pairs of atoms i and j of C_6, C_8, and C_{10} dispersion coefficients, damped to prevent divergences at small interatomic separations:

$$E_{disp} = -\frac{1}{2}\sum_{i\neq j}\left(\frac{C_{6,ij}}{R_{vdW,ij}^6 + R_{ij}^6} + \frac{C_{8,ij}}{R_{vdW,ij}^8 + R_{ij}^8} + \frac{C_{10,ij}}{R_{vdW,ij}^{10} + R_{ij}^{10}}\right). \tag{9.40}$$

$R_{vdW,ij}$ is an effective van der Waals interatomic separation linearly related to a "critical" interatomic separation $R_{c,ij}$ by

$$R_{vdW,ij} = a_1 R_{c,ij} + a_2, \tag{9.41}$$

with the critical separation $R_{c,ij}$ given by the average of $(C_{8,ij}/C_{6,ij})^{1/2}$, $(C_{10,ij}/C_{6,ij})^{1/4}$, and $(C_{10,ij}/C_{8,ij})^{1/2}$. The atom-independent parameters a_1 and a_2 are determined by least-squares fitting to vdW calibration data. On a set of 45 intermolecular complexes ranging from simple systems such as He_2 to $\pi-\pi$ dimers of benzene and naphthalene [127], we obtained $a_1 = 0.83$ and $a_2 = 1.55$ Å for the total energy formula $E_{\rm HF} + E_{\rm DC}^{\rm BR} + E_{disp}$, with $E_{\rm DC}^{\rm BR}$ the dynamical correlation energy of Becke and Roussel as in Appendix 2.

The dispersion coefficients are non-empirical and are given by

$$C_{6,ij} = \frac{\alpha_i\alpha_j < M_1^2 >_i < M_1^2 >_j}{< M_1^2 >_i \alpha_j + < M_1^2 >_j \alpha_i}, \tag{9.42a}$$

$$C_{8,ij} = \frac{3}{2}\frac{\alpha_i\alpha_j(< M_1^2 >_i < M_2^2 >_j + < M_2^2 >_i < M_1^2 >_j)}{< M_1^2 >_i \alpha_j + < M_1^2 >_j \alpha_i}, \tag{9.42b}$$

$$C_{10,ij} = 2\frac{\alpha_i\alpha_j(< M_1^2 >_i < M_3^2 >_j + < M_3^2 >_i < M_1^2 >_j)}{< M_1^2 >_i \alpha_j + < M_1^2 >_j \alpha_i} + \frac{21}{5}\frac{\alpha_i\alpha_j < M_2^2 >_i < M_2^2 >_j}{< M_1^2 >_i \alpha_j + < M_1^2 >_j \alpha_i}, \tag{9.42c}$$

where α_i is the effective atom-in-molecule polarizability of atom i. We estimate this effective polarizability by exploiting the well-known proportionality between polarizability and volume. Thus, for α_i, we use

$$\alpha_i = \left(\frac{< r^3 >_i}{< r^3 >_{i,free}}\right)\alpha_{i,free} = \left(\frac{\int r^3 w_i(\mathbf{r})\rho(\mathbf{r})d^3(\mathbf{r})}{\int r^3 \rho_{i,free}(\mathbf{r})d^3(\mathbf{r})}\right)\alpha_{i,free}, \tag{9.43}$$

where $\alpha_{i,free}$ is the free atomic polarizability [76] and the expectation value $< r^3 >_i$ is assumed to be a measure of effective volume. The functions $w_i(\mathbf{r})$ are Hirshfeld atomic partitioning weights [88] defined by

$$w_i(\mathbf{r}) = \frac{\rho_i^{at}(\mathbf{r})}{\sum_n \rho_n^{at}(\mathbf{r})}, \tag{9.44}$$

where ρ_i^{at} is the sphericalized free atomic density on center i and the n summation is over all atoms in the system.

The quantities $< M_\ell^2 >_i$ in Eqs. (9.42) are atomic expectation values of squared multipoles:

$$< M_\ell^2 >_i = \sum_\sigma \int w_i(\mathbf{r})\rho_\sigma(\mathbf{r})\left[r_i^\ell - (r_i - d_{X\sigma})^\ell\right]^2 d^3\mathbf{r}, \tag{9.45}$$

where r_i is the distance from nucleus i, and $d_{X\sigma}$ is the magnitude of the *dipole moment* of the σ-spin exchange hole and its reference electron at point $\mathbf{r}$. The dipole moment $\mathbf{d}_{X\sigma}(\mathbf{r})$ can be computed from the occupied orbitals by

$$\mathbf{d}_{X\sigma}(\mathbf{r}) = \left[\frac{1}{\rho_\sigma(\mathbf{r})}\sum_{kl}\psi_{k\sigma}(\mathbf{r})\psi_{l\sigma}(\mathbf{r})\int \mathbf{r}'\psi_{k\sigma}(\mathbf{r}')\psi_{l\sigma}(\mathbf{r}')d^3\mathbf{r}'\right] - \mathbf{r} \tag{9.46}$$

or its magnitude may be approximated by the Becke-Roussel model:

$$d_{X\sigma}(\mathbf{r}) = b. \tag{9.47}$$

Here, b is the BR displacement parameter in Appendix 1, Eq. (9.14).

Care must be taken when computing the moment integrals (9.45). High powers of r in the integrand, up to r^6 in the case of C_{10} (r^8 including the volume element), may swamp the density at very large r in numerical codes. Also, the Becke-Roussel b parameter may be ill behaved at very large r even in basis-set codes. In the numerical computation of these integrals, we recommend that the value of $d_{X\sigma}$ be capped at r_i and that integration points with $\rho_\sigma < 10^{-10}$ be excluded.

Please note, as well, that Refs. [121, 127, 134] contain an erroneous constant in the first term of the expression for C_{10}. This error originates with an incorrect value of $\lambda(1,3)$ taken from Ref. [2]. Eq. (9.42c) above is correct.

9.9 Appendix 4: B86 and B88 Exchange GGAs

For completeness, we include in this section expressions for the B86 and B88 exchange functionals. Each consists of a density-gradient correction to the uniform-electron-gas exchange energy (i.e., the LDA):

$$E_X^{\mathrm{LDA}} = -\frac{3}{2}\left(\frac{3}{4\pi}\right)^{1/3} \int \left(\rho_\alpha^{4/3} + \rho_\beta^{4/3}\right) d^3\mathbf{r}. \tag{9.48}$$

B86 is given by [41]

$$E_X^{\mathrm{B86}} = E_X^{\mathrm{LDA}} - 0.0036 \sum_\sigma \int \frac{\rho_\sigma^{4/3} \chi_\sigma^2}{1 + 0.004\chi_\sigma^2} d^3\mathbf{r}. \tag{9.49}$$

B88 is only slightly more complicated [42]:

$$E_X^{\mathrm{B88}} = E_X^{\mathrm{LDA}} - 0.0042 \sum_\sigma \int \frac{\rho_\sigma^{4/3} \chi_\sigma^2}{1 + 0.0252 \chi_\sigma \mathrm{arcsinh} \chi_\sigma} d^3\mathbf{r}, \tag{9.50}$$

where

$$\chi_\sigma = \frac{|\nabla \rho_\sigma|}{\rho_\sigma^{4/3}} \tag{9.51}$$

is the dimensionless local spin-density gradient.

Table 9.1: Atomic exchange and nondynamical correlation energies (au). Computed post-LDA.

Atom	E_X^{exact}	$E_{\rm NDC}^B$	$E_X^{exact} + E_{\rm NDC}^B$	$E_X^{\rm BR}$
H	-0.298	0	-0.298	-0.300
He	-0.998	-0.015	-1.012	-1.015
Li	-1.751	-0.007	-1.757	-1.768
Be	-2.636	-0.014	-2.650	-2.656
B	-3.724	-0.013	-3.737	-3.749
C	-5.020	-0.018	-5.038	-5.053
N	-6.543	-0.025	-6.568	-6.586
O	-8.137	-0.044	-8.181	-8.200
F	-9.952	-0.062	-10.014	-10.037
Ne	-12.008	-0.086	-12.094	-12.116
Na	-13.929	-0.063	-13.992	-14.016
Mg	-15.914	-0.058	-15.972	-15.993
Al	-18.002	-0.037	-18.039	-18.060
Si	-20.213	-0.015	-20.228	-20.249
P	-22.557	0.007	-22.549	-22.570
S	-24.936	0.022	-24.914	-24.926
Cl	-27.444	0.041	-27.403	-27.411
Ar	-30.093	0.062	-30.031	-30.033

Table 9.2: Best-fit DF07 parameters and error statistics.

Quantity	XX	BR
a_{NDC}^{opp}	0.511	0.515
a_{NDC}^{par}	0.615	0.637
a_{DC}^{opp}	1.073	1.070
a_{DC}^{par}	0.886	0.985
a_1	0.54	0.61
a_2	1.89 Å	1.97 Å
a_{RC}	0.25	0.27
RMSE G3	3.8	3.7
MAE G3	2.9	2.8
MaxAE G3	11.7	11.5
RMSPE vdW	15.6	10.1
MAPE vdW	12.0	7.9
MaxAPE vdW	35.5	25.3

G3 error statistics: RMSE (root mean square error), MAE (mean absolute error), MaxAE (maximum absolute error) in kcal/mol. vdW error statistics: RMSPE (root mean square percent error), MAPE (mean absolute percent error), MaxAPE (maximum absolute percent error).

Figure 9.1: Pauli repulsion curves for He_2. Computed post-Hartree-Fock.

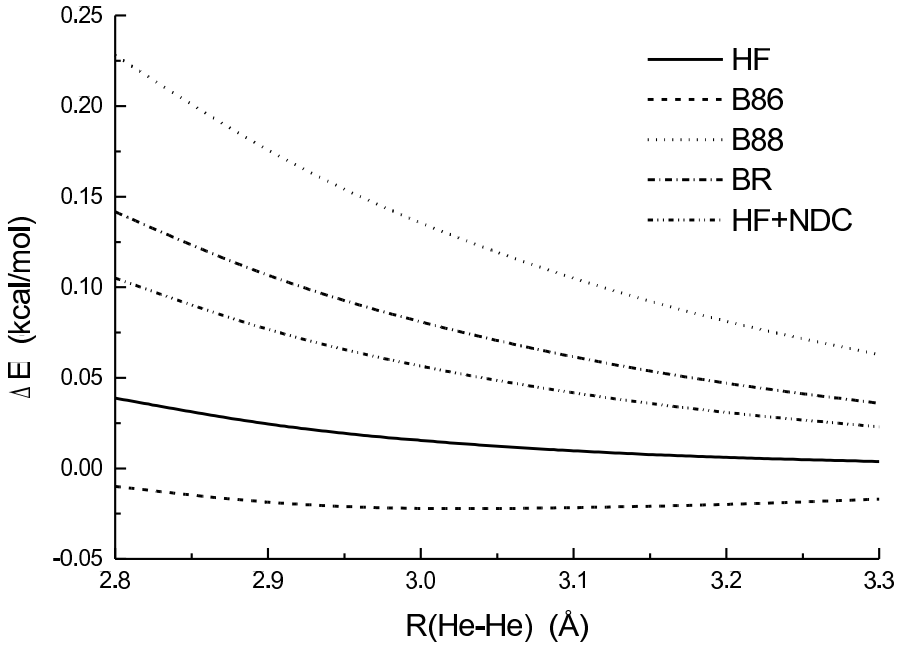

Figure 9.2: Atomic exchange and nondynamical correlation (NDC) energies. Notice that the NDC results mimic the difference between BR and exact (HF) exchange.

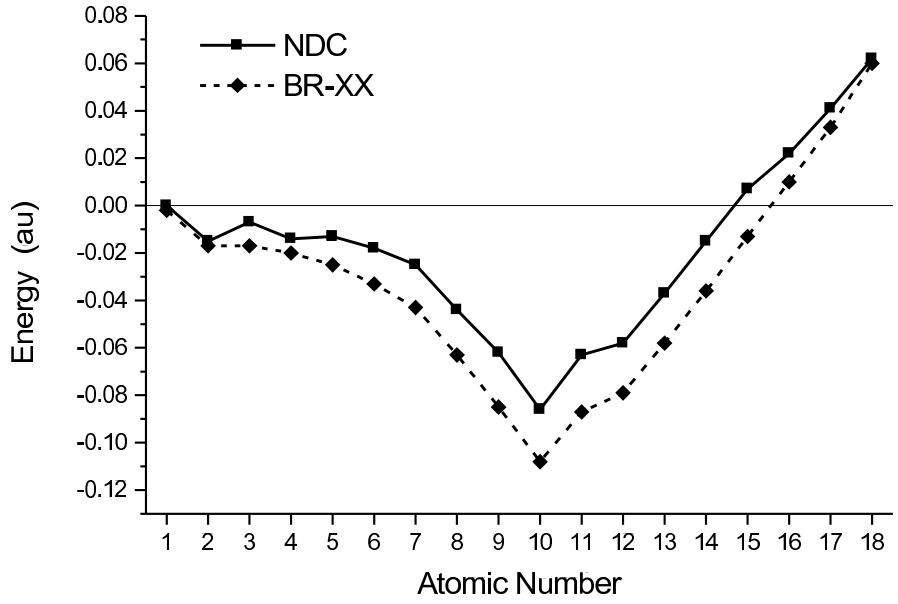

Figure 9.3: Exchange energy curves for the H_2 molecule (spin restricted). Note that the B86 and B88 curves lie virtually on top of each other.

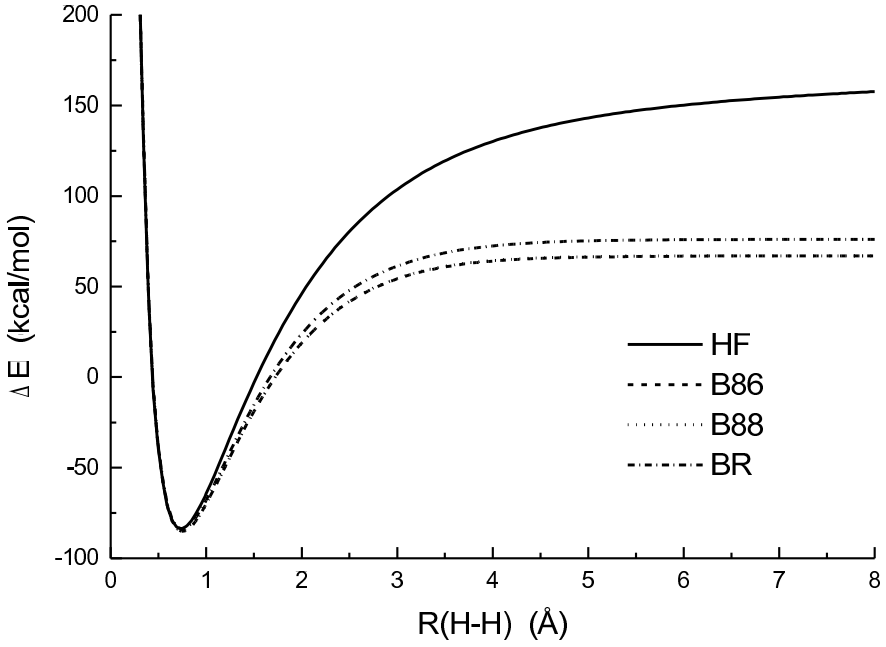

Chapter 10

Exchange-Hole Dipole Moment and the Dispersion Interaction Revisited

Original reference: A. D. Becke and E. R. Johnson, J. Chem. Phys. **127**, 154108 (2007).

Abstract

We have recently introduced a model of the dispersion interaction based on the position-dependent dipole moment of the exchange hole [84]. The original derivation, involving simple dipole-induced-dipole electrostatics, was somewhat heuristic however and lacking in rigour. Here we present a much more satisfying derivation founded on 2nd-order perturbation theory in the closure approximation and a semiclassical evaluation of the relevant interaction integrals. Expressions for C_6, C_8, and C_{10} dispersion coefficients are obtained in a remarkably straightforward manner. Their values agree very well with *ab initio* reference data on dispersion coefficients between the atoms H, He, Ne, Ar, Kr, and Xe. We also highlight the importance of the

exchange contribution to the dispersion coefficients, especially to C_6.

10.1 Introduction

In a previous paper [84] we introduced a conceptually appealing model of C_6 dispersion coefficients generated by the position-dependent dipole moment of an electron and its exchange hole. The model was extended to C_8 and C_{10} coefficients in Ref. [121], incorporated into density-functional theory in Ref. [116], and has been applied to intermolecular and intramolecular vdW potential energy surfaces in Refs. [127, 134, 138].

We use occupied orbitals only, either Hartree-Fock or Kohn-Sham, and our C_6, C_8, and C_{10}'s involve no fitting of parameters whatsoever. Appealing and successful as it is, however, the original derivation of the model was highly intuitive and heuristic. The dipole-induced-dipole approach of Ref. [84] was simplistic, even missing a factor of four. The perturbation-theory approach of Ref. [121] replaced multi-electron expectation values with effective one-electron integrals, only partially supported by the subsequent analysis of Angyan [139].

Here we introduce a much more satisfying approach. We begin with 2nd-order perturbation theory in the closure approximation and then model the dispersion interaction in a semiclassical way. The model is "semi"-classical in that the dispersion interaction is treated as a classical multipole-multipole interaction, yet quantum effects are included through the exchange hole. The resulting derivation of expressions for C_6, C_8, and C_{10} dispersion coefficients is straighforward and, we think, delightfully simple. This work provided an independent verification of our previous expressions [121, 127, 134] based on angular momentum coupling formulas from Ref. [2], and, indeed, uncovered an error in Ref. [2].

To set the stage, we review in Section 10.2 the nature of correlation in electronic

systems and how correlation affects the instantaneous dipole moments generated by electrons in atoms. In Section 10.3 our new dispersion interaction model is developed. Dispersion coefficients are presented in Section 10.4 for all atom pairs between H, He, Ne, Ar, Kr, and Xe to demonstrate the quality of the model and to highlight the importance of the exchange-hole contribution, especially to C_6.

10.2 The Exchange-Hole Dipole Moment

As an electron moves through a multi-electron system, it repels other electrons from its vicinity through a combination of "Pauli" and "Coulomb" correlations. Pauli correlation arises from multi-electron wavefunction antisymmetry and acts between electrons of parallel spin. It has the consequence that the probability of finding *another* electron of parallel spin at the position of a given electron is *zero*. Coulomb correlation arises from the $1/r$ repulsive interaction between electron pairs and acts between electrons of both opposite and parallel spins. Coulomb correlation is much less important than Pauli correlation. In, eg., a single Slater determinant (Hartree-Fock theory) Pauli correlation contributes a significant exchange-energy component to the total energy. Coulomb correlation, on the other hand, contributes nothing in Hartree-Fock theory. We therefore consider only Pauli correlations in this work and assume that each monomer in an intermolecular interaction is described by a single Slater determinant.

If an electron of σ spin is at point $\mathbf{r}_1$ in a system, the extent to which Pauli correlation depletes the probability (with respect to the total statistical electron density) of finding another electron at point $\mathbf{r}_2$ is given by [72]

$$h_{X\sigma}(\mathbf{r}_1, \mathbf{r}_2) = -\frac{1}{\rho_\sigma(\mathbf{r}_1)} \sum_{ij} \psi_{i\sigma}(\mathbf{r}_1)\psi_{j\sigma}(\mathbf{r}_1)\psi_{i\sigma}(\mathbf{r}_2)\psi_{j\sigma}(\mathbf{r}_2) \tag{10.1}$$

called the *exchange* or *Fermi* "hole". The summation is over all occupied orbitals of σ spin, assumed in this paper to be real, and ρ_σ is the total σ-spin electron density. The Fermi hole is a powerful conceptual device. As an electron moves through a system, its Fermi hole accompanies it. The shape of the hole depends on the electron's instantaneous position $\mathbf{r}_1$, and its normalization is always -1 (easy to prove by integrating over $\mathbf{r}_2$ and using orthonormality of the orbitals).

The electron plus its hole is neutral overall. The hole is generally not, however, spherically symmetric around $\mathbf{r}_1$. Even in systems with spherically symmetric total densities, the hole is non-spherical unless $\mathbf{r}_1$ is at the center of the system. Thus the electron plus its hole has an $\mathbf{r}_1$-dependent *non-zero dipole moment* given by [84]

$$\mathbf{d}_{X\sigma}(\mathbf{r}_1) = \left[\frac{1}{\rho_\sigma(\mathbf{r}_1)}\sum_{ij}\psi_{i\sigma}(\mathbf{r}_1)\psi_{j\sigma}(\mathbf{r}_1)\int \mathbf{r}_2\psi_{i\sigma}(\mathbf{r}_2)\psi_{j\sigma}(\mathbf{r}_2)d^3\mathbf{r}_2\right] - \mathbf{r}_1. \qquad (10.2)$$

The situation is depicted for an electron in a spherical atom in Fig. 10.1. When the electron e^- is at distance r from the nucleus and at solid angle Ω, the mean position h^+ of the hole is at distance $(r - d_{X\sigma})$. Notice, furthermore, that higher multipole moments $M_{\ell\sigma}$ with respect to the nucleus as origin can be defined by e^- and h^+ as well [121]:

$$M_{\ell\sigma} = -\left[r^\ell - (r - d_{X\sigma})^\ell\right] \qquad (10.3)$$

all directed along Ω and depending on the magnitude of the exchange-hole dipole moment only.

The two-point picture of Fig. 10.1 is an approximate model of the electron and its hole. Therefore the higher moments, $\ell > 1$, of Eq. (10.3) are approximate. Exact $\ell > 1$ moments *could* be computed by appropriate generalizations of Eq. (10.2) to higher orders. The great strength of the two-point model, however, is its dependence

only on $d_{X\sigma}$. This is the key to transforming our theory into density-functional form as in Refs. [116, 138].

In the *absence* of correlation (i.e., if electron motions were truly independent of each other) an electron at r and Ω in a spherical atom would generate the following moments,

$$M_{\ell\sigma}(\text{uncorrelated}) = -r^{\ell} \tag{10.4}$$

along Ω. In atoms containing only s electrons, the exchange hole is centered at the nucleus ($d_{X\sigma} = r$) and Eqs. (10.3) and (10.4) are identical. In atoms with p, d, f, ... electrons, however, the exchange hole is removed from the nucleus ($d_{X\sigma} < r$) and the uncorrelated moments, Eq. (10.4), are significantly larger than the correlated moments, Eq. (10.3). It has long been known [8] that uncorrelated moments yield highly erroneous, far too large, dispersion coefficients. The effect of Pauli correlation and the exchange hole in p, d, f, ... atoms is therefore critical. This will be aptly demonstrated in Section 10.4.

10.3 The Dispersion Interaction

If the first-order, ground-state energy correction due to a perturbation V_{pert} is zero:

$$E^{(1)} = < V_{pert} > = 0, \tag{10.5}$$

then the second-order correction is approximately given by

$$E^{(2)} = -\frac{< V_{pert}^2 >}{\Delta E_{avg}}, \tag{10.6}$$

where the expectation values are in the ground state and ΔE_{avg} is an *average* excitation energy. This well-known result, derived in many standard textbooks [12], is called the "closure" or Unsöld approximation.

Consider two spherically symmetric atoms separated by a large internuclear distance R, and suppose that an electron is at position $\mathbf{r}_A$ in atom A and an electron is at position $\mathbf{r}_B$ in atom B (see Fig. 10.2). As established in the previous section, the electron at $\mathbf{r}_A$ generates multipole moments with respect to nucleus A given by Eq. (10.3) and directed along $\mathbf{r}_A$. The electron at $\mathbf{r}_B$ similarly generates multipole moments with respect to nucleus B. For the perturbation V_{pert} in Eq. (10.6), we take the multipole-multipole interaction energy as follows:

$$V_{AB}(\mathbf{r}_A, \mathbf{r}_B) = V_{1,1} + V_{1,2} + V_{2,1} + V_{1,3} + V_{3,1} + V_{2,2}, \tag{10.7}$$

where subscripts 1, 2, and 3 denote dipole, quadrupole, and octopole moments respectively and we include all terms contributing to orders r^{-3}, r^{-4}, and r^{-5}.

The individual terms are given by [4]

$$V_{1,1}(\mathbf{r}_A, \mathbf{r}_B) = \frac{M_1(r_A)M_1(r_B)}{R^3}(-3c_Ac_B + c_{AB}), \tag{10.8a}$$

$$V_{1,2}(\mathbf{r}_A, \mathbf{r}_B) = \frac{3}{2}\frac{M_1(r_A)M_2(r_B)}{R^4}(5c_Ac_B^2 - 2c_Bc_{AB} - c_A), \tag{10.8b}$$

$$V_{2,1}(\mathbf{r}_A, \mathbf{r}_B) = \frac{3}{2}\frac{M_2(r_A)M_1(r_B)}{R^4}(-5c_A^2c_B + 2c_Ac_{AB} + c_B), \tag{10.8c}$$

$$V_{1,3}(\mathbf{r}_A, \mathbf{r}_B) = \frac{1}{2}\frac{M_1(r_A)M_3(r_B)}{R^5}(-35c_Ac_B^3 + 15c_B^2c_{AB} + 15c_Ac_B - 3c_{AB}), \tag{10.8d}$$

$$V_{3,1}(\mathbf{r}_A, \mathbf{r}_B) = \frac{1}{2}\frac{M_3(r_A)M_1(r_B)}{R^5}(-35c_A^3c_B + 15c_A^2c_{AB} + 15c_Ac_B - 3c_{AB}), \quad (10.8e)$$

$$V_{2,2}(\mathbf{r}_A, \mathbf{r}_B) = \frac{3}{4}\frac{M_2(r_A)M_2(r_B)}{R^5}(35c_A^2c_B^2 - 20c_Ac_Bc_{AB} - 5c_A^2 - 5c_B^2 + 2c_{AB}^2 + 1), \quad (10.8f)$$

where c_A, c_B, and c_{AB} are the following direction cosines:

$$c_A = \hat{\mathbf{r}}_A \cdot \hat{\mathbf{R}} = \cos\theta_A, \quad (10.9a)$$

$$c_B = \hat{\mathbf{r}}_B \cdot \hat{\mathbf{R}} = \cos\theta_B, \quad (10.9b)$$

$$c_{AB} = \hat{\mathbf{r}}_A \cdot \hat{\mathbf{r}}_B = \cos\theta_A\cos\theta_B + \sin\theta_A\sin\theta_B\cos(\phi_B - \phi_A), \quad (10.9c)$$

$\hat{\mathbf{R}}$ is the unit vector from A to B, and (θ_A, ϕ_A) and (θ_B, ϕ_B) are the polar angles of $\hat{\mathbf{r}}_A$ and $\hat{\mathbf{r}}_B$ with respect to $\hat{\mathbf{R}}$.

Now evaluate the expectation value $< V_{pert}^2 >$ in Eq. (10.6) by *squaring* $V_{AB}(\mathbf{r}_A, \mathbf{r}_B)$ and integrating over all points $\mathbf{r}_A$ in atom A (weighted by the atomic density of A) and all points $\mathbf{r}_B$ in atom B (weighted by the atomic density of B). The result is

$$E_{disp} = -\frac{C_6}{R^6} - \frac{C_8}{R^8} - \frac{C_{10}}{R^{10}} - \ldots, \quad (10.10)$$

with dispersion coefficients given by

$$C_6 = \frac{2}{3}\frac{< M_1^2 >_A < M_1^2 >_B}{\Delta E_{avg}}, \quad (10.11a)$$

$$C_8 = \frac{< M_1^2 >_A < M_2^2 >_B + < M_2^2 >_A < M_1^2 >_B}{\Delta E_{avg}}, \tag{10.11b}$$

$$C_{10} = \frac{4}{3}\frac{< M_1^2 >_A < M_3^2 >_B + < M_3^2 >_A < M_1^2 >_B}{\Delta E_{avg}} + \frac{14}{5}\frac{< M_2^2 >_A < M_2^2 >_B}{\Delta E_{avg}}, \tag{10.11c}$$

and with atomic moment integrals given by

$$< M_\ell^2 >= \sum_\sigma \int \rho_\sigma M_{\ell\sigma}^2 d^3\mathbf{r}. \tag{10.12}$$

The derivation is very straightforward for C_6 and C_8, though laborious for C_{10}. These expressions are the same as our previous expressions in Ref. [121] except for the coefficient of the first term in Eq. (10.11c). The expression in Ref. [121] is incorrect due to an arithmetic error inherited from Ref. [2].

A more elegant derivation based on angular momentum coupling theory is presented in Appendix A.

We assume (see Appendix B) that the average excitation energy ΔE_{avg} is the sum of the average excitation energies of the constituent atoms:

$$\Delta E_{avg} = \Delta E_A + \Delta E_B \tag{10.13}$$

and that, for each atom, ΔE is related to its *polarizability* by the same perturbation theory used to obtain the dispersion energy [8, 84, 121]. The atomic polarizability α is defined by

$$E^{(2)} = -\frac{1}{2}\alpha F^2 = -\frac{< V_{pert}^2 >}{\Delta E}, \tag{10.14}$$

where $\mathbf{F}$ is the electric field vector and, in the present semiclassical approach,

$$V_{pert} = -\mathbf{d}_{X\sigma}(\mathbf{r}) \cdot \mathbf{F} \tag{10.15}$$

when an electron is at position $\mathbf{r}$ in the atom. Squaring V_{pert}, integrating over all points $\mathbf{r}$ in the atom (weighted by the atomic density), and using that $\mathbf{d}_{X\sigma}(\mathbf{r})$ is colinear with $\mathbf{r}$, we get

$$< V_{pert}^2 >= \frac{1}{3} < M_1^2 > F^2, \tag{10.16}$$

where $< M_1^2 >$ is the atomic dipole moment integral, Eq. (10.12) with $\ell = 1$. Solving for ΔE gives

$$\Delta E = \frac{2}{3} \frac{< M_1^2 >}{\alpha}. \tag{10.17}$$

Atomic polarizabilities α are conveniently tabulated in, eg., Ref. [76].

Substituting Eq. (10.17) into Eqs. (10.11), we finally obtain

$$C_6 = \frac{\alpha_A \alpha_B < M_1^2 >_A < M_1^2 >_B}{< M_1^2 >_A \alpha_B + < M_1^2 >_B \alpha_A}, \tag{10.18a}$$

$$C_8 = \frac{3}{2} \frac{\alpha_A \alpha_B (< M_1^2 >_A < M_2^2 >_B + < M_2^2 >_A < M_1^2 >_B)}{< M_1^2 >_A \alpha_B + < M_1^2 >_B \alpha_A}, \tag{10.18b}$$

$$\begin{aligned} C_{10} = 2 \frac{\alpha_A \alpha_B (< M_1^2 >_A < M_3^2 >_B + < M_3^2 >_A < M_1^2 >_B)}{< M_1^2 >_A \alpha_B + < M_1^2 >_B \alpha_A} \\ + \frac{21}{5} \frac{\alpha_A \alpha_B < M_2^2 >_A < M_2^2 >_B}{< M_1^2 >_A \alpha_B + < M_1^2 >_B \alpha_A}, \end{aligned} \tag{10.18c}$$

These are identical to expressions in previous papers [127, 134] except for the coeffi-

cient of the first term in C_{10}. The above C_{10} formula is correct.

The incorrect constant [6/5 instead of 2 in the first term of Eq. (10.18c)] in our previous papers [121, 127, 134] has negligible impact on the previous results or conclusions. Recalculation of the binding energies of our 45 intermolecular benchmark complexes of Ref. [127], for example, insignificantly changes the mean absolute percent error (MAPE) from 14.1% to 13.7%.

10.4 Calculations and Conclusions

Tables 10.1, 10.2, and 10.3 give dispersion coefficients from Eqs. (10.18) for all pairs of the atoms H, He, Ne, Ar, Kr, and Xe. The dipole moments, Eq. (10.2), and moment integrals, Eq. (10.12), are numerically integrated over Hartree-Fock orbitals from the NUMOL program of Becke and Dickson [78]. Atomic polarizabilities are from Ref. [76]. Results for both exchange-hole corrected and uncorrelated moments, Eqs. (10.3) and (10.4) respectively, are presented in order to demonstrate the importance of exchange effects. For C_6, the latter is equivalent to the early Kirkwood-Müller model (see Ref. [8] and references therein). *Ab initio* reference data is from Refs. [80, 113, 114].

Our C_6 values are in excellent agreement with the reference data. The mean absolute percent error (MAPE) is only 3.4%. Our C_8's and C_{10}'s are reasonably good, with MAPEs of 21.5% and 21.5%, though not as good as our C_6's.

The uncorrelated C_6's, on the other hand, have an enormous MAPE of 85.0%. The uncorrelated C_8's and C_{10}'s are fortuitously better than the uncorrelated C_6's due to the fact that the moment integrals $< M_\ell^2 >$ are less affected by exchange as ℓ increases [9]. At the same time, the far-too-large uncorrelated $< M_1^2 >$ integrals in the denominators of Eqs. (10.18b) and (10.18c) drive the C_8 and C_{10} values down.

The importance of Pauli correlation (exchange) in dispersion coefficients, espe-

cially C_6, is well demonstrated by these data. We expect that the effects of Coulomb correlation, ignored here, would be small, reducing our dispersion coefficients slightly.

In conclusion, the present dispersion model is much more satisfying than our previous models [84, 121]. We obtain the same expressions for C_6, C_8, and C_{10} dispersion coefficients as before (with the exception of a corrected constant in the C_{10} expression) in a very straightforward and elegant manner. The generalization from atoms to molecules, and to intermolecular and intramolecular vdW potential energy surfaces, proceeds without change as in Refs. [127, 134, 138]. The present work nicely reinforces the theoretical underpinnings of our vdW methodology.

10.5 Appendix A: Angular Momentum Coupling Theory

Eqs. (10.11) can be derived using the formulas of angular momentum coupling theory as found, eg., in Ref. [2]. The potential energy of interaction, as in Fig. 10.2, between two spherical atoms A and B is given by

$$V_{AB}(\mathbf{r}_A, \mathbf{r}_B) = \sum_{\ell_A=0}^{\infty} \sum_{\ell_B=0}^{\infty} \frac{V_{\ell_A \ell_B}}{R^{\ell_A+\ell_B+1}}. \tag{10.19}$$

If the coordinate axes in A and B are parallel and their z axes point along $\mathbf{R}$ (the vector from A to B), then

$$V_{\ell_A \ell_B}(\mathbf{r}_A, \mathbf{r}_B) = \sum_{m=-\ell_{min}}^{+\ell_{min}} M_{\ell_A}(r_A) Y_{\ell_A}^{m}(\theta_A, \phi_A) M_{\ell_B}(r_B) Y_{\ell_B}^{-m}(\theta_B, \phi_B)$$
$$\times \frac{(-)^{\ell_B} 4\pi(\ell_A+\ell_B)!}{[(2\ell_A+1)(2\ell_B+1)(\ell_A-m)!(\ell_A+m)!(\ell_B-m)!(\ell_B+m)!]^{1/2}}, \tag{10.20}$$

where ℓ_{min} is the smaller of ℓ_A and ℓ_B. If V_{AB} is *squared* and integrated over all $\mathbf{r}_A$ in A (weighted by the atomic density of A) and all $\mathbf{r}_B$ in B (weighted by the atomic density of B), all cross terms vanish thanks to orthogonality of the spherical harmonic functions. We get the dispersion series, Eq. (10.10), again with

$$C_6 = \lambda_{1,1} \frac{< M_1^2 >_A < M_1^2 >_B}{\Delta E_{avg}}, \tag{10.21a}$$

$$C_8 = \lambda_{1,2} \frac{< M_1^2 >_A < M_2^2 >_B + < M_2^2 >_A < M_1^2 >_B}{\Delta E_{avg}}, \tag{10.21b}$$

$$\begin{aligned} C_{10} = \lambda_{1,3} \frac{< M_1^2 >_A < M_3^2 >_B + < M_3^2 >_A < M_1^2 >_B}{\Delta E_{avg}} \\ + \lambda_{2,2} \frac{< M_2^2 >_A < M_2^2 >_B}{\Delta E_{avg}}, \end{aligned} \tag{10.21c}$$

and (see Ref. [2]),

$$\begin{aligned} \lambda_{\ell_A,\ell_B} &= \frac{[(\ell_A+\ell_B)!]^2}{(2\ell_A+1)(2\ell_B+1)} \sum_{m=-\ell_{min}}^{+\ell_{min}} \frac{1}{(\ell_A-m)!(\ell_A+m)!(\ell_B-m)!(\ell_B+m)!} \\ &= \frac{(2\ell_A+2\ell_B)!}{(2\ell_A+1)(2\ell_B+1)(2\ell_A)!(2\ell_B)!}. \end{aligned} \tag{10.22}$$

The atomic moment integrals $< M_\ell^2 >$ are as defined in Eq. (10.12). Evaluating the λ_{ℓ_A,ℓ_B}: $\lambda_{1,1} = \frac{2}{3}$, $\lambda_{1,2} = 1$, $\lambda_{1,3} = \frac{4}{3}$, $\lambda_{2,2} = \frac{14}{5}$, we obtain the same coefficients as in Eqs. (10.11).

10.6 Appendix B: Average Excitation Energies

The assumption, Eq. (10.13), that the average excitation energy of the AB system is the sum of the average excitation energy of A and the average excitation energy of

B may not be obvious. We therefore give a simple proof here.

Denote the excitation energies of A by E_i and the excitation energies of B by E_j, and the number of excited states by N_A and N_B respectively. Then the average excitation energy of A is

$$\Delta E_A = \frac{1}{N_A} \sum_i E_i \tag{10.23}$$

and similarly for B. If A and B interact weakly, the excitation energies of the AB system are $E_i + E_j$ and the number of excited states is $N_A N_B$. The average excitation energy of AB is therefore

$$\begin{aligned} \Delta E_{AB} &= \frac{1}{N_A N_B} \sum_i \sum_j (E_i + E_j) \\ &= \frac{1}{N_A N_B} \sum_i \sum_j E_i + \frac{1}{N_A N_B} \sum_i \sum_j E_j \\ &= \frac{1}{N_A N_B} \times N_B \sum_i E_i + \frac{1}{N_A N_B} \times N_A \sum_j E_j \\ &= \Delta E_A + \Delta E_B \end{aligned} \tag{10.24}$$

as assumed in Eq. (10.13).

Table 10.1: C_6 coefficients for atomic pairs (atomic units).

Atom Pair	Eq. (10.3)	Eq. (10.4)	Ref.
H-H	6.76	6.76	6.49
H-He	2.99	2.99	2.82
H-Ne	5.69	6.74	5.69
H-Ar	20.13	25.91	19.86
H-Kr	29.44	39.25	29.15
H-Xe	45.14	63.52	44.14
He-He	1.64	1.64	1.46
He-Ne	3.09	4.26	3.07
He-Ar	9.81	15.20	9.57
He-Kr	14.08	23.03	13.65
He-Xe	20.91	37.07	19.92
Ne-Ne	5.83	12.52	6.55
Ne-Ar	18.60	41.67	19.75
Ne-Kr	26.71	63.19	28.01
Ne-Xe	39.72	101.23	40.52
Ar-Ar	62.71	144.30	64.54
Ar-Kr	90.93	218.78	93.16
Ar-Xe	137.4	351.4	138.0
Kr-Kr	132.1	331.7	135.1
Kr-Xe	200.1	532.7	201.3
Xe-Xe	304.7	855.8	302.3
MAPE	3.4	85.0	–
MPE	0.3	85.0	–
MaxAPE	12.1	183.1	–

MAPE: mean absolute percent error. MPE: mean percent error. MaxAPE: maximum absolute percent error. Literature values from Ref. [80, 113, 114].

Table 10.2: C_8 coefficients for atomic pairs (atomic units).

Atom Pair	Eq. (10.3)	Eq. (10.4)	Ref.
H-H	152.1	152.1	124.4
H-He	48.37	48.37	41.75
H-Ne	111.7	105.2	97.8
H-Ar	560.5	507.8	442.1
H-Kr	920.6	807.9	732.2
H-Xe	1688	1431	1357
He-He	16.15	16.15	14.11
He-Ne	41.05	39.47	36.18
He-Ar	211.2	201.6	167.5
He-Kr	351.0	328.2	280.0
He-Xe	649.2	600.6	525.0
Ne-Ne	97.40	108.98	90.34
Ne-Ar	464.2	528.9	390.1
Ne-Kr	757.8	864.4	638.1
Ne-Xe	1370	1582	1162
Ar-Ar	2082	2408	1623
Ar-Kr	3329	3866	2617
Ar-Xe	5869	6895	4669
Kr-Kr	5287	6188	4187
Kr-Xe	9234	10978	7389
Xe-Xe	15922	19305	12807
MAPE	21.5	27.2	–
MPE	21.5	27.2	–
MaxAPE	28.2	50.7	–

MAPE: mean absolute percent error. MPE: mean percent error. MaxAPE: maximum absolute percent error. Literature values from Ref. [80, 113, 114].

Table 10.3: C_{10} coefficients for atomic pairs (atomic units).

Atom Pair	Eq. (10.3)	Eq. (10.4)	Ref.
H-H	4438	4438	3286
H-He	1065.3	1065.3	858.7
H-Ne	2619	2267	2221
H-Ar	16496	12977	12617
H-Kr	29671	21956	23441
H-Xe	62297	42843	51088
He-He	214.2	214.2	183.2
He-Ne	598.8	500.3	545.1
He-Ar	4475	3567	3701
He-Kr	8499	6486	7257
He-Xe	18896	13853	16674
Ne-Ne	1625	1317	1536
Ne-Ar	11050	9087	9335
Ne-Kr	20399	16678	17658
Ne-Xe	43819	35826	38978
Ar-Ar	64960	52050	49063
Ar-Kr	114390	90550	88260
Ar-Xe	232344	182168	184250
Kr-Kr	198379	155528	155450
Kr-Xe	395106	307395	316030
Xe-Xe	766727	592409	619840
MAPE	21.5	9.1	–
MPE	21.5	-0.5	–
MaxAPE	35.1	35.1	–

MAPE: mean absolute percent error. MPE: mean percent error. MaxAPE: maximum absolute percent error. Literature values from Ref. [80, 113, 114].

Figure 10.1: Exchange-hole dipole geometry (e^- is the reference position of a σ-spin electron and h^+ is the mean position of its exchange hole).

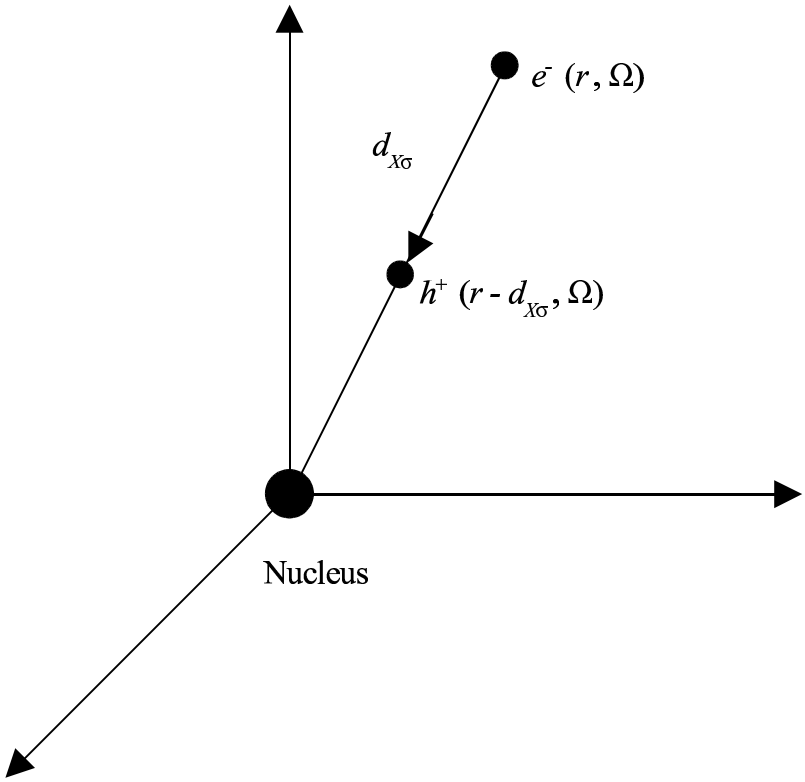

Figure 10.2: Interaction between multipole moments of an electron and its exchange hole at $\mathbf{r}_A$ in atom A and an electron and its exchange hole at $\mathbf{r}_B$ in atom B.

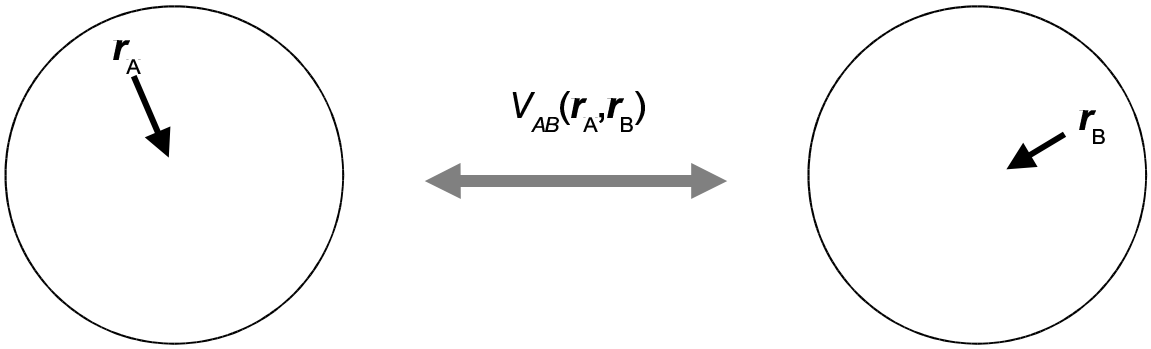

Chapter 11

A Unified Density-Functional Treatment of Dynamical, Nondynamical, and Dispersion Correlations II: Thermochemical and Kinetic Benchmarks

Original reference: E. R. Johnson and A. D. Becke, J. Chem. Phys. Submitted.

Abstract

In previous work [138] we introduced an exact-exchange-based density-functional methodology incorporating dynamical, nondynamical, and dispersion correlations called DF07. In this work, the performance of the DF07 method is assessed on a variety of thermochemical and kinetic benchmark data including ionization potentials, electron affinities, proton affinities, isomerization energies, bond dissociation enthalpies, and barrier heights of radical reactions. DF07 gives uniform accuracy

over all our benchmark data without any refitting of parameters. The importance of the exact-exchange character of DF07 is highlighted through comparison with a 3-parameter hybrid meta-GGA functional.

11.1 Introduction

Hybrid exchange-correlation density functionals are very popular in computational chemistry and are capable of providing highly accurate thermochemistry results in many applications [14]. However, the local exchange component of hybrid functionals drastically over-stabilizes stretched odd-electron systems [15], including transition states of chemical reactions [56] and delocalized radicals [140]. Hybrid functionals also fail to account for the long-range electron correlation responsible for London dispersion interactions [17, 18].

The problems inherent in local exchange approximations are avoided by using exact (Hartree-Fock) exchange. Our recent work has therefore focused on developing post-Hartree-Fock real-space correlation models. The resulting 2005 functional of Becke [25], to be denoted "B05" in this work, starts with exact exchange and adds four correlation terms accounting for dynamical and nondynamical correlation for both opposite- and parallel-spin electron pairs. B05 was designed to give the correct dissociation limits for H_2^+, H_2, He_2^+, and He_2 and performs well for both atomization energies and reaction barrier heights [25, 57].

A density-functional dispersion model has also been developed [127, 141] based on the exchange-hole dipole moment and second-order perturbation theory. Our dispersion model has been combined with B05 to give the "DF07" method [138], a unified density-functional treatment of dynamical, nondynamical, and dispersion correlations. The 7 parameters in DF07 were determined by simultaneously minimizing the RMS error in 222 atomization energies [40] and the RMS percent error in the

binding energies of 45 van der Waals complexes [127].

In this work the performance of the B05 and DF07 methods is assessed on several thermochemical and kinetic benchmark data sets. The data includes ionization potentials [40], electron affinities [40], proton affinities [40], isomerization energies [142], bond dissociation enthalpies [140], and barrier heights of radical reactions [143, 144]. The barrier heights are subdivided into two sets: hydrogen atom transfer (HAT) reactions [143] and non-hydrogen atom transfer reactions [144]. The latter set includes heavy-atom transfers, nucleophilic substitutions, unimolecular, and association reactions. To highlight the importance of the exact-exchange character of B05 and DF07, we also compare to a 3-parameter hybrid meta-GGA, "B3BR", and a dispersion corrected version, "B3BR-D".

11.2 Computational Methods

The geometries of all species in the barrier height sets are from Refs. [143] and [144] and are QCISD/MG3 geometries. In all other cases, geometry optimizations and frequency calculations were performed using the Gaussian 98 program [49] at the B3LYP/6-31G(2df,p) [46, 48] level as recommended in the G3X procedure [135]. Single-point post-LSDA energy calculations were then carried out on all species with the NUMOL program [79] using the PW91 LSDA [38]. Electronic energies were thus obtained for each of B05, DF07, B3BR, and B3BR-D. The various exchange and correlation terms in these functionals are thoroughly reviewed in Ref. [138]. Hence only the general forms of the functionals will be described here.

The B05 functional has the form [25]:

$$E_{\mathrm{XC}}^{\mathrm{B05}} = E_X^{exact} + a_{\mathrm{NDC}}^{opp} U_{\mathrm{NDC}}^{opp} + a_{\mathrm{NDC}}^{par} U_{\mathrm{NDC}}^{par} + a_{\mathrm{DC}}^{opp} E_{\mathrm{DC}}^{opp} + a_{\mathrm{DC}}^{par} E_{\mathrm{DC}}^{par}, \tag{11.1}$$

where E_X^{exact} is the exact exchange energy, $U_{\rm NDC}$ is the potential energy of nondynamical correlation [25], $E_{\rm DC}$ is the dynamical correlation energy [47], and the superscripts indicate opposite or parallel electron spins.

The DF07 functional has the form [138]:

$$E_{\rm XC}^{\rm DF07} = E_X^{exact} + a_{\rm NDC}^{opp} U_{\rm NDC}^{opp} + a_{\rm NDC}^{par} U_{\rm NDC}^{par} + a_{\rm DC}^{opp} E_{\rm DC}^{opp} + a_{\rm DC}^{par} E_{\rm DC}^{par} + E_{disp}^{\rm BR}(a_1, a_2) + a_{\rm RC}(E_X^{\rm B86} - E_X^{\rm B88}), \qquad (11.2)$$

where $E_{disp}^{\rm BR}$ is the BR variant of our dispersion energy (see Ref. [138]) dependent on two universal parameters a_1 and a_2, and $(E_X^{\rm B86} - E_X^{\rm B88})$ is a Pauli repulsion correction.

The B3BR functional is a hybrid of Becke-Roussel meta-GGA exchange [43], $E_X^{\rm BR}$, dynamical correlation [47], and exact exchange:

$$E_{\rm XC}^{\rm B3BR} = (1 - a_0) E_X^{exact} + a_0 E_X^{\rm BR} + a_{\rm DC}^{opp} E_{\rm DC}^{opp} + a_{\rm DC}^{par} E_{\rm DC}^{par}. \qquad (11.3)$$

The B3BR-D functional is obtained by adding the same Pauli repulsion correction and dispersion terms present in DF07 to B3BR:

$$E_{\rm XC}^{\rm B3BR\text{-}D} = (1 - a_0) E_X^{exact} + a_0 E_X^{\rm BR} + a_{\rm DC}^{opp} E_{\rm DC}^{opp} + a_{\rm DC}^{par} E_{\rm DC}^{par} + E_{disp}^{\rm BR}(a_1, a_2) + a_{\rm RC}(E_X^{\rm B86} - E_X^{\rm B88}). \qquad (11.4)$$

Other hybrids are of course conceivable using other local exchange and dynamical correlation parts. The predominantly Becke-Roussel character of DF07 (see Ref. [138]) suggests, however, that the above BR-based hybrids are the most suitable for comparison.

Parameter values for all four functionals are collected in Table 11.1. The B05 and B3BR parameters were fit to the G3/99 atomization energies of Ref. [40]. The DF07 and B3BR-D parameters were obtained as in Ref. [138], by simultaneously minimizing

the RMS error in the G3/99 atomization energies and the RMS percent error in the binding energies of 45 van der Waals (vdW) complexes. DF07 gives a mean absolute percent error (MAPE) of 7.9% and a maximum absolute percent error (MaxAPE) of 25.3% for the vdW binding energies [138]. B3BR-D gives similar vdW statistics, with a MAPE of 7.7% and a MaxAPE of 22.4%.

11.3 Results and Discussion

The error statistics for each of our thermochemical and kinetic benchmark sets are given in Table 11.2. Atomization energies, ionization potentials, electron affinities, and proton affinities are from the G3/99 test set [40], with two exceptions. The ionization energy of CN and the electron affinity of C_2 have been removed from consideration because C_2 and CN^+ both have low-lying *open-shell* singlet excited states that strongly mix with the ground state. It is well known that DFT should not be applied to systems with multi-determinant character [145].

B05 and B3BR perform similarly on the atomization energies, with mean absolute errors (MAEs) of 2.9 and 3.0 kcal/mol. Inclusion of dispersion, as in DF07 and B3BR-D, lowers the MAEs by 0.2 kcal/mol. On the ionization potentials, the exact-exchange-based methods yield MAEs of 3.2 kcal/mol, an improvement over the hybrid methods of 0.4-0.5 kcal/mol. The opposite trend is seen for the proton affinities, with the hybrid methods yielding MAEs of 1.6-1.8 kcal/mol, 0.7 kcal/mol lower than the MAEs of the exact-exchange-based functionals. Electron affinity errors of 2.8-3.0 kcal/mol are obtained with all functionals. All four functionals also perform similarly on the isomerization energies, with MAEs of 2.1-2.3 kcal/mol.

It is generally accepted that hybrid functionals perform well for the thermochemical benchmark sets considered so far and, in these cases, our exact-exchange-based functionals do not offer any significant improvement. However, the final three data

sets considered include delocalized radical species, which are problematic for DFTs based on local exchange approximations. It is in these data sets that we expect B05 and DF07 to outperform the hybrid methods.

In a previous study of main-group X-H and X-Y (X,Y=C,N,O,F,Si,S,Cl,Br) bond dissociation enthalpies (BDEs) [140], we found that the B3P86 [44, 48] hybrid performs well for most of these BDEs, but underestimates the BDE in cases where the resulting radical fragments are highly delocalized (such as allyl or pentadienyl radicals). This is a symptom of the same underlying problem as in stretched H_2^+, that local exchange functionals over-stabilize delocalized odd-electron systems [15]. We also noted [140] under-estimations of several Si-X BDEs, including $(CH_3)_3$Si-N$(CH_3)_2$, $(CH_3)_3$Si-OCH_2CH_3, and $(CH_3)_3$Si-Si$(CH_3)_3$. In these cases there are steric H-H clashes in the parent molecule that are relieved in the separated radicals and the observed errors may be due to neglect of dispersion. The same pattern of errors is observed in the present work for B3BR. On the test set of 76 BDEs of Ref. [140], the hybrid methods B3BR and B3BR-D give MAEs of 3.4-3.6 kcal/mol, even larger than the G3/99 atomization-energy errors. B05 remedies the delocalized radical problem, lowering the MAE to 2.1 kcal/mol. The DF07 method further lowers the MAE to 1.7 kcal/mol, with the dispersion correction greatly improving performance for the problematic Si-X bonds.

Hybrid DFTs fit to atomization-energy data are well known to underestimate the barrier heights of simple HAT reactions [56]. The source of this error is that hybrid functionals over-stabilize the transition state where the unpaired electron is more delocalized than in the separated reactants. Including a greater fraction of exact exchange (ca. 45-50%) improves barrier heights but sacrifices accuracy in thermochemical properties such as bond dissociation energies and electron affinities [146], and can also yield very large errors for barriers outside the parameter fit set [147]. The B05 functional, on the other hand, performs well for barriers *without reparameteri-*

zation [57]. In Table 11.2, we see that B05 and DF07 give MAEs of 1.2-1.3 kcal/mol for the hydrogen-atom transfer barriers and 1.7-2.0 kcal/mol for the non-hydrogen transfer barriers. This is a substantial improvement over B3BR and B3BR-D, which give MAEs of 3.4-3.9 kcal/mol for these barriers.

The only other functional in the literature that, like B05 and DF07, is based entirely on exact exchange is the MCY functional of Ref. [58]. MCY accurately treats the G3/99 atomization energies (MAE of 3.4 kcal/mol) and the HAT barriers (MAE of 2.0 kcal/mol) [58], but does not include dispersion.

11.4 Conclusions

We have compared in this work two density functionals that include dispersion physics: the exact-exchange-based DF07 functional [138] and the hybrid functional B3BR-D. Both perform well on van der Waals complexes, the G3 thermochemical benchmarks, and isomerization energies. However, hybrid DFTs over-stabilize delocalized odd-electron systems, leading to large errors for B3BR-D on barrier heights of radical transfer reactions and some bond dissociation enthalpies.

DF07 is an excellent universal functional for both thermochemistry and kinetics. Full inclusion of both exact exchange and dispersion reduces errors, relative to hybrid functionals, for delocalized radicals, transition states, and species with steric H-H interactions. Our DF07 results approach "chemical accuracy" for main-group chemistry, with MAEs of ca. 3 kcal/mol for atomization energies, ionization potentials, electron affinities, and proton affinities and ca. 2 kcal/mol for isomerization energies, BDEs, and barrier heights. To the best of our knowledge, DF07 is the only DFT that provides a uniformly accurate treatment for all of these benchmark sets without refitting of parameters to each.

Table 11.1: Optimized parameters.

Parameter	B05	DF07	B3BR	B3BR-D
a_0	–	–	0.810	0.826
a_{NDC}^{opp}	0.514	0.515	–	–
a_{NDC}^{par}	0.651	0.637	–	–
a_{DC}^{opp}	1.075	1.070	1.100	1.101
a_{DC}^{par}	1.113	0.985	1.382	1.262
a_1	–	0.61	–	0.59
a_2	–	1.97 Å	–	2.07 Å
a_{RC}	–	0.27	–	0.31

Table 11.2: Mean absolute errors for each of the benchmark sets. Maximum absolute errors are in parentheses. All values are in kcal/mol.

Data set	B05	DF07	B3BR	B3BR-D
Atomization energies (222)	3.0 (11.8)	2.8 (11.5)	2.9 (10.8)	2.7 (11.2)
Ionization potentials (87)	3.2 (14.4)	3.2 (14.3)	3.6 (13.4)	3.7 (13.4)
Electron affinities (57)	2.9 (9.7)	3.0 (9.9)	2.8 (11.0)	2.9 (10.7)
Proton affinities (8)	2.3 (3.8)	2.5 (4.1)	1.6 (2.9)	1.8 (3.4)
Isomerizations (34)	2.3 (11.6)	2.1 (10.0)	2.2 (11.6)	2.1 (9.9)
BDEs (76)	2.1 (7.8)	1.7 (6.8)	3.6 (11.8)	3.4 (10.8)
HAT Barriers (41)	1.2 (7.7)	1.3 (7.0)	3.4 (7.4)	3.9 (7.9)
Non-H Barriers (32)	1.7 (3.8)	2.0 (5.1)	3.4 (8.4)	3.9 (10.0)

Chapter 12

General Discussion

This thesis has described the development and testing of our exchange-hole dipole-moment dispersion model and the DF07 universal DFT. The chapters can be grouped as follows: development of the model for dispersion coefficients (Chapters 3, 6, and 10), extension of the model to computation of potential energy surfaces (Chapters 4, 5, 7, and 9) and application to benchmark systems (Chapters 8 and 11).

The physical picture underlying our dispersion model is that the source of the instantaneous dipoles responsible for the dispersion interaction is the position-dependent exchange-hole dipole moment generated by electrons in non-uniform systems. This model evolved from the simplistic dipole-induced-dipole electrostatic argument of Chapter 3, to approximation of two-electron operators in second-order perturbation theory in Chapter 6. It should be noted that the factor of four error in the dispersion coefficients in Chapter 3 was a result of the simplistic electrostatic model and this error is eliminated in the perturbation theory treatment. Chapter 10 presents our most elegant derivation involving semi-classical evaluation of interaction integrals within second-order perturbation theory.

Our first applications of the model to post-Hartree-Fock calculation of potential energy surfaces in Chapters 4 and 5 included only the leading-order C_6 term of the

dispersion energy. We also used an *energy-based* cut-off of the dispersion energy at small internuclear separations. Both the exact exchange-hole (XX) variant and its DFT reformulation using the BR exchange-hole model were major improvements over conventional DFTs for computation of accurate van der Waals potential energy surfaces. However, this early model had two major shortcomings: dependence on molecular polarizabilities, thus preventing application to intramolecular dispersion interactions, and drastic underbinding of π-stacked complexes.

In chapters 6 and 7 our dispersion model was refined to remedy both these problems, yielding the HFBR-XDM method. Extending the model to include higher-order C_8 and C_{10} dispersion coefficients provided a convenient *separation-based* cut-off at small internuclear separations, as opposed to the previous energy-based cut-off. The C_6 term was shown to account for ca. 60% of the dispersion energy, with C_8 and C_{10} terms contributing ca. 30% and 10%, respectively. Inclusion of the C_8 and C_{10} terms is particularly critical for π-stacked systems, in which there is substantial Pauli-repulsion at the equilibrium geometry and the dispersion energy is up to twice as large as the binding energy. Dependence on molecular polarizabilities was eliminated by exploiting the relationship between polarizability and volume, allowing atom-in-molecule polarizabilities to be obtained from tabulated free atomic polarizabilities and computed atomic volumes. This yielded a unified treatment of interatomic, intermolecular, and even intramolecular dispersion interactions as demonstrated in the bio-organic tests in Chapter 8.

The HFBR-XDM dispersion model accurately describes all classes of van der Waals interactions, from dispersion to hydrogen bonding. To obtain a unified density functional theory, the B05 nondynamical correlation energy [25] was added to HFBR-XDM in Chapter 9, allowing modeling of covalent bonding as well as van der Waals interactions. Inclusion of a "repulsion correction" term was necessary to seamlessly mesh these two models together. The correction term also permitted the use of LSDA

input orbitals as opposed to HF orbitals, which represents a great computational saving for many numerical codes. The resulting DF07 model meets all the requirements for a unified density functional. It includes a balanced treatment of the three distinct correlation types: dynamical, nondynamical, and dispersion correlation. Its seven parameters are all physically motivated and, after simultaneous fitting to van der Waals complexes and the G3 atomization energy set, the optimum values agree with physical intuition. While DF07-XX and DF07-BR give very similar results for thermochemistry, the BR variant performs substantially better for π-stacked complexes [138].

In Chapter 11, DF07 was applied to a variety of thermochemical and kinetic benchmark sets, including ionization potentials, electron and proton affinities, isomerization energies, bond dissociation enthalpies, and barrier heights, with impressive results. The hybrid B3BR-D functional was introduced in this chapter for comparative purposes, to demonstrate the importance of the 100% exact exchange in DF07 for kinetics. B3BR-D and DF07 give similar results for van der Waals complexes, but DF07 is clearly superior in systems involving delocalized unpaired electrons.

Table 12.1 summarizes the performance of all the dispersion-inclusive functionals of this thesis, HFBR-XDM, DF07, and B3BR-D, for each class of interaction type in our test set of 45 van der Waals complexes. Note that the HFBR-XDM results differ slightly from those in Chapter 7 due to an error in the coefficient of the dipole-octopole term in the C_{10} coefficient corrected in Chapter 9 [141]. MP2 results are presented in the table as well. DF07-BR and B3BR-D are roughly three times as accurate as MP2 for dispersion-bound complexes, with particularly notable improvement in the binding energies of the π-stacked complexes. DF07-BR and B3BR-D also out-perform MP2 for dipole-induced dipole and dipole-dipole interactions. This is especially impressive considering the much lower computational cost and much wider range of applicability of these DFTs compared to MP2.

Table 12.1: Mean absolute percent errors in calculated binding energies. The reference data and MP2 results for the 45 complex set are given in Chapter 7. The HFBR-XDM results are revised from those in Chapter 7 to correct for an error in the C_{10} coefficient, as discussed in Chapters 9 and 10.

Interaction Type	MP2	HFBR-XDM	DF07-XX	DF07-BR	B3BR-D
Dispersion	34.7	16.4	15.6	8.9	8.5
Dipole-Induced-Dipole	8.5	10.5	7.6	7.3	6.8
Dipole-Dipole	8.3	8.8	6.4	5.6	5.8
Hydrogen bonded	2.4	8.6	6.3	6.0	7.2
Overall	24.1	13.7	12.3	7.9	7.7

Chapter 13

Conclusions and Outlook

The overall objective of this thesis was to develop a unified density functional theory capable of treating dynamical, nondynamical, and dispersion correlations. The DF07 functional fulfills this objective. DF07 is an exact-exchange-based method which has been shown to provide accurate thermochemistry, kinetics, and van der Waals interactions, including dispersion, with precision approaching "chemical accuracy".

The exchange-hole dipole moment is the central object of the dispersion model used in DF07. The model gives non-empirical C_6, C_8, and C_{10} dispersion coefficients using the occupied orbitals, or the electron density, its gradient and Laplacian, and the kinetic energy density, and from free atomic polarizabilities. The model involves only two universal parameters with well-defined physical interpretation. Its computational cost is negligible compared to the calculation of the Hartree-Fock or Kohn-Sham orbitals themselves.

DF07 has been benchmarked on dispersion coefficients, intermolecular potential energy surfaces, intramolecular conformational energies, atomization energies, ionization potentials, electron and proton affinities, isomerization energies, bond dissociation enthalpies, and reaction barrier heights, all with excellent results. For binding

energies of dispersion-bound complexes, DF07 gives average errors that are three times lower than for basis-set-extrapolated MP2, with lower computational costs and superior scaling. DF07 is the only DFT method at this time that is robust enough to include all three electron-correlation types in chemistry. This method promises to be widely useful in computational chemistry, particularly in organic and biochemical applications.

Future work will focus on benchmarking DF07 for change-transfer complexes and for transition-metal chemistry. GGA functionals generally overbind charge-transfer complexes [148]. This error stems from the tendency of GGAs to underestimate band gaps [16]. Performance for charge-transfer complexes should be improved with exact-exchange-based methods such as DF07. Transition-metal chemistry will be a very sensitive test of DF07 since conventional DFTs give errors in bond dissociation energies of transition-metal complexes that are considerably larger than for organic molecules [149]. Transition-metal complexes are also problematic for Hartree-Fock-based theories due to the importance of both dynamical and nondynamical correlation in the correct description of the binding [150].

DF07 is currently not implemented self-consistently. This is a major limitation. Self-consistent energies and forces are necessary in order to perform full geometry optimizations. However, this will be very difficult with DF07 due to the complicated form of the nondynamical correlation energy expressions (see Chapter 9). The B3BR-D hybrid functional presented in this thesis is a convenient alternative to DF07 since it does not include the nondynamical correlation energy terms. The accuracy of B3BR-D is comparable to DF07 for thermochemistry and van der Waals interactions, but as a hybrid functional, it is susceptible to large errors for delocalized odd-electron systems. Self-consistent orbital calculations, geometry optimizations, and frequency calculations should be straightforward to implement for B3BR-D in Gaussian-based computational chemistry packages. As for DF07, future work will explore simpli-

fications that will hopefully allow self-consistent orbital calculations and geometry optimizations eventually.

Bibliography

[1] F. London, Z. Phys. Chem. B. **11**, 222 (1930).

[2] A. Dalgarno and W. D. Davison, Adv. At. Mol. Phys. **2**, 1 (1966).

[3] G. D. Zeiss and W. J. Meath, Mol. Phys. **33**, 1155 (1977).

[4] A. J. Stone, The Theory of Intermolecular Forces. (Clarendon Press, Oxford, 1996).

[5] H. B. G. Casimir and D. Polder, Phys. Rev. **73**, 360 (1948).

[6] M. Karplus and H. J. Kolker, J. Chem. Phys. **41**, 3955 (1964).

[7] J. C. Slater and J. G. Kirkwood, Phys. Rev. **37**, 682 (1931).

[8] L. Salem, Mol. Phys. **3**, 441 (1960).

[9] F. Mulder, G. F. Thomas, and W. J. Meath, Mol. Phys. **41**, 249 (1980).

[10] J. G. Kirkwood, Phys. Z. **33**, 57 (1932).

[11] A. Müller, Proc. Roy. Soc. A. **154**, 624 (1936).

[12] P. W. Atkins and R. S. Friedman, Molecular Quantum Mechanics, 3rd Ed. (Oxford University Press, New York, 1997).

[13] T. J. Giese and D. M. York, Int. J. Quantum Chem. **98**, 388 (2004).

[14] L. A. Curtiss, K. Raghavachari, P. C. Redfern, and J. A. Pople, J. Chem. Phys. **107**, 1063 (1997).

[15] A. D. Becke, J. Chem. Phys. **119**, 2972 (2003).

[16] L. J. Sham and M. Schlüter, Phys. Rev. B. **32**, 3883 (1985).

[17] J. M. Pérez-Jordá and A. D. Becke, Chem. Phys. Lett. **233**, 134 (1995).

[18] E. R. Johnson, R. A. Wolkow, and G. A. DiLabio, Chem. Phys. Lett. **394**, 334 (2004).

[19] Y. K. Zhang, W. Pan, and W. Yang, J. Chem. Phys. **107**, 7921 (1997).

[20] H. L. Williams and C. F. Chabalowski, J. Phys. Chem. A. **105**, 646 (2001).

[21] V. F. Lotrich, R. J. Bartlett, and I. Grabowski, Chem. Phys. Lett. **405**, 43 (2005).

[22] Q. Wu and W. Yang, J. Chem. Phys. **116**, 515 (2002).

[23] S. Grimme, J. Comput. Chem. **25**, 1463 (2004).

[24] O. A. von Lilienfeld, I. Tavernelli, U. Rothlisberger, and D. Sebastiani, Phys. Rev. Lett. **93**, 153004 (2004).

[25] A. D. Becke, J. Chem. Phys. **122**, 064101 (2005).

[26] W. J. Hehre, L. Radom, P. v. R. Schleyer, and J. A. Pople, Ab Initio Molecular Orbital Theory (John Wiley & Sons, 1986).

[27] A. Szabo and N. S. Ostlund, Modern Quantum Chemistry (McGraw-Hill Publishing Company, New York, 1989).

[28] I. N. Levine, Quantum Chemistry, 5th Ed. (Prentice-Hall, New Jersey, 2000).

[29] P. Hohenberg and W. Kohn, Phys. Rev. B. **136**, 864 (1964).

[30] R. G. Parr and W. Yang, Density-Functional Theory of Atoms and Molecules (Oxford University Press, 1989).

[31] W. Kohn and L. J. Sham, Phys. Rev. A. **140**, 1133 (1965).

[32] A. D. Becke, in Modern Electronic Structure Theory, Ed. D. R. Yarkony (World Scientific, 1995) 1022.

[33] J. Harris and R. O. Jones, J. Phys. F. **4**, 1170 (1974).

[34] O. Gunnarsson and B. I. Lundqvist, Phys. Rev. B. **13**, 4274 (1976).

[35] D. C. Langreth and J. P. Perdew, Phys. Rev. B. **15**, 2884 (1977).

[36] J. Harris, Phys. Rev. A. **29**, 1648 (1984).

[37] S. H. Vosko, L. Wolk, and M. Nusair, Can. J. Phys. **58**, 1200 (1980).

[38] J. P. Perdew and Y. Wang, Phys. Rev. B. **45**, 13244 (1992).

[39] A. D. Becke, J. Chem. Phys. **88**, 1053 (1988).

[40] L. A. Curtiss, K. Raghavachari, P. C. Redfern, and J. A. Pople, J. Chem. Phys. **112**, 7374 (2000).

[41] A. D. Becke, J. Chem. Phys. **84**, 4524 (1986).

[42] A. D. Becke, Phys. Rev. A. **38**, 3098 (1988).

[43] A. D. Becke and M. R. Roussel, Phys. Rev. A. **39**, 3761 (1989).

[44] J. P. Perdew, Phys. Rev. B. **33**, 8822 (1986).

[45] J. P. Perdew, in Electronic Structure of Solids, Ed. P. Ziesche and H. Eschrig (Akademie Verlag, Berlin, 1991) 11.

[46] C. Lee, W. Yang, and R. G. Parr, Phys. Rev. B. **37**, 785 (1988).

[47] A. D. Becke, Int. J. Quantum Chem. Symp. **28**, 625 (1994).

[48] A. D. Becke, J. Chem. Phys. **98**, 5648 (1993).

[49] Gaussian 98, Revision A.6, M. J. Frisch, *et al.* Gaussian, Inc., Pittsburgh PA, 1998.

[50] Gaussian 98 User's Reference (Gaussian, Inc., Pittsburgh PA, 1998).

[51] D. Feller and K. A. Peterson, J. Chem. Phys. **108**, 154 (1998); D. Feller and D. A. Dixon, J. Chem. Phys. **115**, 3484 (2001).

[52] A. D. Becke, J. Chem. Phys. **107**, 8554 (1997).

[53] F. A. Hamprecht, A. J. Cohen, D. J. Tozer, and N. C. Handy, J. Chem. Phys. **109**, 6264 (1998).

[54] P. J. Wilson, T. J. Bradley, and D. J. Tozer, J. Chem. Phys. **115**, 9233 (2001).

[55] M. A. Buijse and E. J. Baerends, Mol. Phys. **100**, 401 (2002).

[56] B. J. Lynch and D. G. Truhlar, J. Phys. Chem. A. **105**, 2936 (2001).

[57] R. M. Dickson and A. D. Becke, J. Chem. Phys. **123**, 111101 (2005).

[58] P. Mori-Sanchez, A. J. Cohen, and W. Yang, J. Chem. Phys. **124**, 091102 (2006).

[59] T. Sato, T. Tsuneda, and K. Hirao, Mol. Phys. **103**, 1151 (2005).

[60] S. Grimme, J. Comput. Chem. **27**, 1787 (2006).

[61] Y. Andersson, D. C. Langreth, and B. I. Lundqvist, Phys. Rev. Lett. **76**, 102 (1996).

[62] T. Sato, T. Tsuneda, and K. Hirao, J. Chem. Phys. **123**, 104307 (2005).

[63] R. Ahlrichs, R. Penco, and G. Scoles, Chem. Phys. **19**, 119 (1977).

[64] M. Elstner, P. Hobza, S. Suhai, and E. Kaxiras, J. Chem. Phys. **114**, 5149 (2001).

[65] X. Wu, M. C. Varga, S. Nayak, V. Lotrich, and G. Scoles, J. Chem. Phys. **115**, 8748 (2001).

[66] U. Zimmerli, M. Parrinello, and P. Koumoutsakos, J. Chem. Phys. **120**, 2693 (2004).

[67] R. Jurecka, J. Cerny, P. Hobza, and D. R. Salahub, J. Comput. Chem. **28**, 555 (2007).

[68] J. P. Perdew, K. Burke, and M. Ernzerhof, Phys. Rev. Lett. **77**, 3865 (1996).

[69] J. F. Stanton, Phys. Rev. A. **49**, 1698 (1994).

[70] G. D. Mahan, J. Chem. Phys. **76**, 493 (1982); S. J. A. van Gisbergen, J. G. Snijders, and E. J. Baerends, J. Chem. Phys. **103**, 9347 (1995).

[71] M. A. Spackman, J. Chem. Phys. **95**, 1295 (1991).

[72] J. C. Slater, Phys. Rev. **81**, 385 (1951); J. C. Slater, Quantum Theory of Molecules and Solids, Vol. 4, The Self-Consistent Field for Molecules and Solids (McGraw-Hill, New York, 1974).

[73] See Ref. [28], pages 466-468, for a virial theorem analysis of kinetic and potential energies of dispersion.

[74] M. J. Allen and D. J. Tozer, J. Chem. Phys. **117**, 11113 (2002).

[75] See R. Cambi, D. Cappelletti, G. Luiti, and F. Pirani, J. Chem. Phys. **95**, 1852 (1991), for a good discussion of the Slater-Kirkwood formula.

[76] CRC Handbook of Chemistry and Physics, 76th Ed., edited by D. R. Lide (CRC, Boca Raton, 1995).

[77] A. D. Becke, J. Chem. Phys. **88**, 2547 (1988).

[78] A. D. Becke, Int. J. Quantum Chem. Quantum Chem. Symp. **23**, 599 (1989); A. D. Becke and R. M. Dickson, J. Chem. Phys. **92**, 3610 (1990).

[79] The NUMOL program has been revised to perform fully numerical Hartree-Fock computations.

[80] K. T. Tang, J. M. Norbeck, and P. R. Certain, J. Chem. Phys. **64**, 3063 (1976).

[81] P. J. Stephens, F. J. Devlin, C. F. Chabalowski, and M. J. Frisch, J. Phys. Chem. **98**, 11623 (1994).

[82] T. A. Halgren, J. Am. Chem. Soc. **114**, 7827 (1992).

[83] Accurate values of molecular C_6's are collected from Refs. [22] and [71] as well as (a) A. Kumar, G. R. G. Fairley, and W. J. Meath, J. Chem. Phys. **83**, 70 (1985). (b) A. Kumar, W. J. Meath, P. Bundgen, and A. J. Thakkar, J. Chem. Phys. **105**, 4927 (1996). (c) A. Kumar, J. Mol. Struct. Theochem. **591**, 91 (2002). (d) M. Kumar, A. Kumar, and W. J. Meath, Mol. Phys. **100**, 3271 (2002). (e) A. Kumar, M. Kumar, and W. J. Meath, Chem. Phys. **286**, 227 (2003). (f) A. Kumar, M. Kumar, and W. J. Meath, Mol. Phys. **101** 1535 (2003).

[84] A. D. Becke and E. R. Johnson, J. Chem. Phys. **122**, 154104 (2005), Chapter 3 in this work.

[85] K. J. Miller, J. Am. Chem. Soc. **112**, 8533 (1990).

[86] W. T. M. Mooij, F. B. van Duijneveldt, J. G. C. M. van Duijeneveldt-van de Rijdt, and B. P. van Eijck, J. Phys. Chem. A. **103**, 9872 (1999).

[87] See Ref. [55] for representative plots of exchange holes.

[88] F. L. Hirshfeld, Theoret. Chim. Acta (Berl.) **44**, 129 (1977).

[89] M. J. Jamieson, A. Dalgarno, and L. Wolniewicz, Phys. Rev. A. **61**, 042705 (2000).

[90] K. Patel, P. R. Butler, A. M. Ellis, and M. D. Wheeler, J. Chem. Phys. **119**, 909 (2003).

[91] R. Prosmiti, C. Cunha, P. Villarreal, and G. Delgado-Barrio, J. Chem. Phys. **119**, 4216 (2003).

[92] E. R. Johnson and G. A. DiLabio, Chem. Phys. Lett. **397**, 314 (2004).

[93] The CCSD geometry optimizations were performed using Gaussian 03, Revision C.02, M. J. Frisch, *et al.* Gaussian, Inc., Wallingford CT, 2004.

[94] S. B. Boys and F. Bernardi, Mol. Phys. **19**, 553 (1970).

[95] J. M. L. Martin, Chem. Phys. Lett. **259**, 669 (1996).

[96] S. J. Chakravorty, S. R. Gwaltney, E. R. Davidson, F. A. Parpia, and C. Froese Fischer, Phys. Rev. A. **47**, 3649 (1993).

[97] S. Tsuzuki and H. P. Lüthi, J. Chem. Phys. **114**, 3949 (2001).

[98] A. Bondi, J. Phys. Chem. **68**, 441 (1964).

[99] E. R. Johnson and A. D. Becke, J. Chem. Phys. **123**, 024101 (2005), Chapter 4 in this work.

[100] A. D. Becke, Can. J. Chem. **74**, 995 (1996).

[101] A. D. Becke, J. Chem. Phys. **117**, 6935 (2002).

[102] W. H. Press, S. A. Teukolsky, W. T. Vetterling, and B. P. Flannery, Numerical Recipes in Fortran 77, 2nd Ed., Cambridge University Press, Cambridge, 1992.

[103] R. F. W. Bader, Atoms in Molecules: A Quantum Theory, Oxford University Press, Oxford, 1990.

[104] M. O. Sinnokrot and C. D. Sherrill, J. Phys. Chem. A. **108**, 10200 (2004).

[105] Y. Zhao and D. G. Truhlar, J. Chem. Theory Comput. **1**, 415 (2005).

[106] S. Tsuzuki, T. Uchimaru, M. Mikami, and S. Urata, J. Chem. Phys. **116**, 3309 (2002).

[107] S. Tsuzuki, K. Honda, T. Uchimaru, M. Mikami, and K. Tanabe, J. Am. Chem. Soc. **122**, 3746 (2000).

[108] S. Tsuzuki, T. Uchimaru, M. Mikami, and K. Tanabe, J. Chem. Phys. **109**, 2169 (1998).

[109] R. G. A. Bone, Chem. Phys. Lett. **206**, 260 (1993).

[110] E. R. Johnson and G. A. DiLabio, Chem. Phys. Lett. **419**, 333 (2006).

[111] S. Tsuzuki, K. Honda, T. Uchimaru, M. Mikami, and K. Tanabe, J. Am. Chem. Soc. **122**, 11450 (2000).

[112] R. McWeeny, Rev. Mod. Phys. **32**, 335 (1960); Int. J. Quantum Chem. Quantum Chem. Symp. **1**, 351 (1967).

[113] A. J. Thakkar, H. Hetterna, and P. E. S. Wormer, J. Chem. Phys. **97**, 3252 (1992).

[114] W. Rijks and P. E. S. Wormer, J. Chem. Phys. **88**, 5704 (1988).

[115] H. Hetterna, P. E. S. Wormer, and A. J. Thakkar, Mol. Phys. **80**, 533 (1993).

[116] A. D. Becke and E. R. Johnson, J. Chem. Phys. **123**, 154101 (2005), Chapter 5 in this work.

[117] J. D. Jackson, Classical Electrodynamics, 2nd Ed. (Wiley, New York, 1975), pp. 60-62.

[118] D. Tabor, Gases, Liquids and Solids (Penguin, Harmondsworth, 1969), pp. 238-239.

[119] T. Brinck, J. S. Murray, and P. Politzer, J. Chem. Phys. **98**, 4305 (1993).

[120] O. A. van Lilienfeld, I. Tavernelli, U. Rothlisberger, and D. Sebastiani, J. Chem. Phys. **122**, 014113 (2005).

[121] A. D. Becke and E. R. Johnson, J. Chem. Phys. **124**, 014104 (2006), Chapter 6 in this work.

[122] R. J. Wheatley and W. J. Meath, Mol. Phys. **80**, 25, 1993.

[123] E. Clementi, D. L. Raimondi, and W. P. Reinhardt, J. Chem. Phys. **38**, 2686 (1963).

[124] S. Tsuzuki, K. Honda, T. Uchimaru, and M. Mikami, J. Chem. Phys. **120**, 647 (2004).

[125] W. Klopper, J. G. C. M. van Duijneveldt-van de Rijdt, and F. B. van Duijneveldt, Phys. Chem. Chem. Phys. **2**, 2227 (2000).

[126] J. M. L. Martin and G. de Oliveira, J. Chem. Phys. **111**, 1843 (1999).

[127] E. R. Johnson and A. D. Becke, J. Chem. Phys. **124**, 174104 (2006), Chapter 7 in this work.

[128] P. Jurecka and P. Hobza, J. Am. Chem. Soc. **125**, 15608 (2003).

[129] X. Xu and W. A. Goddard, Proc. Natl. Acad. Sci. USA. **101**, 2673 (2004).

[130] J. Cerny and P. Hobza, Phys. Chem. Chem. Phys. **7**, 1624 (2005).

[131] R. Vargas, J. Garza, B. P. Hay and D. A. Dixon, J. Phys. Chem. A. **106**, 3213 (2002).

[132] A. J. Weldon, T. L. Vickrey, and G. S. Tschumper, J. Phys. Chem. A. **109**, 11073 (2005).

[133] T. Kubar and P. Hobza, Personal communication.

[134] E. R. Johnson and A. D. Becke, Chem. Phys. Lett. **432**, 600 (2006), Chapter 8 in this work.

[135] L. A. Curtiss, P. C. Redfern, K. Raghavachari, and J. A. Pople, J. Chem. Phys. **114**, 108 (2001)

[136] T. Schwabe and S. Grimme, Phys. Chem. Chem. Phys. in press (2007).

[137] E. R. Johnson, R. M. Dickson, and A. D. Becke, J. Chem. Phys. **126**, 184104 (2007).

[138] A. D. Becke and E. R. Johnson, J. Chem. Phys. **127**, 124108 (2007), Chapter 9 in this work.

[139] J. G. Angyan, J. Chem. Phys. **127**, 024108 (2007).

[140] E. R. Johnson, O. J. Clarkin, and G. A. DiLabio, J. Phys. Chem. A. **107**, 9953 (2003).

[141] A. D. Becke and E. R. Johnson, J. Chem. Phys. **127**, 154108 (2007), Chapter 10 in this work.

[142] S. Grimme, M. Steinmetz, and M. Korth, J. Org. Chem. **72**, 2118 (2007).

[143] B. J. Lynch and D. G. Truhlar, J. Phys. Chem. A. **107**, 3898 (2003).

[144] Y. Zhao, N. González-García, and D. G. Truhlar, J. Phys. Chem. A. **109**, 2012 (2005).

[145] T. Ziegler, A. Rauk, and E. J. Baerends, Theoret. Chim. Acta. **43**, 261 (1977).

[146] Y. Zhao, N. E. Schultz, and D. G. Truhlar, J. Chem. Theor. Comput. **2**, 364 (2006).

[147] G. A. DiLabio and E. R. Johnson, J. Am. Chem. Soc. **129**, 6199 (2007).

[148] E. Ruiz, D. R. Salahub, and A. Vela, J. Phys. Chem. **100**, 12265 (1996).

[149] F. Furche and J. P. Perdew, J. Chem. Phys. **124**, 044103 (2006).

[150] A. Veillard, Chem. Rev. **91**, 743 (1991).